Universidade do Minho
Escola de Engenharia

Manuel António de Sousa Cortez Gonçalves de Oliveira

# New Eco-Efficient Polymers for Phosphorus Recovery

abril de 2012

Manuel Oliveira New Eco-Efficient Polymers for Phosphorus Recovery

UMinho | 2012

FCT Fundação para a Ciência e a Tecnologia
MINISTÉRIO DA EDUCAÇÃO E CIÊNCIA Portugal

Universidade do Minho
Escola de Engenharia

Manuel António de Sousa Cortez Gonçalves de Oliveira

# New Eco-Efficient Polymers for Phosphorus Recovery

Tese de Doutoramento
Ciência e Engenharia de Polímeros e Compósitos

Trabalho efetuado sob a orientação da
Professora Doutora Ana Vera Machado

e co-orientação da
Professora Doutora Regina Nogueira

abril de 2012

DECLARAÇÃO

Manuel António de Sousa Cortez Gonçalves de Oliveira

Endereço electrónico: moliveira@dep.uminho.pt Telefone: 963468015

Número do Bilhete de Identidade: _12530122

Título tese:

Novos Polímeros Eco-eficientes para a Recuperação de Fósforo / New Eco-efficient Polymers for Phosphorus Recovery

Orientadora:

Professora Doutora Ana Vera Machado

Co-Orientadora:

Professora Doutora Regina Nogueira

Ano de conclusão: 2012

Designação do Ramo de Conhecimento do Doutoramento:

Ciência e Engenharia de Polímeros e Compósitos

Nos exemplares das teses de doutoramento ou de mestrado ou de outros trabalhos entregues para prestação de provas públicas nas universidades ou outros estabelecimentos de ensino, e dos quais é obrigatoriamente enviado um exemplar para depósito legal na Biblioteca Nacional e, pelo menos outro para a biblioteca da universidade respectiva, deve constar uma das seguintes declarações:

É AUTORIZADA A REPRODUÇÃO PARCIAL DESTA TESE (indicar, caso tal seja necessário, nº máximo de páginas, ilustrações, gráficos, etc.), APENAS PARA EFEITOS DE INVESTIGAÇÃO, MEDIANTE DECLARAÇÃO ESCRITA DO INTERESSADO, QUE A TAL SE COMPROMETE.

Universidade do Minho, ____/____/_____

Assinatura: _____

***“Tudo parece impossível até que seja feito.”*** Nelson Mandela

# ACKNOWLEDGEMENTS

The present thesis is a result of work that was carried out between 2008 and 2012 in the Departments of Polymer Engineering and Biological Engineering of the University of Minho.
This thesis represents a crucial achieving at professional level, however it would not have been possible to write without the help and support of the kind people around me. Therefore, I would like to express my gratitude to the following persons and institutions:

I wish to thank, first and foremost, my supervisor Professor Ana Vera Machado. She has not only been my greatest supervisor, but also a teacher, mentor and role model. I consider it an honour to work with you Professor.

To my co-supervisor, Professor Regina Nogueira. Many thanks for support, scientific guidance, encouragement and valuable suggestions!

To Professor António Brito for all scientific guidance and valuable suggestions!

I would like to thank Véronique Bounor-Legare and Flavien Melis, from University of Lyon 1, for the kind hospitality and scientific support during my stay in France, where part of this work was performed.

To my colleagues that work with me along this time, which encourage me in bad moments and help me with always pertinent scientific discussions. Thus, I would like to thanks to Alexandrina Rodrigues, Andrea Santos, Isabel Moura, Jorge Fernandes, Rui Gomes, Daniel Ribeiro, Joana Barbas, Catarina Domingues, Bruno Oliveira, Sara Amorim, Raquel Santos, Gilberto Martins, Luciana Peixoto and Maria Matos.

An important thanks to academic technicians from Department of Polymer Engineering and Biological Engineering from the University of Minho, which help me along this path. Especially to Manuel Santos, Madalena Vieira, Mauricio Malheiro, Francisco Mateus, Manuel Escourido and João Paulo.

To all the persons and entities that contribute to my work, but are not directly mentioned here, my sincere gratefulness and appreciation.
To Fundação para Ciência e Tecnologia (FCT), for the financial support without it was not possible to carried out this work (SFRH/BD/39085/2007). Thanks!

Importantly I would like to acknowledge to my family, especially to my parents and aunts Laura e Manuela for the opportunities, love and life experiences that given me the strength to make it through each day. To my little sister for the kind and happiness of every day, who is a role model for me.

Finally, I would like to dedicate this thesis to Joana, who has endured my growth with her love and support. I thank you for your infinite understanding, patience and persistence!

# PUBLICATIONS

## International Journals Publications

**This doctoral thesis is based on following papers:**

**Oliveira, M.** Ribeiro, D. Nobrega, J.M. Machado, A.V. Brito, A.G. Nogueira, R. 2011. Removal of Phosphorus from Water Using Active Barriers: $Al_2O_3$ Immobilized onto Polyolefins. *Environmental Technology* 32(9):989-995 (Chapter 3).

**Oliveira, M.** Nogueira, R. Machado, A.V. 2012. Synthesis of Aluminium Nanoparticles in a PP Matrix During Melt Processing: Effect of the Alkoxide Organic Chain. Submitted to *Reactive & Functional Polymer* (Chapter 4).

**Oliveira, M.** Nogueira, R. Machado, A.V. 2012. Preparation of EVA Containing Aluminium Nanoparticles in the Melt. Submitted to *Polymer Advanced Technologies* (Chapter 5).

**Oliveira, M.** Nogueira, R. Machado, A.V. 2012. Hybrid Nanocomposite Containing Al Nanoparticles: Comparison of Materials by Twin Screw Extruder and Batch Mixer. Submitted to *Advanced in Polymer Technologies* (Chapter 6).

**Oliveira, M.** Machado, A.V. Nogueira, R. 2011. Phosphorus Removal from Eutrophic Waters with an Aluminium Hybrid Nanocomposite. Accepted for publication in *Water, Air, & Soil Pollution* DOI: 10.1007/s11270-012-1239-9 (Chapter 7)

**Oliveira, M.** Rodrigues, A.L. Ribeiro, D. Machado, A.V. Brito, A.G. Nogueira, R. 2012. A Novel Hybrid Polymer Nanocomposite Biofilm Reactor for Phosphorus Removal: Start-Up and Operation. Submitted to *Science of Total Environment* (Chapter 8).

## International Conferences Proceedings books

### Oral Communications:

**Oliveira, M.** Machado, A.V. Nogueira, R. Development of Permeable Reactive Barrier for Phosphorus Removal. 5th International Materials Symposium Conference. 5-8 April, 2009 Lisboa, Portugal.

**Oliveira, M.** Machado, A.V. Nogueira, R. Hybrids Nanocomposites for Phosphorus Removal. Encontro com a Ciência. 29-30 July, 2009 Lisboa, Portugal.

**Oliveira, M.** Machado, A.V. Nogueira, R. Hybrid Nanocomposites for Phosphorus Removal. Dia da Engenharia, Universidade do Minho. 20-23 October, 2009 Braga, Portugal.

**Oliveira, M.** Machado, A.V. Nogueira, R. Nanocomposite for Water Treatment. 3rd Young Polymer Scientist Conference. 28-30 April, 2010 Madrid, Spain.

**Oliveira, M.** Machado, A.V. Nogueira, R. Nanomaterials for Water Treatment. MPA 2010, 4th International Meeting on Developments in Materials, Processes and Applications of Emerging Technologies. 28-30 July, 2010 Braga, Portugal.

**Oliveira, M.** Nogueira, R. Machado, A.V. "In-situ" Generation of Aluminum Nanoparticles into PP Matrix. 6th International Materials Symposium Conference. 18-20 April, 2011 Guimarães, Portugal.

**Oliveira, M.** Nogueira, R. Machado, A.V. Hybrid Polymer Containing In-Situ Generated Aluminum Nanoparticles. Polymer Processing Society 27th Annual Meeting. 10-14 May, 2011 Marrakech, Morocco.

### Papers in Conference Proceedings:

**Oliveira, M.** Machado, A.V. Nogueira, R. Phosphorus Removal from Water by Polyolefins: Effect of $Al_2O_3$ Addition. Chempor. 4-6 September, 2008 Braga, Portugal.

**Oliveira, M.** Machado, A.V. Bounor-Legare, V. Nogueira, R. Permeable Reactive Barrier for Phosphorus Removal. EPF 4th Summer School, Bioplastics and Related Materials. 24-29 May, 2009 Gargnano, Italy.

**Oliveira, M.** Machado, A.V. Nogueira, R. Development of Hybrid Nanocomposites Containing Aluminium. 6th International ECNP Conference on Nanostructured Polymers and Nanocomposites. 28-30 April, 2010 Madrid, Spain.

**Oliveira, M.** Machado, A.V. Nogueira, R. Hybrid Polymers for Phosphorus Removal. Polymer Processing Society 26th Annual Meeting. 4-8 July, 2010 Banff, Canada.

**Oliveira, M.** Machado, A.V. Nogueira, R. Nanomaterials for Water Treatment. MPA 2010, 4th International Meeting on Developments in Materials, Processes and Applications of Emerging Technologies. 28-30 July, 2010 Braga, Portugal.

**Oliveira, M.** Nogueira, R. Machado, A.V. Nanocomposites for Eutrophic Waters Treatment. I3N Meeting, 11-12 February, 2011 Fátima, Portugal.

**Oliveira, M.** Nogueira, R. Machado, A.V. Hybrid Polymer Containing In-Situ Generated Aluminum Nanoparticles. Polymer Processing Society 27th Annual Meeting. 10-14 May, 2011 Marrakech, Morocco.

**Posters:**

**Oliveira, M.** Machado, A.V. Nogueira, R. Phosphorus Removal from Water by Polyolefins: Effect of $Al_2O_3$ Addition. Chempor. 4-6 September, 2008 Braga, Portugal.

**Oliveira, M.** Machado, A.V. Bounor-Legare, V. Nogueira, R. Permeable Reactive Barrier for Phosphorus Removal. EPF 4th Summer School, Bioplastics and Related Materials. 24-29 May, 2009 Gargnano, Italy.

**Oliveira, M.** Machado, A.V. Nogueira, R. Nanocomposites for Water Treatment. I3N Meeting. 5-6 February, 2010 Fátima, Portugal.

**Oliveira, M.** Machado, A.V. Nogueira, R. Development of Hybrid Nanocomposites Containing Aluminium. 6th International ECNP Conference on Nanostructured Polymers and Nanocomposites.

28-30 April, 2010 Madrid, Spain.

**Oliveira, M.** Machado, A.V. Nogueira, R. Hybrid Polymers for Phosphorus Removal. Polymer Processing Society 26th Annual Meeting. 4-8 July, 2010 Banff, Canada.

**Oliveira, M.** Nogueira, R. Machado, A.V. A New Hybrid Nanocomposite for Eutrophic Waters Treatment. I3N Meeting, 11-12 February, 2011 Fátima, Portugal.

**Oliveira, M.** Nogueira, R. Machado, A.V. Preparation of EVA Containing Aluminium Nanoparticles by Reactive Extrusion. I3N Meeting, 9-10 March, 2012 Quiaios, Portugal.

**Patent:**

**Oliveira, M.** Nogueira, R. Machado, A.V. 2011. Hybrid nanocomposite for aquatic mediums remediation and respective production method – national patent PCT nº 105441 and international patent PCT/PT 2011/000044.

**National award:**

National award **BES Inovação 2011** in the Category of *Natural Resources & Alimentation*.

# ABSTRACT

NEW ECO-EFFICIENT POLYMERS FOR PHOSPHORUS RECOVERY

In the last 50 years a considerably decline on quality of superficial natural waters, in special for aquatic environments, where the water residence time is higher (more than one year), has been witnessed. Discharge of wastewaters without appropriate treatment, leaching of fertilisers and slurry from agricultural land resulted in a massive input of nutrients to superficial waters, especially phosphorus and nitrogen. As a consequence of this nutrient enrichment, aquatic plants start to overgrow impairing the waters, a process describe as *eutrophication*. The eutrophication prevents the use of water for recreational proposes, increases the cost of water purification for human and animal consumption and has severe consequences for biodiversity.

Therefore, the main of this thesis was to develop a new polymeric material able to remove phosphorus from eutrophic waters without any environmental contamination. Hybrid nanocomposites containing aluminium nanoparticles were prepared by sol-gel reaction in the melt in an internal mixer. Polypropylene (PP), polypropylene grafted with maleic anhydride (PP-g-MA) and poly(ethylene vinyl acetate) (EVA) were used as organic components to prepared the nanocomposites. Two different aluminium precursors, aluminium isopropoxide ($Al(Pr\text{-}i\text{-}O)_3$) and aluminium acetylacetonate ($Al(acac)_3$) were used to produce the aluminium nanoparticles. Several analytical techniques were used to characterize the nanocomposites produced.

The results shows that aluminium precursor with short organic chain ($Al(Pr\text{-}i\text{-}O)_3$) allow faster and extensive reactions without a post step treatment. The nanoparticles are smaller and well dispersed. Regarding to phosphorus removal efficiency, the nanocomposite based of PP was the one that exhibited better performance. Therefore, this material was also produced in a twin-screw to evaluate the scale-up production. The results in a pilot scale, where real eutrophic water was treated using this material, confirm that it is able to remove phosphorus from natural waters. Moreover, it can be used several times and the phosphorus can be recovery.

# RESUMO

NOVOS POLÍMEROS ECO-EFICIENTES PARA RECUPERAÇÃO DE FÓSFORO

Nos últimos 50 anos tem-se assistido a uma diminuição considerável na qualidade das águas superficiais, especialmente em meios aquáticos onde o tempo de residência da água é elevado (superior a 1 ano). Descargas de águas residuais sem tratamento suficiente, lixiviação de fertilizantes e escorrências de terrenos agrícolas, têm contribuído para a introdução massiva de nutrientes, especialmente fósforo e azoto, nas águas superficiais. Como consequência deste enriquecimento, plantas aquáticas começaram a crescer descontroladamente comprometendo a qualidade das águas, um processo denominado por *eutrofização*. A eutrofização impede o uso dos meios aquáticos para fins lúdicos, aumenta os custos de purificação da água para consumo humano e animal e tem graves consequências para a biodiversidade.

Posto isto, o objectivo da presente tese foi desenvolver um novo material polimérico capaz de captar o fósforo de águas eutrofizadas sem provocar contaminações. Para esse efeito, foram preparados por reação de sol-gel no fundido num misturador interno, vários nanocompositos contendo nanoparticulas de alumínio. Polipropileno (PP), polipropileno enxertado com anidrido maleico (PP-g-MA) e poli(etileno vinil acetato) (EVA), foram usados como componentes orgânicos na preparação dos nanocompositos. Dois precursores de alumínio, alumínio isopropoxido ($Al(Pr\text{-}i\text{-}O)_3$) e alumínio acetilacetonato ($Al(acac)_3$) foram usados para produzir as nanoparticulas de alumínio. Várias técnicas analíticas foram empregues para caracterizar os nanocompositos produzidos.

Os resultados obtidos mostram que o precursor de alumínio com menor cadeia orgânica ($Al(Pr\text{-}i\text{-}O)_3$) permitiu reações mais rápidas e extensas sem necessidade de tratamento posterior. As nanoparticulas geradas são pequenas e encontram-se dispersas homogeneamente. Relativamente à eficiência na remoção de fósforo, o nanocomposito baseado no PP foi o que exibiu a melhor performance. Posteriormente, este material foi produzido numa extrusora duplo

fuso de modo a avaliar a sua produção a nível industrial. Resultados obtidos num estudo à escala piloto, onde água real foi tratada usando este material, confirmaram a sua eficiência na remoção de fósforo. Por ultimo, este pode ser usado consecutivamente e o fósforo recuperado.

# CONTENTS

# LIST OF FIGURES

# LIST OF TABLES

# List of Abbreviations and Symbols

**Abreviations:**

acac – Acetylacetonate

Al – Aluminium

$Al(acac)_3$ – Aluminium acetylacetonate

$Al(Pr\text{-}i\text{-}O)_3$ – Aluminium isopropoxide

$Al(OH)_3$ – Aluminium hydroxide

$Al_2O_3$ – Aluminium oxide

AlOOH – Aluminium oxide hydroxide

AlOR – Aluminium alkoxide

Al-PE – Polyethylene containing aluminium oxide

Al-PE-g-MA – Polyethylene grafeted with maleic anhydryde with aluminium oxide

BSE – Back-scattered electrons microscopy

Ca – Calcium

DGGE – Denaturing of temperature gradient gel electrophoresis

DSC – Differential scanning calorimetry

$E_a$ – Activation energy

EDS – Energy dispersive X-ray spectroscopy

EEA – European Environmental Agency

EVA – Poly(ethylene vinyl acetate)

EVA12 – Poly(ethylene vinyl acetate) with 12 % of vinyl acetate

EVA27 – Poly(ethylene vinyl acetate) with 27 % of vinyl acetate

Fe – Iron

FT-IR – Fourier transform infrared

HCl – Hydrochloric acid

HPN – Hybrid polymer nanocomposite

HPNEVA12 – Hybrid polymer nanocomposite synthesised with aluminium isopropoxide and EVA12

HPNEVA27 – Hybrid polymer nanocomposite synthesised with aluminium isopropoxide and EVA27

HPN-acac – Hybrid polymer nanocomposite synthesised with aluminium acetylacetonate

HPN-ext – Hybrid polymer nanocomposite synthesised in the extruder

HPN-int – Hybrid polymer nanocomposite synthesised in the internal mixer

HPN-Pr – Hybrid polymer nanocomposite synthesised with aluminium isopropoxide

MA – Maleic anhydryde

Mg – Magnesium

MSFD – Marine Strategy Framework Directive

NaOH – Sodium hydroxide

O – Oxygen

$O_a$ – Oxygen adsorbed

$O_o$ – Oxygen atributed to oxides

OH – Hydroxide

P – Phosphorus

PE – Polyethylene

PE-g-MA – Polyethylene grafeted with maleic anhydryde

$pH_{ZPC}$ – pH at zero point charge

PP – Polypropylene

PP-g-MA – Polypropylene grafted with maleic anhydryde

$Sb_2O_3$ – Antimony trioxide

SRP – Soluble reactive phosphorus

SEM – Scanning electron microscopy

TEM – Transmission electron microscopy

TGA – Thermalgravimetric analysis

TS – Total solids

TSS – Total suspended solids

VA – Vinyl acetate

$X_c$ – Crystallinity degree

XPS – X-ray photoelectron spectroscopy

XRD – X-ray diffraction

WFD – Water Framework Directive

**SYMBOLS:**

Å – Ångström

$C/C_0$ – Equilibrium concentration per initial concentration

°C – Celsius degree

°C/min – Celsius degree per minute

cm – Centimeter

$cm^2$ – Square centimer

d – day

eV – Electron volt

g – Gram

g/kg – Gram per kilogram

g/L – Gram per liter

$g/m^2$ – Gram per square meter

$g/dm^3$ – Gram per cubic decimeter

G' – Storage modulous

$G_e$ – Equilibrium shear elasticity modulus

h – Hour

ha – Hectare

Hz – Hertz

kg – Kilogram

kg/h – Kilogram per hour

kJ/mol – Kilojoules per mole

km – Kilometer

kV – Kilovolt

L – Liter

M – Molar concentration

ma – Milliamper

$m^2/g$ – Square meter per gram

mm – Millimeters

mg – Milligram

$mg/cm^2$ – Milligram per square centimeter

mg/L – Milligram per liter

mg/g – Milligram per gram

mgP/g – Milligram of phosphorus per gram

mL – Milliliter

mL/min – Milliliter per minute

nm – Nanometer

Pa – Pascal

Pa.s – Pascal second

R – Universal gas constant

rpm – Revolutions per minute

t – Tone

t/year – Tone per year

T – Absolute temperature

Tg – Teragram

Tg/year – Teragram per year

V – Molar volume

$\nu$ – Crosslinking density

$\nu_r$ – Polymer volume fraction at swelling equilibrium

$\chi$ – Polymer/solvent interaction parameter

$\rho$ – Density

$\delta$ – Solubility parameter

µg/L – Microgram per liter

µg/cm – Microgram per centimeter

$\mu g/cm^2$ – Microgram per square centimeter

µm – Micron

$\mu m^2$ – Micron per square meter

w/w – Weight per weight

wt% – Weight percentage

% – Percentage

$\Delta H_f$ – Melt enthalpy

$\Delta H_f^\circ$ – Theoretical melt enthalpy

CHAPTER

# 1 THESIS OVERVIEW AND GENERAL INTRODUCTION

This chapter makes a brief introduction about the thesis subject, follow by an explanation about the motivation for the present work. After, the thesis outline is show to give a general picture about the organisation and subjects consider in each chapter.

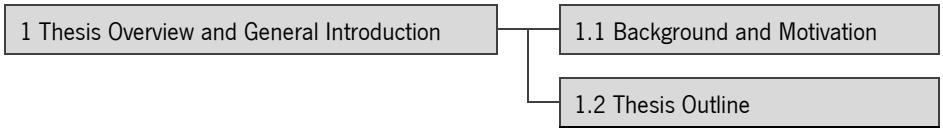

## 1.1 BACKGROUND AND MOTIVATION

The massive input of phosphorus in agriculture land has been contributing for natural stress observed on aquatic bodies and surrounding wetlands. As a result of this excessive nutrient enrichment, an excessive algae growth has been observed. This phenomenon is described as eutrophication. The eutrophication of natural surface waters prevents its use for recreational and domestic consumption and limits the use by native biota. Thus, the reduction of phosphorus in eutrophic waters becomes an imperative task with legal importance in the Europe (WFD-2000/60/EC and MSFD-2008/56/EC).

Treatments based on direct application of chemical salts, like iron, aluminium or calcium, industrial by-products and adsorption with clays have been used for decades. However, these approaches are focus mainly on phosphorus precipitation and the applied agent cannot be recovery, resulting in an increase of the water turbidity and slug production, possibility of phosphorus release and possible contamination of the aquatic medium with toxic compounds. Moreover, as the phosphorus rock is a non-renewable source, with depletion predictions of world reserves ranging from 50 to 400 years, its recovery and recycling are imperative.

The present thesis investigates the development of a hybrid nanocomposite containing aluminium nanoparticles able to remove phosphate from eutrophic waters. Using this material a different approach can be apply, it can be placed in the water and then removed after some time. This way the phosphorus removed can be recovery and the material can be re-used.

Organic-inorganic hybrids have been increasing the academic interest, due to its unique properties, which result from the combination of organic and inorganic structures at molecular level. The hybrid nanocomposites were obtained by a sol-gel process, which consists in mixing a polymer in the molten state with an aluminium precursor. The latter produces aluminium nanoparticles, which are chemically bond to the polymer chain and allow phosphorus removal without contamination.

## 1.2 THESIS OUTLINE

This thesis is organised in nine chapters:

**CHAPTER 1** makes an overview about the thesis subject, explaining the motivation and the objectives of the present work.

**CHAPTER 2** explains the historical rule of phosphorus on eutrophication process and the future perspectives for this non-renewable essential nutrient. Presents a review on the negatives effects of eutrophication in natural aquatic ecosystems and an overview about common methods, results and commercial products available. A review on historical evolution of hybrid nanocomposites, synthesis, principal properties and applications is also given.

**CHAPTER 3** presents the development of polymeric barrier to remove the dissolved phosphorus from water. Composite materials of polyethylene (PE) and polyethylene grafted with maleic anhydride (PE-g-MA) with aluminium oxide ($Al_2O_3$) were prepared and tested. The effect of pH and zero point charge were assed to each composite being the phosphorus removal capability study by kinetic removal tests. The experimental to be used to tests the developed materials will be presented and discuss.

**CHAPTER 4** discusses the preparation of hybrid nanocomposite by melt processing. A new nanocomposite based on polypropylene grafted with maleic anhydride (PP-g-MA)/aluminium was prepared by sol-gel reaction in the melt. To produce the aluminium nanoparticles into PP-g-MA two aluminium precursors were used. Moreover, the chemical and morphological characterization as well as reaction mechanism for both precursors are presented.

**CHAPTER 5** reports the preparation of poly(ethylene vinyl acetate) (EVA)/aluminium nanocomposite by sol-gel reaction in the melt. In this chapter, the effect of vinyl acetate (VA) content on sol-gel reaction was assessed by crosslinking density and rheology measurements.

**CHAPTER 6** deals with a comparative study of nanocomposite preparation in an internal batch mixer and in a twin-screw extruder. The extension of sol-gel reaction was assessed by FT-IR, rheological and crosslinking density measurements. The aluminium nanoparticles size and dispersion by SEM and TEM is shown.

**CHAPTER 7** exposes the application of hybrid nanocomposites developed in chapter 3 on phosphorus removal. The capacity of the prepared nanocomposites to remove phosphorus was tested. The possibility of aluminium contamination and the possibility of regenerate and reused of the material is also presented and discuss. Then, column tests were preformed to assess the behaviour of nanocomposites under continuous phosphorus loads.

**CHAPTER 8** deals with a laboratory simulation of real treatment. The nanocomposites produced in the twin-screw extruder were used on the treatment of natural eutrophic water. The eutrophic water was treated by passing it through fixed bed columns, which contains the developed material.

**CHAPTER 9** presents the general conclusions of the work carried out and suggestions for future work.

Table 1.1 – Organization of the thesis

| |
|---|
| 1. Thesis Overview and General Introduction |
| 2. Literature Review |
| 3. Removal of Phosphorus from Water Using Active Barriers: $Al_2O_3$ Immobilized on to Polyolefins |
| 4. Synthesis of Aluminium Nanoparticles in a PP Matrix During Melt Processing: Effect of the Alkoxide Organic Chain |
| 5. Preparation of EVA Containing Aluminium Nanoparticles in the Melt |
| 6. Hybrid Nanocomposite Preparation in a Batch Mixer and a Twin-Screw Extruder |
| 7. Phosphorus Removal from Eutrophic Waters with an Aluminium Hybrid Nanocomposite |
| 8. A Novel Hybrid Polymer Nanocomposite Biofilm Reactor for Phosphorus Removal: Start-Up and Operation |
| 9. Conclusions and Future Work |

CHAPTER

# 2 LITERATURE REVIEW

This chapter aims to make an overview about the eutrophication process in natural waters, giving an historical approach on the role of phosphorus in the process and an assessment of the current eutrophication level, especially in the Europe. Moreover, an analysis of the actual methods used to control/reduce the eutrophication is provided. It also presents a description of nanocomposites properties, preparation methods and inorganic precursors.

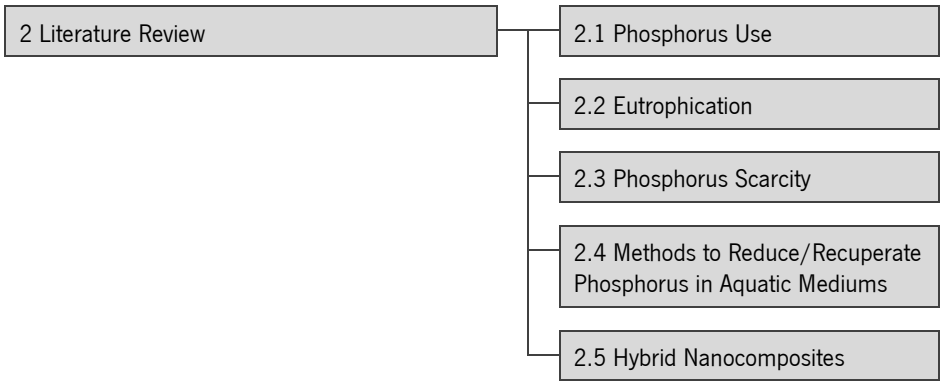

## 2.1 PHOSPHORUS USE

Since industrial revolution the human population is growing and with these the need for food supply. The use of fertilizers becomes an imperative to answer the global food necessities. Phosphorus (P), which was removed from soil by crops, was replaced using waste products as manure, crop residues and human excretes. The use of these methods allowed, at that time, to improve the agriculture fertility and maintenance the level of crop production [1,2].

In 1840, the German chemist Justus von Liebig demonstrated, for the first time, that the growth of terrestrial plants was conditioned by the nutrient in less quantity in the environment relative to the plant growth demand, his theory becomes known as Liebig's Law of the Minimum [3]. The Liebig theory comes to contradict the humus theory accepted until that time. This theory, very popular in the 18th century, defends that the organic compounds were the most important nutrients for plants growth. The fertilization with organic compounds was considered essential to improve the yield and increase the soil fertility. Liebig rejected this and demonstrated that only inorganic salts of P and nitrogen should be used as nutrient sources for plants growth, he also considered that humus only gives $CO_2$ to be used by plants [4]. Therefore, he assumed that nutrients, such as, P, nitrogen and potassium should be introduced into the soil to improve the production [2,4].

In the middle-to-late of 19th century, the increase of soil degradation and famines led the Europe to search for new sources of fertilizers. Guano (bird excreta rich in mineral P) started to be imported to Europe to be used as source of inorganic P [5]. The worldwide guano demand increased rapidly, which resulted in a decline in production by the end of 19th century. Since this become economic unfeasible, the P rock was seen as unlimited source of concentrated P. The mining of the P rock had begun [6]. The fertilisers industry grew rapidly together with improvements in hygiene condition. Humana excreta was no longer used as soil fertilizers and started to be discharge into water bodies.

After the industrial revolution, the natural P biochemical cycle was interrupted and public health concerns required the disposal of excreta rather than reuse (Figure 2.1). P was no more recycled and mine phosphate rock started to be intensively used in agriculture. The use of fertilizers allowed a rapid replace of P levels in soil, after crops harvested. The modern civilization went from a P recycling society to a P throughput society. A sustainable cycle was interrupted, the P

that used to be recycled is now moving from mines to oceans at levels much higher than the natural biogeochemical cycle, which takes tens of millions of years [5]. Reported by Ritmann and co-workers, the P content in worldwide fresh water systems increased at least 75 % since pre-industrial revolution. The P fluxes went from 8 to 22 million metric tons per year in the same period. The P as becomes an environmental pollutant for oceans, lakes and rivers waters [7].

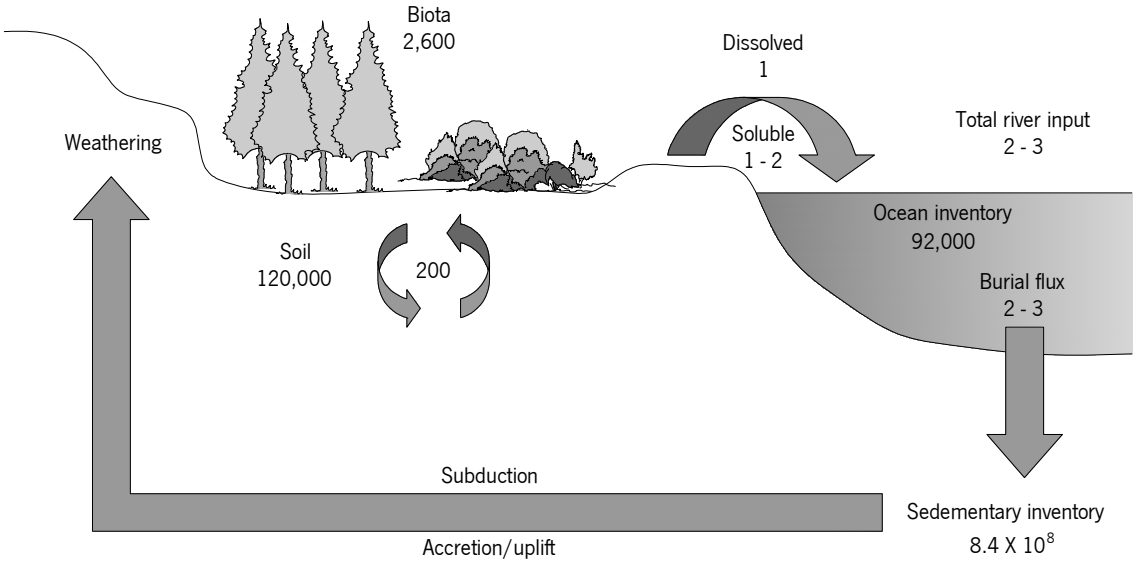


(a)

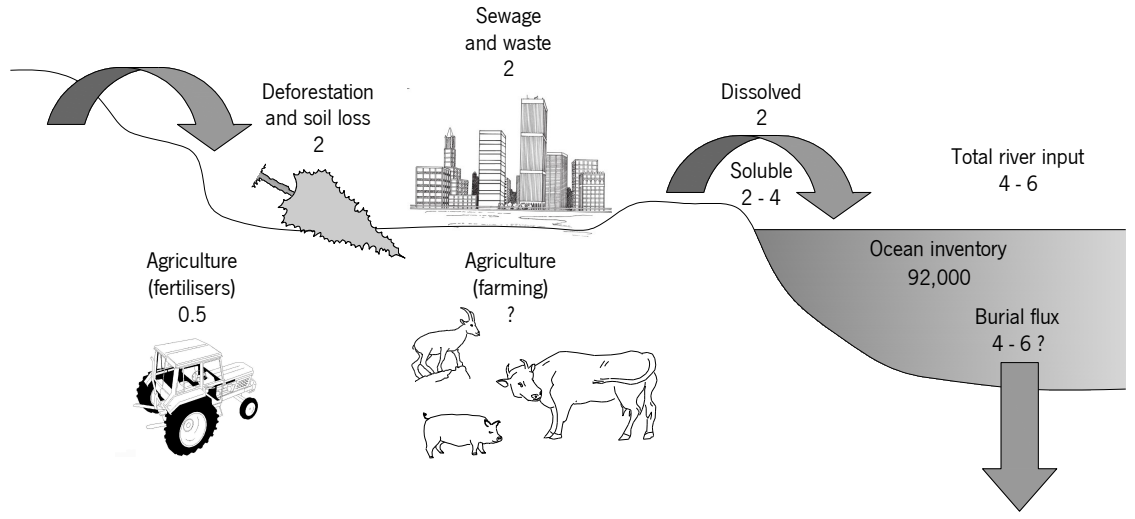


(b)

Figure 2.1 – The dissolved phosphorus cycle a) prior to human influence and b) after to human influence (adapted from Filippelli, 2002 [8]). Reservoirs capacities in Tg phosphorus and fluxes indicated by arrows in Tg/year phosphorus.

## 2.2 EUTROPHICATION

As an effect of the phosphorus (P) movement to aquatic bodies, an over enrichment of nutrients occurred, this was define as "eutrophication". Etymologically "eutrophic" means "good nourishment" and eutrophication is the process by which water bodies grow in biomass productivity [9]. The term eutrophication initially applied in limnology by Naumann in 1919, to provide a classification scheme according to plant production and nutrient available. Later, in 1929 Naumann transposed this classification on trophic degrees for lakes water types based on production of organic matter by phytoplankton creating oligotrophic-eutrophic paradigm (Figure 2.2) [10,11]. The historical episodes of freshwaters eutrophication through Europe and North America are reflex of modern industrial society evolution. Ashley and co-workers enumerate a few cases, the Wisconsin lakes – Mendota and Monona in 1882, Lake of Zurich, Switzerland in 1896, Lake Erie in 1930 and Lake Washington in the 1950s [5]. Around 50 years ago became clear that this good nourishment have tragic environmental effects in fresh waters environments as rivers, dams and lakes. As a result of this concern, many political actions have been taken around the world, being express into programs started by Coastal Zone Management Act (PL 92-583, 1972) and Clean Water Act (PL 92-500, 1972) in the United States, the Barcelona convention (MEDPOL) for the Mediterranean and legislative instruments for Urban Wastewater Treatment Directive (UWWTD-CEC, 1991a) and Nitrates Directive (ND, CEC, 1991b), Helsinki Convention (HELCOM, 1994) for the Protection of Baltic Sea and Oslo-Paris Convention for the Protection of Northeast Atlantic (OSPAR, 2002). Thus, at the end of 20th Century eutrophication had a scientific and legal meaning in Europe, it was defined in OSPAR as: "*Eutrophication means the enrichment of water by nutrients causing an accelerated growth of algae and higher forms of plant life to produce an undesirable disturbance to the balance of organisms present in the water and to the quality of the water concerned, and therefore refers to the undesirable effects resulting from anthropogenic enrichment by nutrients...*"[10]. To implement the reduction of nutrients level over enrichment in fresh water environments, Europe developed more specific legislation describe in the Water Framework Directive (WFD-2000/60/EC) and in the Marine Strategy Framework Directive (MSFD-2008/56/EC) which establish environmental policy for all European countries.

The MSFD Directive describes the negative effects that result from the eutrophication process. Lost of biodiversity, ecosystem degradation, harmful algae blooms and oxygen deficiency in bottom waters are expected on degraded eutrophic fresh water environments. The abundance of algal blooms, often cyanobacteria, provokes a reduction of dissolve oxygen levels, which is one of most common consequence. The depletion of oxygen can be great enough to create anoxia and consequently fish death, leading gradually a biodiversity reduction and creation of "death zones". As a result of this, more than 400 costal death zones were identified this number increases 10 % per decade [7]. In severe cases toxins might also be present in the water resulting from the domination of phytoplankton by blue-green algae (cyanobacteria), where some of produced compounds more toxic than "snake poison" making water unsafe for consumption [12-15]. These serious problems have been reported in literature from centuries, with narration of animal group death by ingesting large quantities of infested water. In the Bible (Exodus, 7: 20-24) is possible to read "*all the water of the Nile river became red as blood and fish which were in the river died. And the river was poisoned and the Egyptians could not drink its waters*". In 1878, it was published the first scientific report in Australia about domestic animals that die as consequence of poisoning after drinking water from lake Alexandrina, impaired by blue/green algae bloom. In 1988, Brazil dealt with 2000 gastroenteritis cases, which resulted in 88 deaths. The reason was a toxin produced by cyanobacteria (Anabaena and Microcystis) present in the dam water used to supply the area [16]. Smol in 1996 describe the case of a farm near Baldur, Manitoba (Canada), where 16 cows were killed by nerve toxins from cyanobacteria blooming in a pond used for watering [17]. Dokulil and Teubner, 2011 summarized the principal consequences caused by eutrophication on watersheds [11]:

- Increase of biomass of phytoplankton and macrophyte vegetation;
- Shift to bloom-forming algal species that might be toxic or inedible;
- Increase of biomass of benthic and epiphytic algae;
- Change in species composition of macrophyte vegetation;
- Increase of biomass of consumer species;
- Increase of incidence of fish kills;
- Reduction in species diversity;
- Reduction in harvestable fish biomass;
- Decrease in water transparency;
- Oxygen depletion in the water body;

- Taste, odour, and drinking water treatment problems;
- Decrease in perceived aesthetic value of the water body;
- pH variation.

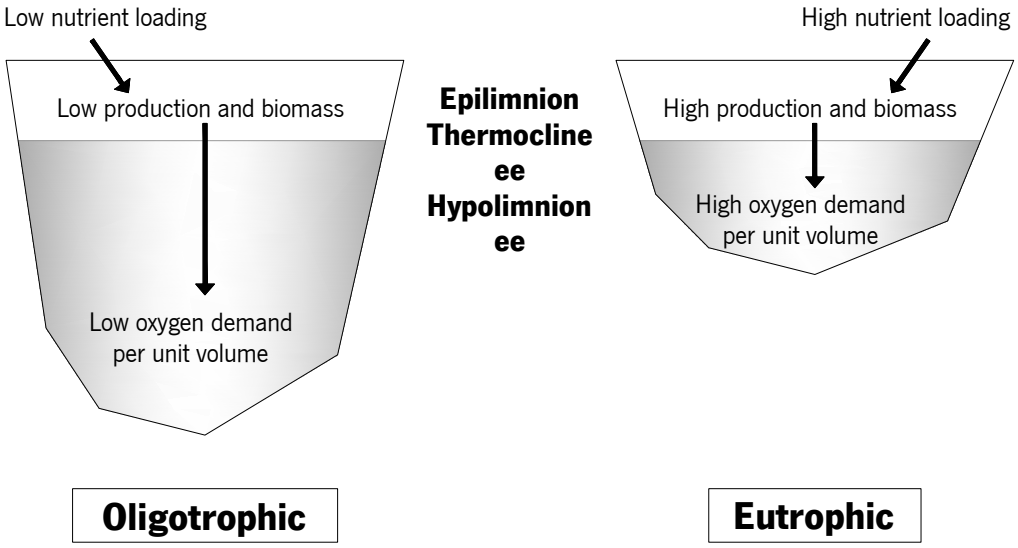


Figure 2.2 – The oligotrophic-eutrophic paradigma (from Dokulil and Teubner, 2011 [11]).

Examples of lakes, rivers and dams eutrophication are spread around the world. Meybeck in his studies indicated that streams and rivers have double nitrogen and P concentrations worldwide, with local concentrations, sometimes, higher than 50 times [18,19]. The Water Wheel reported that 54 % of the lakes and reservoirs in Asia are impaired by eutrophication, 53 % in Europe, 48 % in North America, 41 % in South America, and 28 % in Africa [20].

The Portuguese Ministry of Environment, Spatial Planning and Regional Development published, in July 2008, a report of the data collected between 2004 – 2007, where the level of Portuguese dams eutrophication were assessed. The results revealed that 72 % of the tested stations had P excess, which corresponds to 21 eutrophic dams (Figure 2.3) [21]. The excessive nutrients soils load led to eutrophication of several lakes in Azores. The most famous are Lagoa das Sete Cidades and Furnas, which began to suffer cyanobacteria blooms after the year 2000. However, in the report of the triennium 2004 – 2007, only Lagoa Negra in Flores Island was considered eutrophic [21].

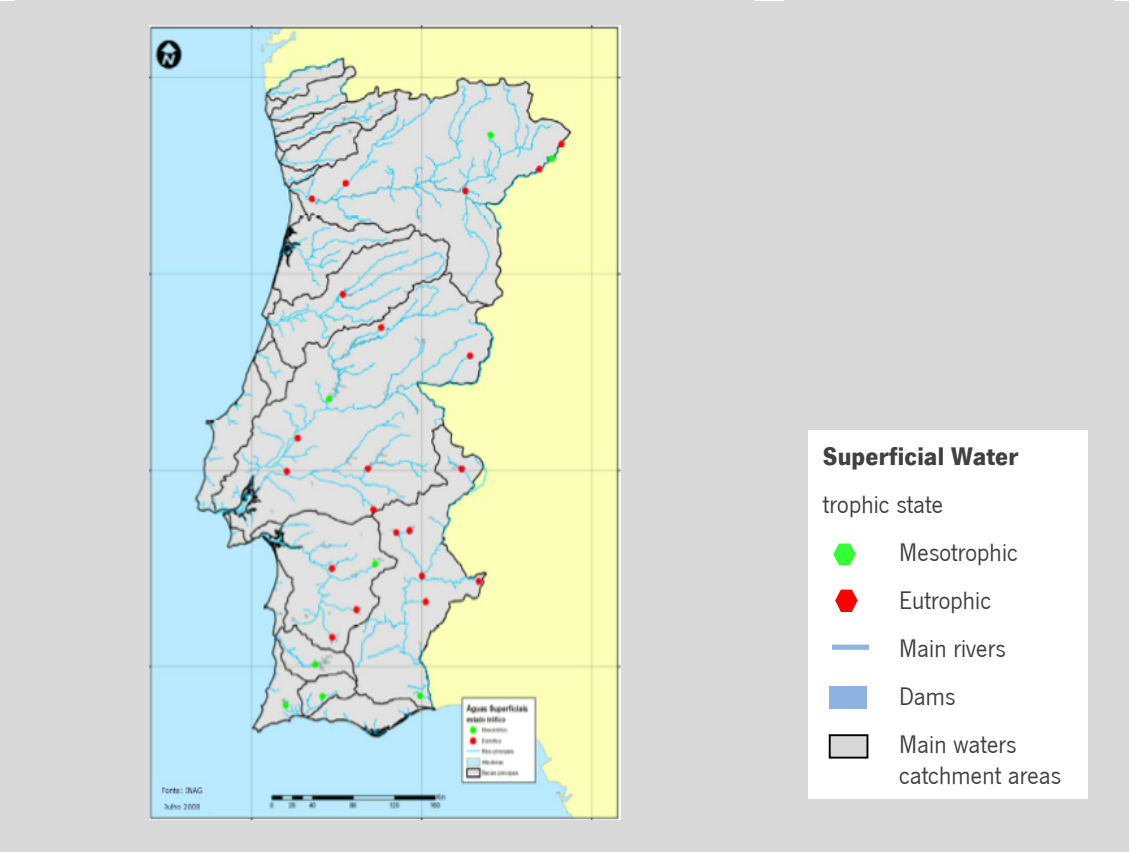


Figure 2.3 – Representative map of superficial waters trophic state in Portugal [21].

The European Environmental Agency (EEA) in a report from 2009 indicated that rivers and lakes eutrophication is generally higher in central and southern Europeans countries and lower in the northern and alpines countries (Figure 2.4) [10,22]. The European costal and marine waters were also target of assessment by EEA agency. Published in July 2011, Waterbase CSI021 identified the critical points in European seas (Figure 2.5) [23].

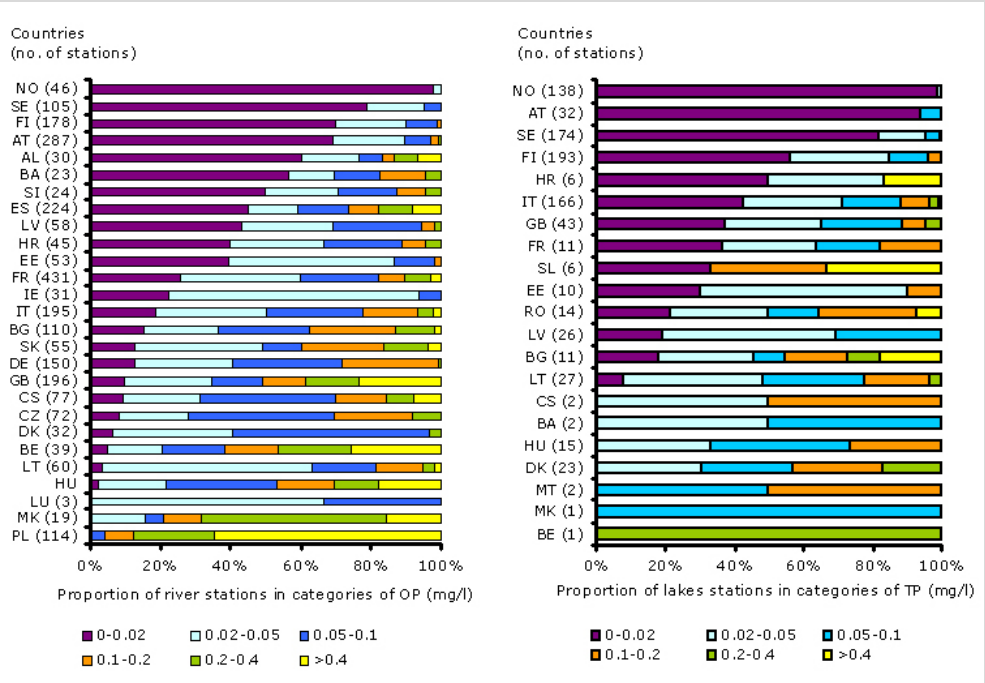


Figure 2.4 – Concentration of phosphorus in rivers (left; ortophosphate) and lakes (right; total phosphorus) in European countries. The number of monitoring stations in each country is given in brackets. Figures are based on the most recent year for which data are available: this is 2005 for all countries except for France (lakes: 2000), Czech Rep. (lakes: 2003), Bulgaria and Denmark (rivers and lakes: 2004) [22].

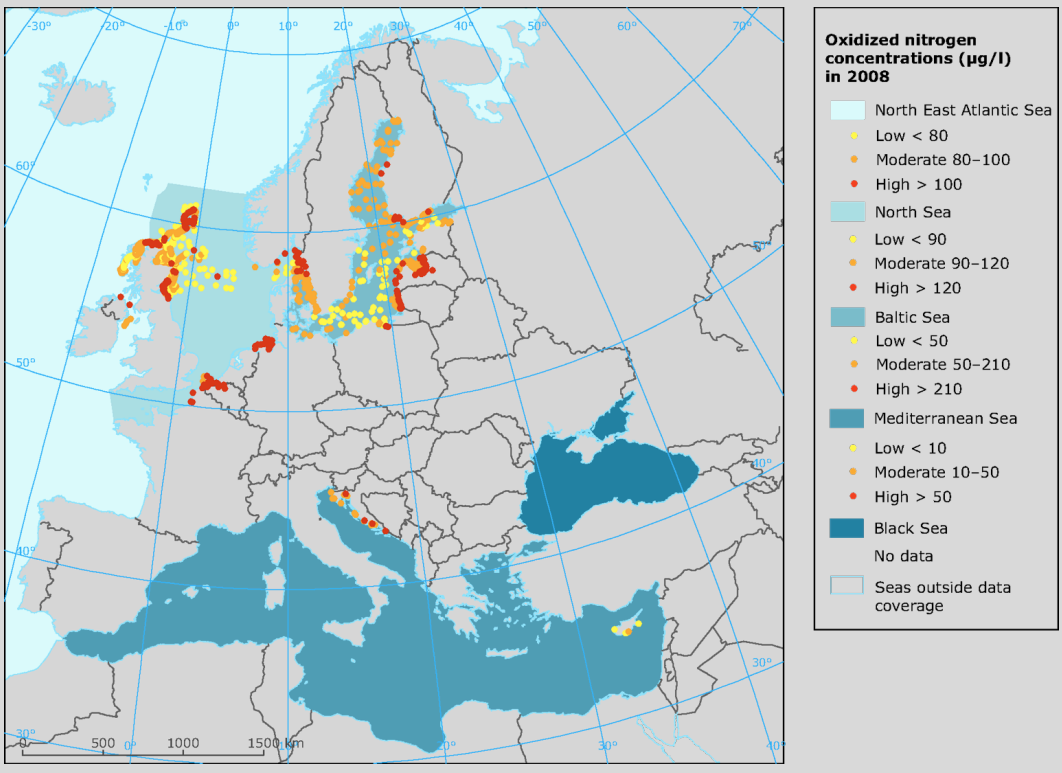


Figure 2.5 – Winter orthophosphate concentrations in European seas in 2008 [23].

In the Baltic Sea the highest P concentrations (> 25 µg/L) were registered at Finnish coastal stations in the Gulf of Finland and in Gulf of Riga. These high concentrations were provoked by internal P loading, which resulted from P release by bottom sediments during anoxic conditions [23]. As describe by Voss and co-workers, the Baltic Sea is especially sensible to nutrients inputs because water have a long residence time. It suffers visible nutrients loadings since 1950s, with lot of episodes of phytoplankton bloom [24]. Figure 2.6 shows a picture took in 2005, where it is possible to see a cyanobacteria bloom.

In the North Sea the highest P concentration (> 100 µg/L) was registered in French and Belgium coastal waters. However, due to improvements on wastewater treatment, most of North Sea countries reduced there P loadings in 50 % between 1985 and 2005, which result in a decrease of the P concentration in 28 % [23,25].

The Mediterranean Sea had low P concentration in open sea and the eutrophication was only observed in some costal waters. The highest P concentration (> 30 µg/L) was registered along western Italian coast [23].

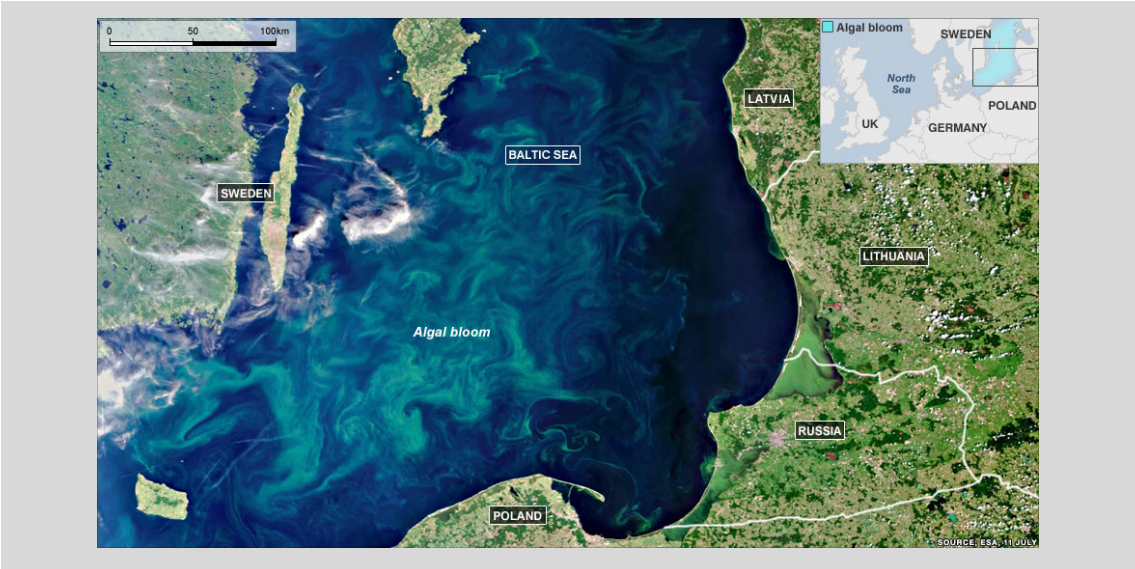


Figure 2.6 – Extensive surface blooms of cyanobacteria in 2005, Baltic Sea [26].

For Black Sea no data referring to the winter nutrient concentrations in 2008 has been submitted to the EEA. However, eutrophication effects have been noticed during the last 30 years (Figure 2.7). Between 1973 and 1990 were estimated that five million tons of fish died as a consequence of eutrophication. Moreover, a reduction in tourism occured, which was estimated in 1995 by Black Sea Environmental Program as annual loss of 360 million US $ [16].

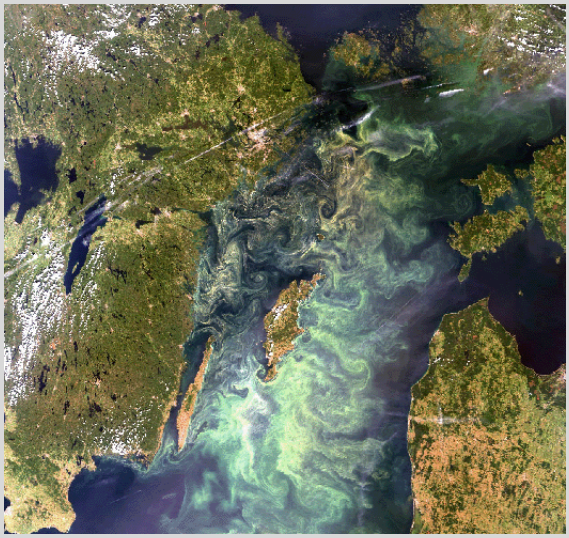

Figure 2.7 – Satellite image of Black sea algae bloom, captured in July 2010 by a camera on the European Space Agency's Envisat satellite [27].

Hans and co-workers describe the case of Taihu lake as the 3rd largest freshwater lake in China. It supplies approximately 40 million people. Taihu has experienced an accelerating eutrophication in the past three decades, went from mesotrophic diatom-dominance to a hyper-eutrophic cyanobacteria dominated system with severe consequences (Figure 2.8) [28].

Figure 2.8 – Pictures from eutrophic Taihu lake [29].

## 2.3 PHOSPHORUS SCARCITY

While the research for efficient ways to control eutrophication still in progress, a newer and serious concerned is the depletion of mineral phosphate rock. Phosphorus (P) is an essential element for life [1]. Moreover, as a key element on fertilizers to improve the crop productions, P cannot be substituted, as describe in 1974 by Isaac Asimov:

*We may be able to substitute nuclear power for coal, and plastics for wood, and yeast for meat, and friendliness for isolation – but for phosphorus there is neither substitute nor replacement (Asimov, 1974 [30]).*

Also, the European Commission in Landfill Waste Directive of 1999, encourage to a sustainable society where renewable resources should substitute non-renewable wherever is possible. In cases where this cannot be done, recovery, reuse and recycling should be practice [31]. Many scientists have been advertising for P scarcity. It is expected that the world population will reach 9 billion people in 2050, thus assures enough P to guarantee the food production will be critical. The International Water Management Institute points out an increase of 70 % of food production by 2050 to face the global demand.

At the present, the main source of P is phosphate rock, a non-renewable source, which is becoming scarce and expensive. Describe in Prud'Homme (2010b), around 90 % of phosphate is for food production, being 82 % used in fertilizers, 7 % for animal feed and 1-2 % for food additives [32]. Accept and recognize by fertilizer industries, the reserves quality is declining and the cost of extraction, processing and shipping increasing [1,2].

In 2008, 17.8 t of P was consumed as fertilizers [33]. If this amount had been spread equality by the 5 billion ha of global land, this means that 4 kg of P per ha. Moreover, if it was spread only by 1.4 billion ha of arable soils, the average amount increase to 13 kg of P per ha. However, in 2008 the P fertilizers distributions average was 10 kg per ha in Asia and North America, around 6 kg per ha in Europe and less than 2 kg per ha in Africa (FAOSTAT). Heffer and Prud'Homme (2008), expect an annual grow on P fertilizers consumer of 2.7 %, increasing from 17.8 t in 2008 to 19.8 t in 2012 [33].

As non-renewable resource, a peak on phosphate rock production is expected around 2030-2040, if the current demand for fertilizers is maintained. Déry and Anderson have a more pessimistic

opinion, they state that the peck on phosphate production already occurred in 1989 [34]. Nevertheless, this was a mini-peck provoked by the disaggregation of Soviet Union [2,5]. In 1949, Hubbert and later other scientist claim that the critical period will be not when 100 % of reserves will be depleted but when the high quality reserves will be depleted and the cost to reach a new high quality reserves unfeasible [1]. Approximately 85 % of world phosphate rock reserves are controlled by five countries, being the most important United States, Morocco and China (Figure 2.9). To prevent the excessive export and ensure the domestic supply, China recently imposes 135 % export tariff.

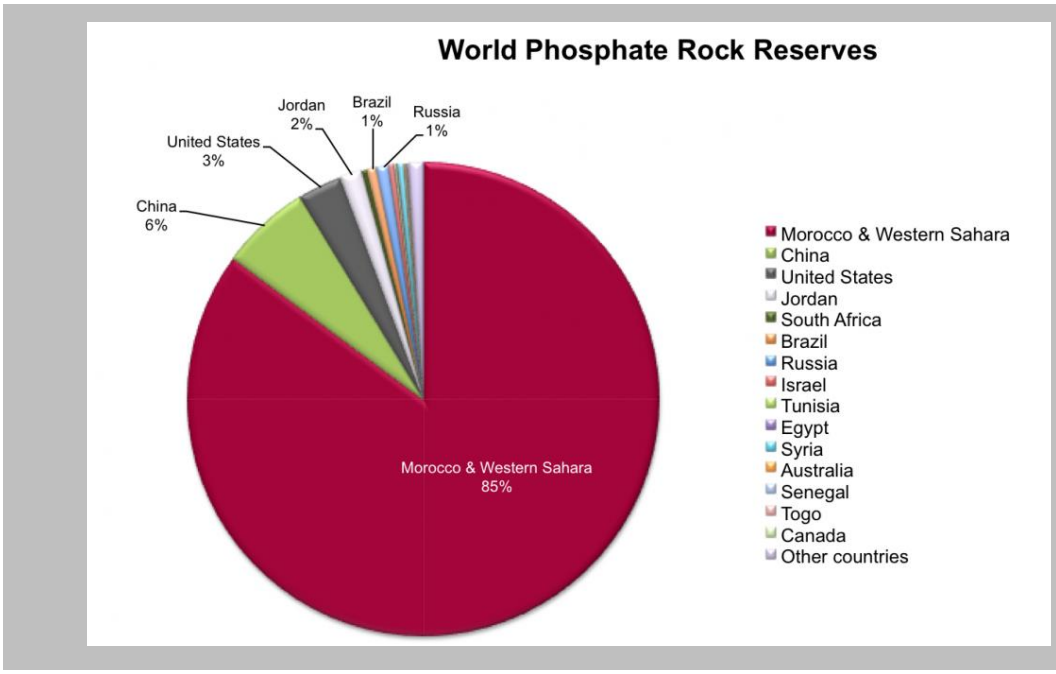


Figure 2.9 – USGS estimates of reported remaining world phosphate rock reserves in 2009, indicated by country/region. Units are in million tones of phosphate rock. Data: USGS, 2010 [1].

## 2.4 METHODS TO REDUCE/RECUPERATE PHOSPHORUS IN AQUATIC MEDIUMS

Concerns about environmental sustainability are increasing and reflected in governmental policy and international agreements. Development of technologies for phosphorus (P) removal started in 1950s aiming to reduce the amount of P arriving in surface waters. The establishment of P removal technologies open the possibility for P recycling and sustainability [35]. The common P removal technologies are based on chemical precipitation, biological adsorption, combination of both and occasionally auto-precipitation (struvite) [36].

Chemical precipitation is the main commercial process for removing P from eutrophic mediums and wastewater in nowadays. Started in 1950s in Switzerland as response to the growing problem of eutrophication, chemical precipitation is based on direct application of salts like aluminium, iron or calcium, industrial by products and mineral clays [35-37].

### 2.4.1 ALUMINIUM

The most common flocculation agent is aluminium sulphate (alum) that dissociated in water forming hydrated ions. The hydrolysis reaction in correct pH range (6 to 8) gives aluminium hydroxide ($Al(OH)_3$). This is an amorphous flock with high coagulation capability and P adsorption properties, which precipitates P almost immediately [38]. The amount of aluminium to be used in the treatments depends on the concentration of reactive P and colloidal particles. From Equation 2.1 the stoichiometric indicates that alum and P molar ratio is 1:2, where 0.87 kg of aluminium are able to remove 1 kg of P, if complete precipitation occurs [39,40].

$$Al_2(SO_4)_3xH_2O + 2PO_4^{2-} \rightarrow 2AlPO_4\downarrow + 3SO_4^{2-} + xH_2O \qquad \text{Equation 2.1}$$

A large number of examples of alum application can be found in the literature [28,41]. Conover patented the use of aluminium hydroxide sulphate for water lake treatment. However, for pH values lower than 5.5 and higher than 8.0, the solubilisation of aluminium phosphate occurred, the adsorbed P is released again for the water column [42]. Cooke and co-workers described in 1993 the case of Rockwell lake on Ohio, an eutrophic water reservoir supplied in 90 % by Cuyahoga river, which drains a vast agriculture and forested catchment areas. Between the summer and autumn, the lake was treated with aluminium sulphate, aluminium hydroxide was

formed which was deposited in bottom of the river and affected the water flow. At the same time, an increase of $Al^{3+}$ concentration and a decrease of pH were registered [39,43].

The main disadvantages of the use of aluminium sulphate are the possibility of toxicity, pH reduction, low flock stability, need to ensure dosage rate, smothering of benthos and a restriction period for drinking water, irrigation and stock watering. However, it has low cost, is applied in liquid form and the treatment cases are well documented [39,44].

### 2.4.2 IRON

Iron is generally applied as iron salts or as industrial by-product. Occurs in two different forms: iron (II) and iron (III), the latter is more commonly used and the former has lower cost benefits resulting in an attractive alternative option [44,45]. Depending on the physico-chemical parameters, when iron (II) is applied to precipitated P two different products can be obtained [39,45].

a) $Fe^{3+} + PO_4^{3-} \rightarrow FePO_4\downarrow$ Equation 2.2

b) $3Fe^{2+} + 2PO_4^{3-} + 8H_2O \rightarrow Fe_3(PO_4)_2.8H_2O\downarrow$ Equation 2.2

The application of iron compounds to remove P requires always water aeration and pH control. Hickey and Gibbs assumed that the reaction of Equation 2.2 only occurs for pH above 7. According to this equation it requires 1.8 kg of iron ion to remove 1 kg of P. Since the addition of iron to lakes water results in water pH reduction, it is necessary to use buffers with low alkalinity [39]. In the bottom of lakes near to sediments, reduction conditions are predominant during hypolimnion seasonally stratification. The absence of oxygen results in released of the P adsorbed, as consequently of microbial reduction of iron (III) to iron (II) [39].

Boers and co-workers, in 1989, applied a daily dose of 100 $g/m^2$ of iron (III) to the sediments of eutrophic Lake Groot Vogelenzang in the Netherlands. The treatment was preformed during two months, October and November. They registered a decrease of the total P and chlorophyll-a three weeks after finishing the treatment. However three months later the total P rose again [46].

### 2.4.3 CALCIUM

Among the three salts, calcium is the less commonly applied due to handling difficulties and large sludge production [45]. Limestone, which is a sedimentary rock composed by $CaCO_3$ (more than 50 %) removes P according to Equation 2.3.

$$10Ca^{2+}+6PO_4^{3-}+OH^- \rightarrow Ca_{10}(PO_4)_6(OH)_2\downarrow \qquad \text{Equation 2.3}$$

The pH range where this reaction occurs still under discussion, different ranges have been proposed (8.0 to 11.0, 7.5 to 8.5 or for pH>10.5) [47]. The P removal with calcareous compounds induces an increase of water pH that might not be compatible with life in aquatic systems [46]. Moreover, literature studies reported that carbonate and phosphate ions compete for calcium, which inhibits the precipitation of calcium phosphate [44,48].

There are several examples worldwide where limestone has been used for P removal. In Melbourne, Australia, different grades of limestone were tested to reduce the P concentration in a small urban lake. The results indicated that only the fine grained was able to precipitate P [44].

### 2.4.4 INDUSTRIAL BY-PRODUCTS

The most common industrial by-products are alum residuals, red mud, fly ash, cement kiln dust and bone char, these are mainly composed by a significant fraction of divalent and trivalent ions as aluminium, iron and calcium [7].

In spite of higher P adsorption capacity revealed in batch tests, the use of industrial by-products have serious limitations since they contain high concentrations of heavy metals that may contaminate the aquatic environment, increase water turbidity and pH [49].

### 2.4.5 MINERAL CLAYS

Mineral clays are widely available in soil and sediments and have been used as flocculated and sorbent of suspended particles, disease bearing organisms and toxic compounds in water. Clays can be used in their natural form or after chemical treatment. The clays adsorption capability is

due to its high specific surface area (external and internal), which extends to a few hundred $m^2/g$. Another important property is the presence of electrical charges of $Al^{3+}$ and/or $Si^{4+}$ that can be changed by cations of low valence, allowing to adapt the surface charge to the pH change of the solution [39].

Allophane is a group of mineral clays compose by alumina, silica and water. Results from volcanic ash materials, it has a large superficial area and is highly porous with lower bulk density. Gibbs and co-workers in 2008 assess the allophane capability to remove P and compared it with alum, Phoslock™ and modified zeolite. They showed that allophane was the sediment capping that allowed higher P removal [37].

### 2.4.6 BIOLOGICAL

The biological P removal can be divided into two independent mechanisms. First, suspended growing cells or plants could directly absorb P. Second, P can be storage as polyphosphates by microbial biomass presented on active sludge on treatment facilities. Construction of wetlands is the common way to perform biological P removal [36]. This low-cost and low-tech process has been used for decades to reduce the excess of nutrients present in domestic and industrial wastewater and agriculture runoffs [50]. Wetlands are artificial ponds planted with aquatic and sometimes terrestrial plants [36]. The biggest difference between wetlands is the type of subtract used for plants growth, which in some cases has also cleaning capacity. The variety of substrates includes, pumice, quartzite, light expanded clay aggregates, lightweight aggregates, wollastonite, shale, sand, maerl, zeolite, bauxite, synthetic hydrotalcite, blast furnace slag and fly ash [50]. In bottom of the wetlands the plants roots forms an enormous biological filter. At the same time, microorganism that lives in submerged roots, degrade other pollutants, which are later absorbed by plants.

### 2.4.7 STRUVITE

Struvite is a mineral formed by magnesium ammonium phosphate in equal molar concentrations (Equation 2.4), which precipitate spontaneously in wastewater [36]. Identified in wastewater treatment plants in 1939 as crystalline deposits, which requires regular cleaning due to pipes

obstruction. Although struvite is a problem on wastewater treatment plants it has potential to be used in fertilizers [51,52].

$$Mg^{2+} + NH_4^+ + PO_4^{3-} + 6H_2O \rightarrow MgNH_4PO_4 6(H_2O)\downarrow \quad \text{Equation 2.4}$$

The interest on struvite precipitation has been growing since it allows P recovery, which has a positive impact taking into account the energy cost of mining and the increase scarcity of natural P resources [53]. As examples, UK alone has the capability to produce 67 t/year of $P_2O_5$ fertilizer and Western Europe 270 t [36].

### 2.4.8 COMMERCIAL PRODUCTS

On international market some products are available to reduce the level of nutrients present in natural eutrophic waters. The next paragraphs make an overview about four commercial solutions with the principal properties described in Table 2.1. However, most of these commercial products only reduce the P concentration in aquatic medium, they do not recovered it.

Plocher™ is a product developed in 1980 by Roland Plocher. This was developed to stimulate the auto-regeneration processes, promoting the rebalance of ecological and biological cycles. Plocher have been used in many countries along Europe, but the better results were obtained in Switzerland (Heidsee lake), Germany (Gernshein lake), France (des Spains lake) and Austria (lake Oedt) [54,55]. The Plocher product is protected by patent, thus information on the compositions is not available. The available information describes Plocher as a material composed by cylindrical tubes containing aluminium, which can be applied directly in aquatic medium as powder or dispersed in solution [55]. In Portugal, Plocher was used in the eutrophic lake Casal da Cambra (Figure 2.10) where treatments start in 2006 with 3 g/m$^2$ [56].

(a) (b)

Figure 2.10 – Picture from Casal de Cambra lake treated with Plocher: a) before treatment and b) after treatment [56].

Phoslock™ is commercial product developed by Commonwealth Scientific and Industrial Research Organization, is based on bentonite clay with surface treatment, where sodium and calcium ions were changed by lanthanum [57]. P is removed by precipitation with lanthanum giving lanthanum phosphate. According to Equation 2.5, 1 kg of P requires 4.5 kg of lanthanum.

$$La^{3+} + PO_4^{3-} \rightarrow LaPO_4\downarrow \qquad \text{Equation 2.5}$$

Phoslock™ is dispersed granular form with 1 – 3 mm directly on aquatic medium, it stays on bottom near the sediments [36,57].

Baraclear™ is another commercial product based on aluminium-modified smectite, developed to remove dissolved solids and organic mater and ions, such as, fluride, chloride and total P [38]. It has on its composition pH buffer agents and algaecide and is produced in many forms, pellets, briquettes or tablets. P removal occurs by aluminium delivery on target aquatic medium [44].

AlgalBLOCK™ was developed to binds to soluble P, consisting in a special calcium carbonate that forms an insoluble natural mineral, hydroxy-apatite. When it reaches the bottom, it forms a sediment capping to prevent further seasonal P release. Studies performed by Water Studies Centre at Monash University demostrate that 1 kg of AlgalBLOCK are able to remove 50 g of P [44].

Table 2.1 – Resume about principal properties of Plocher, Phoslock, Baraclear and AlgalBLOCK.

| | Advantages | Disadvantages | Mechanism | Cost |
|---|---|---|---|---|
| Plocher [56] | • uses the self-cleaning power of water;<br>• organic compounds are split up in $H_2O$, $CO_2$ and minerals;<br>• supports plant growth to encourage spawning. | • Not available | • Not available | • 2 kg around 90 €<br>(3 to 5 g/m² $H_2O$ surface) |
| Phoslock [36,57] | • application either in granular or slurry;<br>• rapid dispersion even in bed distribution;<br>• not release phosphorus under anoxic conditions. | • partial smothering of benthos;<br>• restriction period for drinking water, irrigation and stock watering;<br>• sediment recovery reduces the efficiency;<br>• slower action and reduce uptake at high pH. | • Lanthanum-phosphate | • 25 kg around 110 € |
| Baraclear [38,44] | • design to surface application without mixing tanks, injections or specialized equipment;<br>• precipitate organic and inorganic materials;<br>• suitable to be use in relatively high-energy flow as canal, ditches or streams. | • partial smothering of benthos;<br>• potential toxicity due to aluminium release. | • Not available (form a complex with aluminium) | • 22 kg around 65 € |
| AlgalBLOCK [44] | • environmental benign, composed by natural compounds;<br>• easy to dispersed;<br>• without presence of artificial/toxic additives. | • partial smothering of benthos. | • precipitation of phosphorus as hydroxyl-apatite. | • Not available |

The target of this thesis was to investigate the removal of phosphate from eutrophic waters using a new approach. Therefore, research on the development of new materials, mainly hybrid nanocomposite was also very important. Some relevant concepts about these new materials will be presented below.

## 2.5 HYBRID NANOCOMPOSITES

Nature combines organic and inorganic components, at the nanoscale, to construct smart materials with remarkable properties and functions (mechanics, density, permeability, colour, hydrophobicity, etc). Crustacean carapaces, mollusc shells, bone and tissues are examples of organic-inorganic natural materials [58]. Oriakhi, in 1998, published a paper entitled "*Nano sandwiches*", writing, "*Nature is a master chemist with incredible talent*" [59]. Hybrid composites are not only a physical mixture of organic and inorganic elements, they are intimately mixed at nanometer level. These materials belong to a new class of composites designated by Theng in 1970 as nanocomposites [58,60]. Hybrid nanocomposites are new materials, which properties are not the sum of the initial components but a result of a synergistic effect between them [59,60]. Examples of man-made hybrid nancomposites can be found in green bodies of china ceramics, blue Maya pigments and some prehistoric frescos. The Maya blue for example, is a man-made hybrid nanocomposite, which combined the resistance of the inorganic clay palygorskite with organic pigment blue indigo [61].

In industrial context, mixing organic and inorganic components started in 1940s in some companies, like, Dupont, Dow Corning, 3M and others. Paints (where inorganic nano-pigments were suspended in organic mixtures), paper (metal oxo-species crosslinking with cellulosic polymers) and coupling agents (silanes, silicones or metallo-organic molecules) are products examples [58,61].

Since the eighties, polymeric nanocomposites have been intensely studied, due to the performance properties improvement observed when a small amount of nano-sized particles was added to a polymer matrix [62,63]. The remarkable changes on physical and mechanical properties are due to the addition of inorganic solid nanoparticles (typically in form of fibres, flakes, spheres or fine particles) with huge surface area, which increases the interaction with the polymer [62]. Moreover, nanocomposites can be produce by similar processes used for conventional polymer composites, which makes them particularly interesting from the production point of view [59]. The hybrid interface plays a central role on the final nanocomposite properties. Based on the interface two distinct categories exist. While *Class I* has only weak bonds (hydrogen, van der Waals or ionic), *Class II* has covalent bonds between organic and inorganic components [59,61,63].

Nowadays, market offers many hybrid materials, with good future perspectives, where new and exigent applications are imposed to achieve great harmony between human activities and environment [58]. Figure 2.11 evidences the increasing impact that hybrid materials research has on academic and industry.

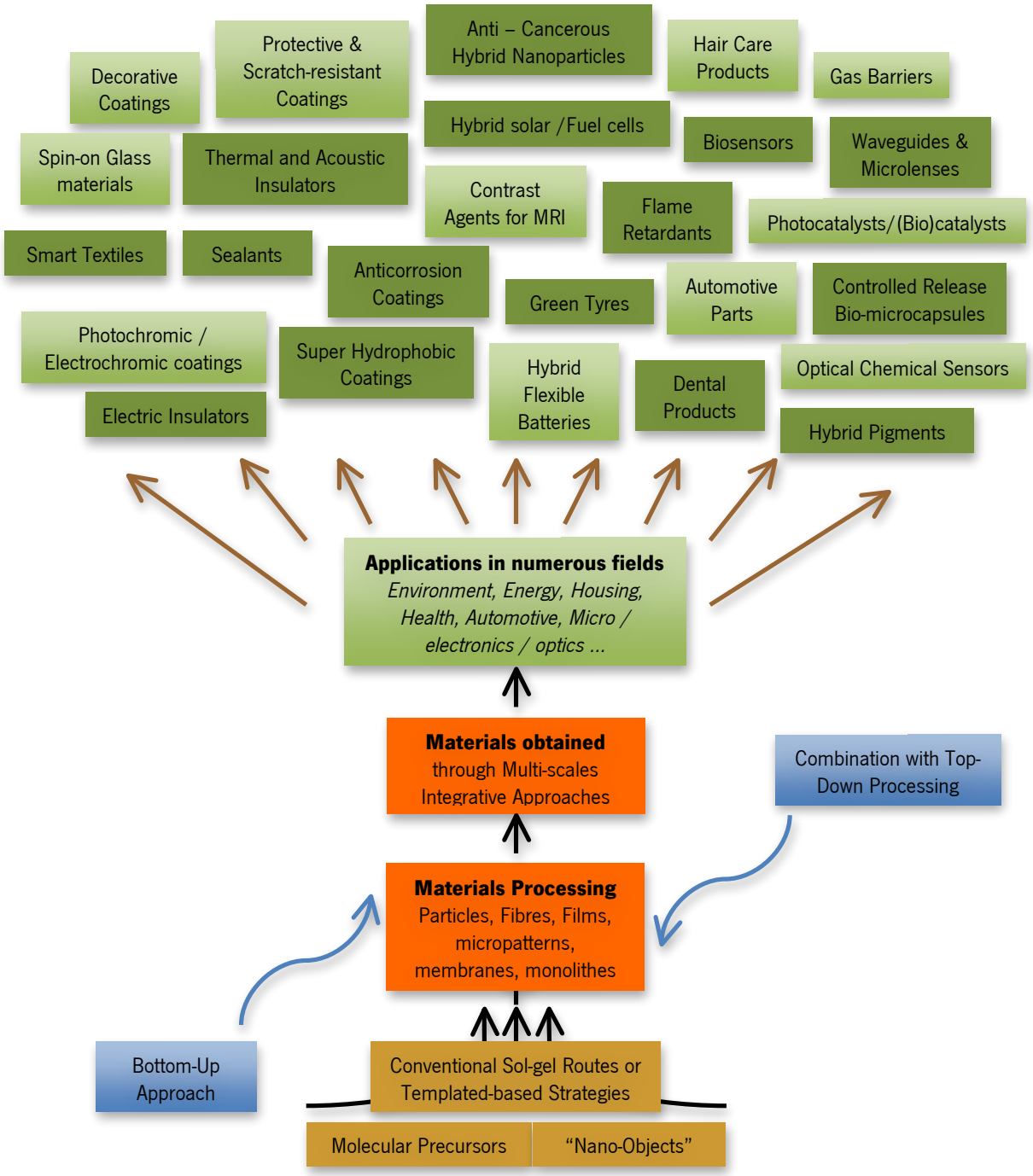


Figure 2.11 – Arborescence representative of hybrid materials on both academic and industrial scenes (from Sanchez and co-workers, 2011 [61]).

Although a lot of research has been performed on the preparation of these materials, homogeneous dispersion of the nanoparticles in polymeric matrices still a difficult task [64]. In most cases the van der Waals attraction between nanoparticles promotes formation of clusters and agglomerates. In addition, hydrophilic nanoparticles and hydrophobic polymers are not compatible, which results in poor interfacial bonding and consequently bad dispersion. Therefore, frequently nanocomposites exhibited worst properties than conventional polymers, which limits their effective application [65-67].

There are three principal methods used to disperse nanoparticles in a polymeric matrix: solution dispersion, melting dispersion and in situ nanoparticles formation by sol–gel process (Figure 2.12). Solution dispersion is a direct route, which is a convenient way to study and understand, at laboratory scale, the interaction between polymer and inorganic nanoparticles. Even though, it is the simplest process, it cannot be used at industrial scale due to solvent elimination. Melt dispersion seems to be the most suitable and environmental friendly method, whereas is solvent free and it is compatible with current industrial process likes extrusion or injection molding. Nevertheless, due to poor compatibility between polymeric matrices and nanoparticles, mainly with nonpolar matrices, agglomerates are often obtained. A way to improve dispersion is by using an in-situ sol-gel method, which is based on a reaction between a precursor and a polymer followed by hydrolysis-condensation of the precursor molecules [62,68,69].

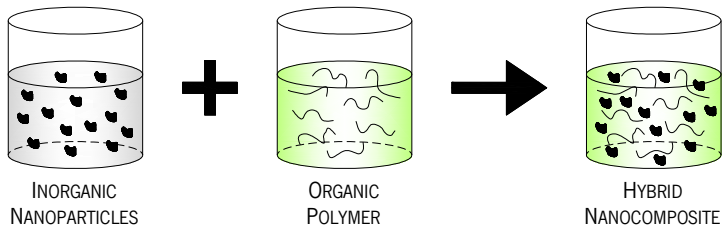


(a)

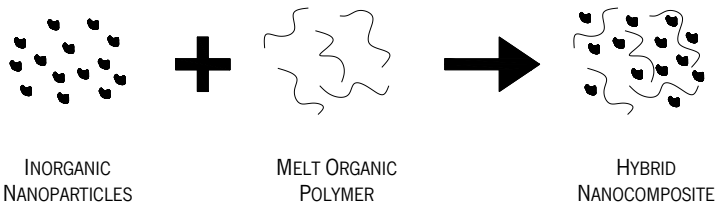


(b)

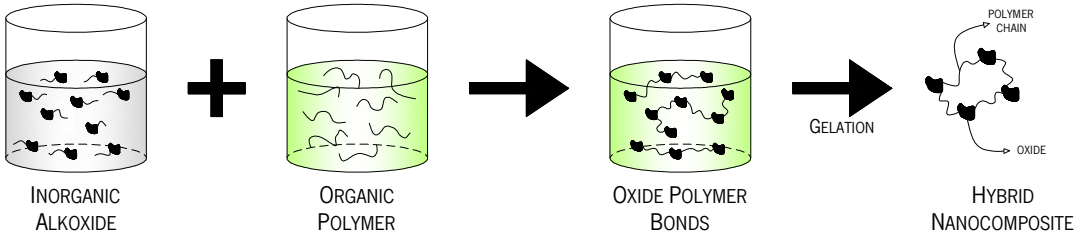


(c)

Figure 2.12 – Methods for nanocomposites preparation a) solution dispersion, b) melt dispersion and c) sol-gel process.

### 2.5.1 OVERVIEW ON SOL-GEL CHEMISTRY

Sol-gel technic is a method that allows engineers and scientists to design a new generation of advanced materials with unique properties [61,70,71]. The inorganic precursor reacts to form a inorganic structure. If well dispersed, small amounts of inorganic filler can improve significantly the material properties, such as gas permeability, flame retardance, mechanical performance or chemical resistance [72].

In the middle of 19th century, Edelman and Graham, studied silica gels and found out that the compound gelled by exposure to atmosphere. Since then sol-gel processing research increased and still very important nowadays [73,74]. The term sol-gel is derived from the two reaction

components, sol and gel. Sol is a colloidal suspension of solid particles in a liquid phase and gel an the interconnected network formed between phases [70,75].

The sol-gel process consists in two main reactions: hydrolysis (Equation 2.6a) and condensation (Equation 2.6b). Being both multi-steps processes, they happened sequentially and in parallel. Hydrolysis is a cleaving of organic chain bonding to metal and subsequent replacement with OH groups through nucleophilic addition. The protonated species leaves the hydrolyzed metal as an alcohol (alcoxolation). Condensation is based on oxygen, metal, oxygen bond formation (-O-M-O-). By definition, condensation reaction released small molecules, such as, water or alcohol [70,75,76].

a) $M(OR)_4 + H_2O \rightarrow HO\text{-}M(OR)_3 + ROH$ Equation 2.6

b) $(OR)_3M\text{-}OH + HO\text{-}M(OR)_3 \rightarrow (OR)_3M\text{-}O\text{-}M(OR)_3 + H_2O$ Equation 2.6

The metal reactivity, amount of water, solvent, temperature and the use of complexing agents or catalysts are the reaction main parameters. The use or not of a catalyst depends on the chemical nature of the metal atom and steric hindrance of the alkoxide group. Regarding to metal atom, electrophilic character and its ability to increase the coordination number, seems to be the main parameters [64,70].

### 2.5.2 SOL-GEL PRECURSORS

Precursors can be either metals alkoxides or inorganic and organic salts. A common example of inorganic salts and inorganic compounds, as precursors for aluminium oxide, are aluminium nitrate ($Al(NO)_3$) and aluminium isopropoxide ($Al(OC_3H_7)_3$), respectively [71,76]. In the present thesis, only metals alkoxides will be discussed, since these are the one that will be used.

In general metal alkoxides are very reactive species due to the presence of highly electronegative OR groups, which stabilize the metal atom in its highest oxidation state and make it susceptible for nucleophilic attack [75]. The extent of sol-gel reaction depends mainly on the steric hindrance of the alkoxide ligand. This group is bonded to the metal by hydrolytacally in a stable way. Metal with alkoxide ligands type $–O\text{-}CH_2\text{-}R$, where R is $n\text{-}C_4H_9$, $i\text{-}C_4H_9$, $n\text{-}C_5H_{11}$, etc., has lower steric hindrance as a result of the molecules symmetry. However, if the alkoxide groups has a OR as

secondary or tertiary, the conversion of the tetrahedral metal atoms to penta or octahedral coordination, results in the formation of less species, like dimers or trimers and consequently lower reactivity [70].

### 2.5.3 ALUMINIUM PRECURSORS

Aluminium is the second must abundant metal in the earth's crust, which belongs to the IIIB section of the periodic table. It has an ionic radius of 0.5 Å and a hydration number of 6. The common mineral source of aluminium is bauxite, which is composed mainly by aluminium hydroxide and oxo-hydroxides. Yolda, in late 1970s, developed the study of aluminium precursors. The two last species (aluminium hydroxide and oxo-hydroxide) have been highly studied as precursors to transition aluminas, catalyst supports and as absorbents. The general formula of aluminium alkoxide precursor is $Al(OR)_3$ where R is $Pr^i$, $Bu^n$, $Bu^s$ are normally used [70,74,75].

### 2.5.4 HYBRID NANOCOMPOSITE CONTAINING ALUMINIUM

In the field of hybrid nanocomposites, Al has been used mainly to improve the fire retardance properties of the polymers and not as metal that is able to give new properties and functionalities to the polymeric material [76]. Therefore, the study of hybrid polymeric nanocomposites has been focus mainly on silica and titanium nanoparticles. Then, this thesis deals with a new type of hybrid polymeric nanocomposites, which contain Al and can have an important positive environmental impact.

## 2.6 BIBLIOGRAPHY

[1] Schröder, J.J. Cordell, D. Smit, A.L. Rosemarin, A. 2009. Sustainable use of phosphorus (report). *EU Tender ENV.B.1/ETU/2009/0025*:1–71.

[2] Cordell, D. Drangert, J. White, S. 2009. The story of phosphorus: global food security and food for thought. *Global Environmental Change* 19(2):292–305.

[3] Smith, V.H. Tilman, G.D. Nekola, J.C. 1999. Eutrophication: impacts of excess nutrient inputs on freshwater, marine and terrestrial ecosystems. *Environmental Pollution* 100(1-3):179–196.

[4] Krasil'nikov, N.A. 1958. Soil microorganisms and higher plants. Published by the Academy of Sciences of the USSR Moscow. Chapter III.

[5] Ashley, K. Cordell, D. Mavinic, D. 2011. A brief history of phosphorus: From the philosopher's stone to nutrient recovery and reuse. *Chemosphere* 84(6):737–746.

[6] Neset, T.S. Bader, H. Scheidegger, R. Lohm, U. 2008. The flow of phosphorus in food production and consumption — Linköping, Sweden, 1870–2000. *Science of Total Environmental* 396(2-3):111–120.

[7] Rittmann, B.E. Mayer, B. Westerhoff, P. Edwards, M. 2011. Capturing the lost phosphorus. *Chemosphere* 84(6):846–853.

[8] Filippelli, G.M. 2002. The global phosphorus cycle. *Reviews in Mineralogy and Geochemistry* 48(1):391–425.

[9] Kitsiou, D. Karydis, M. 2011. Coastal marine eutrophication assessment: A review on data analysis. *Environment International* 37(4):778–801.

[10] Ferreira, J.G. Andersen, J.H. Borja, A. Bricker, S.B. Camp, J. Silva, M.C. Garcés, E. Heiskanen, A.S. Humborg, C. Ignatiades, L. Lancelot, C. Menesguen, A. Tett, P. Hoepffner, N. Claussen, U. 2011. Overview of eutrophication indicators to assess environmental status within the European Marine Strategy Framework Directive. *Estuarine, Costal and Shelf Science* 93(2):117–131.

[11] Dokulil, M.T. Teubner, K. 2011. Eutrophication and climate change: present situation and future scenarios. Ansari, A.A. Gill, S.S. Lanza, G.R. Rast, W. editors. *Etrophication: causes, consequences and control*:1–16.

[12] Yeoman, S. Stephenson, T. Lester, J.N. Perry, R. 1988. The Removal of Phosphorus During Wastewater Treatment: A Review. *Environmental Pollution* 49(3):183–233.

[13] Correll, D.L. 1999. Phosphorus: A Rate Limiting Nutrient in Surface Waters. *Poultry Science* 78(5):674–682.

[14] Skulberg, O.M. Codd, G.A. Carmichael, W.W. 1984. Toxic Blue-Green Algal Blooms in Europe: A Growing Problem. *Ambio* 13(4):244–247.

[15] Carmichael, W.W. 1991. Toxic freshwater blue-green algae (cyano-bacteria): an overlooked health threat. *Health Environment Digest* 5:1–4

[16] Volterra, L. Boualam, M. Ménesguen, A. Duguet, J.P. Duchemin, J. Bonnefoy, X. 2002. Eutrophication and health. Office for Official Publications of the European Communities editor:11–18.

[17] Smol, J.P. 2008. Eutrophication: the environmental consequenes of over-fertilization. Pollution of Lakes and Rivers. Blackwell Publishing editor 2nd ed.:180–228.

[18] Meybeck, M. 1982. Carbon, nitrogen and phosphorus transport by Worl Rivers. *American Journal of Science* 282:401–450.

[19] Meybeck, M. 2003. Global analysis of river systems: from Earth system controls to antropocene syndromes. *Philosophical Transactions Royal Society of London B.1*. 1379:1–21.

[20] Nyenje, P.M. Foppen, J.W. Uhlenbrook, S. Kulabako, R. Muwanga, A. 2010. Eutrophication and nutrient release in urban areas of sub-Saharan Africa — A review. *Science Total Environment* 408(3):447–455.

[21] Lopes, A. Nunes, J. Fialho, R. Castro, A. Orlando, M. Salvado, J. Santos, I. Nunes, J. Leal, M. Medeiros, M. Pacheco, D. Cruz, J. Amorim, M. José, M. Valente, A. 2008. Poluição provocada por nitratos de origem agrícola, *Instituto da Água I.P.* editor:6–7.

[22] EEA (2009) CSI 020 – Nutrients in Freshwater – Assessment published Dec 2010. http://www.eea.europa.eu/data-and-maps/indicators/nutrients-in-freshwater/nutrients-in-freshwater-assessment-published-4, accessed in October 2011.

[23] EEA http://www.eea.europa.eu/data-and-maps/indicators/nutrients-in-transitional-coastal-and/nutrients-in-transitional-coastal-and-3, accessed in October 2011.

[24] Voss, M. Dippner, J.W. Humborg, C. Hürdler, J. Korth, F. Neumann, T. Schernewski, G. Venohr, M. 2011. History and scenarios of future development of Baltic Sea eutrophication. *Estuarine, Coastal and Shelf Science* 92(3):307–322.

[25] OSPAR Commission. 2008. Nutrient Reduction Scenarios for the North Sea. *Eutrophication Series* 9–10.

[26] NASA, GES Distributed Active Center, as processed by SMHI, http://www.smhi.se/weather/baws_ext/info/2005/Baltic_algae_2005_en.htm, accessed in Nuvember 2011.

[27] BBC News – Science and Environment 23 July 2010. www.bbc.co.uk/news/science-environment-10740097, accessed in October 2011.

[28] Paerl, H.W. Xu, H. McCarthy, M.J. Zhu, G. Qin, B. Li, Y. Gardner, W.S. 2011. Controlling harmful cyanobacterial blooms in a hyper-eutrophic lake (Lake Taihu, China): The need for a dual nutrient (N & P) management strategy. *Water Research* 45(5):1973–1983.

[29] Whats on Xiamen 27 Octuber 2007. www.whatsonxiamen.com/news2688.html, accessed in November 2011.

[30] Asimov, I. 1974. Asimov on Chemistry. ISBN 0385041004. *Doubleday & Company*, New York.

[31] EC 1999. Council Directive (99/31/EC) on the landfill of waste. The European Commission Brussels.

[32] Prud'homme, M. 2010b. World Phosphate Rock Flows, Losses and Uses. *International Fertilizer Industry Association*. Phosphates 2010 International Conference, 22–24 March 2010 Brussels.

[33] Heffer, P. Prud'homme, M. 2008. Medium-Term Outlook for Global Fertilizer Demand, Supply and Trade 2008 – 2012. 76th IFA Annual.

[34] Déry, P. Anderson, B. 2007. Peak phosphorus. *Energy Bulletin*. 08/13/2007. Available: energybulletin.net/node/33164.

[35] Morse, G.K. Brett, S.W. Lester, J.N. 1998. Review: Phosphorus removal and recovery technologies. *The Science of Total Environment* 212(1):69–81.

[36] de-Bashan, L.E. Bashan, Y. 2004. Recent advances in removing phosphorus from wastewater and its future use as fertilizer (1997-2003). *Water Research* 38(19):4222–4246.

[37] Yuan, G. Wu, L. 2007. Allophane nanoclay for the removal of phosphorus in water and wastewater. *Science Technology Advance Materials* 8(1-2):60–62.

[38] Landis, C.R. Gray, S.R. 2003. Methods to making water treatment compositions and compositions thereof. *US Application Patent* US2003/0213753 A1.

[39] Hickey, C.W. Gibbs, M. 2009. Lake sediment phosphorus release management – Decision support and risk assessment framework. *New Zealand Journal Marine and Freshwater Research* 43:819–856.

[40] Yeoman, S. Stephenson, T. Lester, J.N. Perry, R. 1988. The removal of phosphorus during wastewater treatment: A review. *Environmental Pollution* 9(3):183–233.

[41] Miller, M.L. Bhadha, J.H. O'Connor, G.A. Jawitz, J.W. Mitchell, J. 2011. Aluminum water treatment residuals as permeable reactive barrier sorbents to reduce phosphorus losses. *Chemosphere* 83(7):978–983.

[42] Conover, B.R. 1991. Method of treating lake water with aluminium hydroxide sulfate. *US Patent* US1991/5039427.

[43] Cooke, G.D. Welch, E.B. Peterson, S.A. Newroth, P.R. 1993. "Lake Protection" in Restoration and management of lakes and reservoirs. *CRC Press LLC*, Boca Raton, Florida:177–230.

[44] Miller, N. 2005. Locally available sorbents materials. *Analytical and Environmental Consultants Report*:1–17.

[45] Clark, T. Stephenson, T. Pearce, P.A. 1997. Phosphorus removal by chemical precipitation in a biological aerated filter. *Water Research* 31(10):2557–2563.

[46] Gulati, D.R. van Donk, E. 2002. Lakes in the Netherlands, their origin, eutrophication and restoration: state-of-the-art review. *Hydrobiologia* 478(1-3):73–106.

[47] Westholm, L. 2006. Substrates for phosphorus removal – Potential benefits for on-site wastewater treatment?. *Water Research* 40(1):23–36.

[48] Drizo, A. Frost, C.A. Grace, J. Smith, K.A. 1999. Physical-chemical screening of phosphate removing substrates for use in constructed wetland systems. *Water Research* 33(17):3595–3602.

[49] Ballantine, D.J. Tanner, C.C. 2010. Substrate and filter materials to enhance phosphorus removal in constructed wetlands treating diffuse farm runoff: a review. *New Zealand Journal of Agricultural Research* 53(1):71–95.

[50] Cui, L. Zhu, X. Ma, M. Ouyang, Y. Dong, M. Zhu, W. Luo, S. 2008. Phosphorus sorption capacities and physicochemical properties of nine substrate materials for constructed wetland. *Archives of Environmental Contamination and Toxicology* 55(2):210–217.

[51] Doyle, J.D. Parsons, S.A. 2002. Struvite formation, control and recovery. *Water Research* 36(16):3925–3940.

[52] Jaffera, Y. Clarkb, T.A. Pearceb, P. Parsons, S.A. 2002. Potential phosphorus recovery by struvite formation. *Water Research* 36(7):1834–1842.

[53] Moermana, W. Carballab, M. Vandekerckhovec, A. Derycked, D. Verstraete, W. 2009. Phosphate removal in agro-industry: Pilot- and full-scale operational considerations of struvite crystallization. *Water Research* 43(7):1887–1892.

[54] Lopes, A. 2009. Estudo do Estado Trófico da Lagoa da Malagueira (Évora) e Proposta de Reabilitação. *Master Thesis*:19–35.

[55] Plocher, Water Presentation 22.11.2010, obtained in www.plocher.de/englisch accessed, in October 2011.

[56] Wallenstein, Report of Lake in Casal de Cambra 2006, obtained in www.wallenstein.pt, accessed in October 2011.

[57] Douglas, G.B. 2002. Remediation material and remediation process for sediments. *US Patent* US2002/635038.

[58] Sanchez, C. Julián, B. Belleville, P. Popall, M. 2005. Applications of hybrid organic–inorganic nanocomposites. *Journal of Materials Chemistry* 15:3559–3592.

[59] Hussain, F. Hojjati, M. Okamoto, M. Gorga, R.E. 2006. Polymer-matrix nanocomposites, processing, manufacturing, and application: an overview. *Journal of Composite Materials* 40(17):1511–1575.

[60] Pomogailo, A.D. 2000. Hybrid polymer-inorganic nanocomposites. *Russian Chemical Reviews* 69(1):53–80.

[61] Sanchez, C. Belleville, P. Popall, M. Nicole, L. 2011. Applications of advanced hybrid organic-inorganic nanomaterials: from laboratory to market. *Chemical Society Reviews* 40(2):696–753.

[62] Dou, Q. Zhu, X. Peter, K. Demco, D.E. Möller, M. Melin, C. 2008. Preparation of polypropylene/silica composites by in-situ sol-gel processing using hyperbranched polyethoxysiloxane. *Journal Sol-Gel Science Technology* 48(1-2):51–60.

[63] Cao, G. 2004. Nanostructures & Nanomaterials. Synthesis, Properties & Applications. *Imperial College Press,* editor:263–266.

[64] Judeinstein, P. Sanchez, C. 1996. Hybrid organic-inorganic materials: a land of multidisciplinarity. *Journal Materials Chemistry* 6(4):511–525.

[65] Xu, C. Ohno, K. Ladmiral, V. Composto, R. 2008. Dispersion of polymer-grafted magnetic nanoparticles in homopolymers and block copolymers. *Polymer* 49(16):3568–3577.

[66] Rong, M.Z. Zhang, M.Q. Zheng, Y.X. Zeng, H.M. Walter, R. Frieddrich, K. 2001. Structure-propertiy relationships of irradiation grafted nano-inorganic particle filled polypropylene composites. *Polymer* 42(1):167–183.

[67] Liua, X. Wu, Q. 2001. PP/clay nanocomposites prepared by grafting-melt intercalation. *Polymer* 42(25):10013–10019.

[68] Bounor-Legaré, V. Angelloz, C. Blanc, P. Cassagnau, P. Michel, A. 2004. A new route for organic-inorganic hybrid material synthesis through reactive processing without solvent. *Polymer* 45(5):1485–1493.

[69] Rong, M.Z. Zhang, M.Q. Pan, S.L. Friedrich K. 2003. Interfacial effects in polypropylene–silica nanocomposites. *Journal of Applied Polymer Science* 92(3):1771–1781.

[70] Maneeratana, V. 2007. Alkoxide based precursors for direct electrospinning of alumina fibers. *PhD Thesis*:25–30.

[71] Wright, J.D. Sommerdijk, N. 2001. Sol-gel materials chemistry and applications. *CRC Press,* editor:1–8.

[72] Sanchez, C. Belleville, P. Popall, M. Nicole, L. 2011. Applications of advanced hybrid organic–inorganic nanomaterials: from laboratory to market. *Chemical Society Review* 40:696–753

[73] Bahloul, W. Bounor-Legaré, V. David, L. Cassagnau, P. 2010. Morphology viscosity of PP/$TiO_2$ nanocomposite prepared by in situ sol-gel method. *Journal Polymer Science, Part B: Polymer Physics* 48(11):1213–1222.

[74] Hench, L. West, J. 1990. The sol-gel process. *Chemical Reviews* 90(1):33–72.

[75] Turova, N. Turevskaya, E. Kessler, V. Yanovskaya, M. 2002. The chemistry of metal alkoxides. *Kluwer Academic Publishers,* Editor:1–6.

[76] Brinker, C. Scherer, G. 1990. Sol-gel science. The physics and chemistry of sol-gel processing. *Academic Press,* editor:1–12.

[77] Zhang, X. Guo, J. Chen, J. Wang, G. Liu, H. 2005. Investigation of interfacial modification for flame retardant ethylene acetate copolymer/alumina trihydrate nanocomposites. *Polymer Degradation and Stability* 87(3):411–418.

CHAPTER

# 3 REMOVAL OF PHOSPHORUS FROM WATER USING ACTIVE BARRIERS: $AL_2O_3$ IMMOBILIZED ON TO POLYOLEFINS

Phosphorus is known to contribute to eutrophication of fresh water systems, as generally it is the limiting nutrient controlling algae growth. Laboratory studies were conducted to develop and test active barriers composed of aluminium oxide immobilized on to polyolefins to remove phosphorus from water. For this purpose, flat plates of polyethylene and polyethylene grafted with maleic anhydride were prepared and tested. The adsorption mechanism of phosphorus on to aluminium oxide was described by the Freundlich isotherm. The optimum pH interval for phosphorus removal was between 5.2 and 7.8, which includes the pH of natural waters. The maximum phosphorus removal capacity was around 11.1 μg/cm$^2$ for both active barriers. Both barriers removed more than 90 % of phosphorus from a 100 μg/L solution in a static batch experiment carried out for 90 d. The *in situ* implementation of the active barriers developed in the present study might be a valuable strategy to sequester phosphate and thus to control eutrophication in natural ecosystems, though further work is required to evaluate possible interferences coming from other substances present in the water.

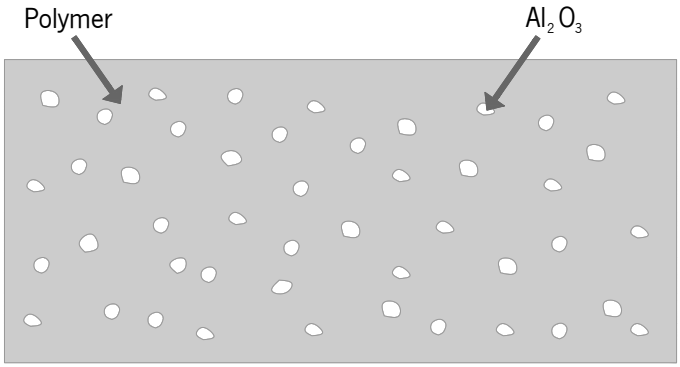


Oliveira, M. Ribeiro, D. Nobrega, J.M. Machado, A.V. Brito, A.G. Nogueira, R. 2011. *Environmental Technology* 32(9):989–995

## 3.1 INTRODUCTION

Phosphorus (P) is an essential nutrient for plant growth and has been intensively used as a fertilizer in agriculture. This practice contributes to the eutrophication of aquatic ecosystems (e.g. lakes, rivers and marshes), causing algal blooms which ultimately lead to oxygen depletion and generally poor water quality [1]. Re-dissolution of phosphate accumulated in sediments, under certain environmental conditions (temperature, redox potential, pH, dissolved oxygen concentration, bacterial activity), might also be responsible for the occurrence of algae blooms, especially when external nutrient sources are controlled [2].

Remediation solutions aimed at decreasing the P content of the water column (P precipitation) and/or delaying P release from sediments have been tested for a long time but with limited success. Chemical precipitation with aluminium, iron and calcium salts added to the water column has several disadvantages, namely it is inadequate to remove low concentrations of P, it contaminates water with high concentrations of sulphate and chloride ions, and generates large quantities of flocs that settle to the sediment at the bottom of aquatic systems [3–5]. Sediment capping also has some drawbacks since it may promote ebullition of sediment gases, bioturbation and wave action [6].

A literature review on materials used for phosphate removal, classified in appropriate groups, is presented in Table 3.1. Calcium compounds, composed largely of calcium carbonate ($CaCO_3$) in the form of calcite, present a phosphate removal capacity that is, in general, lower than those of aluminium and iron compounds. Literature studies reported that carbonate and phosphate ions compete for calcium, which inhibits the precipitation of calcium phosphate [7,8]. Moreover, phosphate removal with calcareous compounds induces an increase in water pH that might not be compatible with life in aquatic systems [9]. Phosphate removal with iron compounds occurs only under aerobic conditions, whereas under anaerobic conditions ferric phosphate compounds dissolve, as a result of the reduction of $Fe^{3+}$ to $Fe^{2+}$, and phosphate is released into the water column [10]. Among the compounds presented in Table 3.1, industrial by-products present the highest removal capacity, which is strongly influenced by their content of metallic oxides such as those of Ca, Mg, Fe and Al [11]. An important disadvantage of these materials is that they can contain heavy metals and thus contaminate the aquatic environment and increase the water pH [12,13]. Clay minerals have a tendency to disperse into very fine particles when applied to the water, which may increase turbidity for long periods. Moreover, the application of dispersible

materials into aquatic systems for phosphate removal is not ideal because the immobilized P remains within the materials and could again be released [14]. Of all the compounds shown in Table 3.1, activated alumina (aluminium oxide activated at 600 °C, $Al_2O_3$) seems to be the most suitable material for removing phosphate from aquatic systems with eutrophication problems. Activated alumina has a very high surface area, is insoluble in water and is selective for P in the presence of chloride and sulphate ions [3,4].

The objective of the present study was to develop and test active barriers composed of aluminium oxide ($Al_2O_3$) immobilized on to polyolefins to remove phosphate from water. The concept of an active barrier, placed *in situ* to sequester phosphate and withdrawn from the system when its phosphate removal capacity is exhausted, is advantageous compared with conventional precipitation methods. This new approach to the eutrophication problem prevents the dispersion of materials into aquatic systems, so avoiding the consequent increase in water turbidity, avoids water contamination with other ions and metals, and eliminates the formation of flocs that settle to the sediment at the bottom of the aquatic system.

Table 3.1 – Literature review on materials used for phosphorus removal (amount of phosphorus removal in g/kg).

| **Aluminium** | **Calcium** | **Iron** | **Industrial by-products** | **Clay** |
|---|---|---|---|---|
| [3]Acti. alumina – 7<br>[7]Shale – 0.73<br>[7]Bauxite – 0.36<br>[15]Zeolite – 2.15 | [16]Wollastonite – 0.85<br>[13]Limestone – 0.68<br>[17]Dolomite – 0.30 | [12]Iron oxide – 12.65<br>[18]Iron coated sands – 1.50<br>[19]Red mud – 0.58 | [11]Steel slags – 18<br>[20]Blast furnace slags – 8.89<br>[20]Coal fly ash – 8.81 | [14]Allophane – $q = 5.620C^{0.264}$<br>[14]Phoslock™ – 11-12<br>[18]Bentonite – $1.5\times10^{4}$ |

## 3.2 MATERIALS AND METHODS

### 3.2.1 MATERIALS AND PREPARATION OF ACTIVE BARRIERS

Polyolefins, namely high density polyethylene and polyethylene modified with 1.9 wt.% maleic anhydride (Total Petrochemicals), further referred in the text as PE and PE-g-MA, respectively, were used to prepare active barriers and functioned as polymeric matrices to support the reactive

material. Aluminium oxide activated at 600 °C ($Al_2O_3$, Sigma Aldrich), provided in pellets of 3 mm, was used as the reactive material to remove phosphate. Potassium dihydrogenophosphate ($KH_2PO_4$, Merck) was used as the P source.

Active barriers were prepared as flat plates (4.0 × 1.0 × 0.2 cm) by compression moulding of 60 g of polymer (PE or PE-g-MA) with 3 g of $Al_2O_3$ (previously crushed and sieved to an effective size in the range of 500 µm to 1000 µm) in a hot plat press (Moore) at 200 °C using a final pressure of 30 t. As a result, $Al_2O_3$ was simply pressed into one the surfaces of the polymeric matrix. The active barrier containing PE as the polymeric matrix was further referred in the text as Al-PE and the one containing PE-g-MA as Al-PE-g-MA.

### 3.2.2 P ADSORPTION ISOTHERM ON GRANULATED ACTIVATED ALUMINIUM OXIDE

The extent of P removal from solution was studied using a batch contacting method. Granulated $Al_2O_3$, previously crushed and sieved to a granular size of 500 µm to 600 µm, was weighed in a range of weights from 10 mg to 500 mg. The weighed solids were contacted with 100 mL solution containing 10 mg/L P in sealed plastic Erlenmeyer flasks clamped into an orbital shaker at 100 rpm and 22 °C during 14 d. Initial and final pH values of the solutions were measured using an ORION pH meter (model 420A). Experiments were carried out in triplicate. At equilibrium, the concentration of P in solution was analyzed by the ascorbic acid colorimetric method using a Shimadzu spectrophotometer [21]. The amount of P adsorbed on $Al_2O_3$ at equilibrium was calculated according to Equation 3.1, where $X$ (g/kg) is the mass of P (g) removed per mass of $Al_2O_3$ (kg), $C_{ini}$ is the initial concentration of P (g/L), $C_{eq}$ is the equilibrium concentration of P (g/L), $V$ is the solution volume (L), and $M$ is the mass of $Al_2O_3$ (kg).

$$X = \left(C_{ini} - C_{eq}\right) \times \frac{V}{M} \qquad \text{Equation 3.1}$$

### 3.2.3 REMOVAL OF P BY ACTIVE BARRIERS

The P saturation potential for Al-PE and Al-PE-g-MA active barriers was assessed using a sequential batch contacting method. Both barriers were contacted with 100 mL solution containing 100 µg/L P at 100 rpm and 22 °C. The solution was replaced weekly until no

changes in the concentration of P could be detected. The experiment was done during 14 weeks in triplicate. The concentration of P was measured both before and after the replacement step.

To simulate P removal in a natural water body characterised by a long hydraulic retention time, as for example a lake, an experiment was carried out in batch for 90 d under static conditions. Both Al-PE and Al-PE-g-MA active barriers were placed in 100 mL solution containing 100 µg/L P in sealed plastic beakers. Experiments were carried out in triplicate. Samples were collected regularly for P concentration analyses. The amount of P removed at equilibrium was calculated according to Equation 3.1, described above, with the exception that *M* was replaced by *A*, the area of the polymeric plate ($cm^2$).

### 3.2.4 EFFECT OF PH ON P REMOVAL

The zero point charge is usually defined as the pH value at which a solid submerged in an electrolyte exhibits zero net electrical charge on the surface. To determine the zero point charge pH ($pH_{zpc}$) of $Al_2O_3$, 0.1 g of the solid was placed in 50 mL of 0.1 M NaCl solution (used as an inert electrolyte) with initial pH in a range of 2 to 12. The pH was adjusted by either addition of chloridric acid or sodium hydroxide. The experiment took place in sealed plastic Erlenmeyer flasks clamped into an orbital shaker at 100 rpm and 22 °C. Chemical equilibrium was attained after 24 h and the pH was measured. Experiments were carried out in triplicate.

The effect of pH on P removal by Al-PE and Al-PE-g-MA active barrier was studied in batch. The barriers were contacted with 100 mL solution containing 100 µg/L P with initial pH in a range of 2 to 9, at 100 rpm and 22 °C for 7 d. Experiments were done in triplicate. The concentration of P was measured in the beginning and at the end of the experiment.

## 3.3 RESULTS AND DISCUSSION

The literature review on materials used for phosphate removal presented in Table 3.1 suggested that activated aluminium oxide might be one of the most suitable materials to be used in the remediation of aquatic systems with eutrophication problems because it has a high removal capacity and is insoluble in water. Therefore, in this study active barriers composed of aluminium

oxide immobilized onto polyolefins (PE and PE-g-MA) were develop and tested to remove phosphate from water. Specifically, the mechanism of P removal, the maximum P removal capacity of active barriers, and the effect of pH on P removal were assessed. It was also investigated long term P removal under static conditions simulating a natural system.

### 3.3.1 P ADSORPTION BY GRANULATED ACTIVATED ALUMINIUM OXIDE

The adsorption isotherm of P onto aluminium oxide was determined to assess the adsorption mechanism. The results were fitted by the Freundlich model (Figure 3.1 and Equation 3.2) with a correlation coefficient of 0.9

$$S = 5.1 \times [C]^{0.46} \qquad \text{Equation 3.2}$$

where *S* is the amount of P adsorbed (g/kg), *C* the equilibrium concentration (mg/L), K=5.1 $mg^{1-n}.g^{-1}.L^{n}$ and 1/n=0.46. These results suggested that the adsorption of P onto $Al_2O_3$ followed a multilayer mechanism. Similar results were reported in literature for the adsorption of P onto aluminium oxide hydroxide [22].

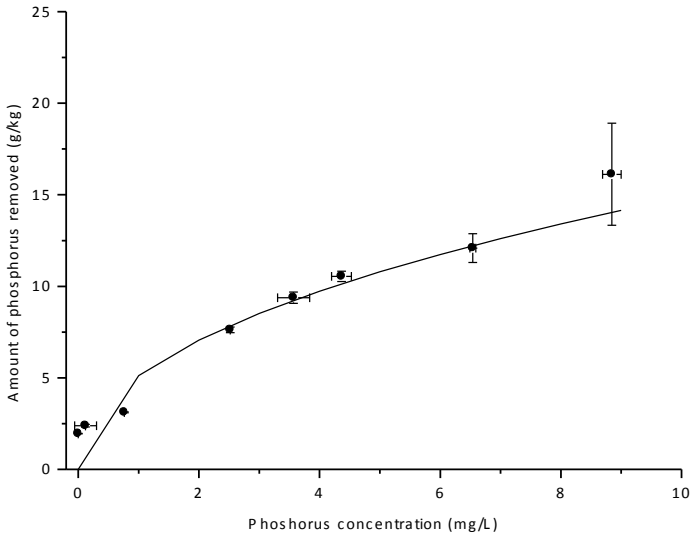


Figure 3.1 – Phosphorus adsorption isotherm onto granulated $Al_2O_3$. The experiment was conducted 22 ± 1 °C for 14 d at 100 rpm.

### 3.3.2 REMOVAL OF P BY ACTIVE BARRIERS

The maximum P removal of both Al-PE and Al-PE-g-MA active barriers was 11.1 ± 0.3 μg/cm² P from the 35 μg/cm² P theoretically available (100 μg/L × 0.1 L × 14 weeks / 4 cm²). Although Al-PE and Al-PE-g-MA active barriers removed almost the same amount of P, the initial removal rate of Al-PE-g-MA was higher than that of Al-PE, as depicted in Figure 3.2. The geometric surface area of the aluminium oxide layer deposited on top of PE and PE-g-MA matrices was used in the calculation of the maximum P removal instead of the available surface area. Experimentally determination of the available surface area might have improved the accuracy of results obtained since aluminium oxide distribution might have not been homogenous. It is also not straightforward to compare the maximum P removal obtained in this study with those reported in literature (Table 3.1) because previously explored strategies used granular adsorbing materials and consequently removal is listed per mass of material. Considering that the calculated amount of activated aluminium oxide in the adsorbing layer is 13.9 mg/cm² the maximum P removal per mass of aluminium oxide would be around 1 g/kg. This value is lower than others obtained with granulated aluminium oxide (Table 3.1 and this study) and the possible explanation is that the removal of P onto active barriers is limited by the surface area.

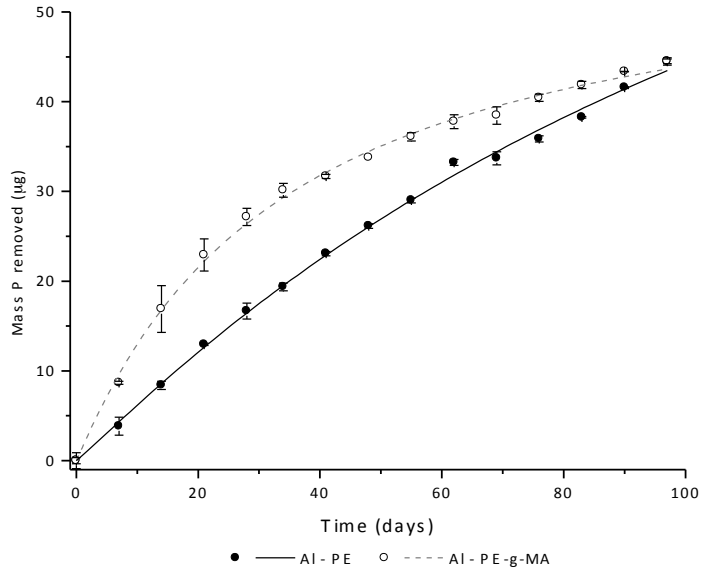


Figure 3.2 – Cumulative phosphorus adsorption onto Al-PE and Al-PE-g-MA activated barriers. Experiments were conducted 22 ± 1 °C for 14 weeks at 100 rpm.

Long-term batch experiments (90 d) were carried out using the maximum concentration of P expected in natural waters, 100 μg/L, under static conditions. The experimental results showed that the concentration of P decreased faster in the first 30 d in the presence of Al-PE-g-MA than in the presence of Al-PE (Figure 3.3). The amount of P removed was 2.3±0.1 μg/cm$^2$ for Al-PE and 2.5±0.1 μg/cm$^2$ for Al-PE-g-MA, and the concentration of P at equilibrium for both barriers was lower than 10 μg/L.

Although the Al-PE-g-MA active barrier had a higher affinity to phosphate than the Al-PE, corresponding to a higher initial rate of phosphate removal, the presence of maleic anhydride in the polymer matrix did not contribute in a long term experiment to a superior removal of P from solution. Because the extent of P removal was smaller than the maximal possible one, these results suggested that the amount of P used in this experiment was the limiting factor and not the available surface area. Considering that the minimum P concentration needed to attain an algae bloom in a lake is about 20 μg/L at the hipolimnium [1], the active barriers prepared in the present study can reduce the P concentration in water to values lower than 10 μg/L, the critical value for the algae growth, at a pH compatible to those found in natural ecosystems.

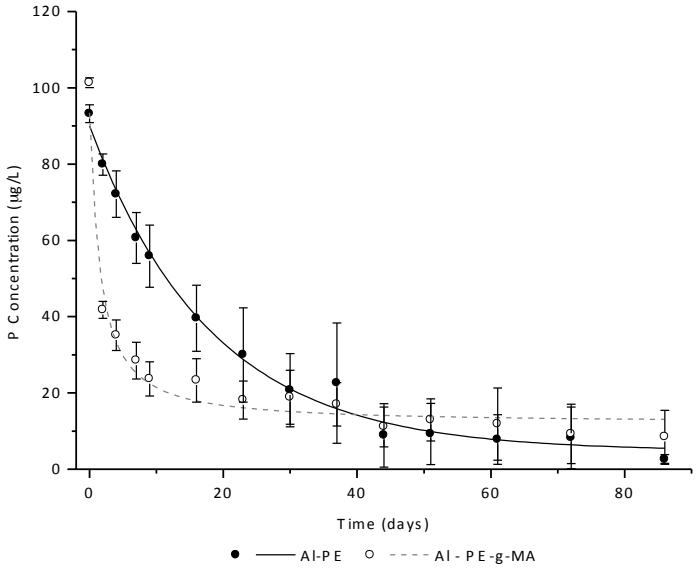


Figure 3.3 – Phosphorus concentration profiles along time. Experiments were conducted at 22 ± 1 °C for 90 d under static conditions.

### 3.3.3 EFFECT OF PH ON P REMOVAL

Point zero charge ($pH_{ZPC}$) is an important parameter to understand the surface chemistry of a material in aqueous solution and is defined as the pH value where net surface charge of particles is zero. As depicted in Figure 3.4, the $pH_{ZPC}$ determined for aluminium oxide was around 8.0 which is consistent with literature values [23]. Below the $pH_{ZPC}$, the acidic water donates more protons than hydroxide groups, and so the aluminium oxide surface is positively charged (attracting anions). On the contrary, above $pH_{ZPC}$ the aluminium oxide is negatively charged (attracting cations).

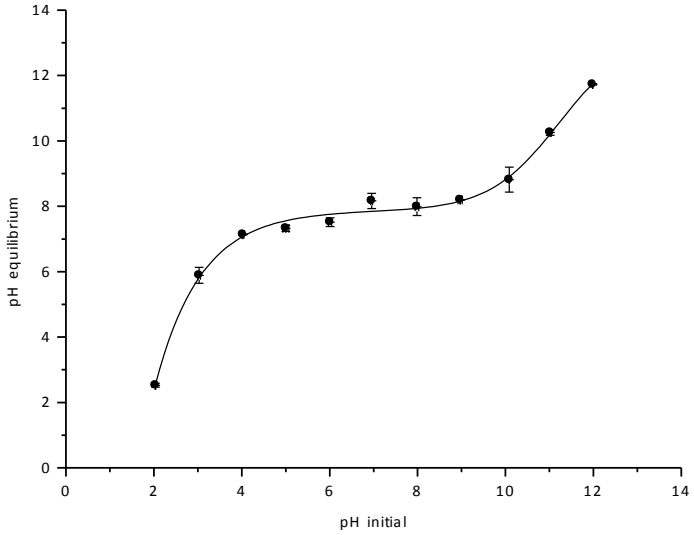


Figure 3.4 – Point of zero charge for activated aluminium oxide.

The influence of pH in the extent of P removal onto Al-PE-g-MA is depicted in Figure 3.5. Al-PE-g-MA was used in this experiment because it presented a faster initial kinetics of P removal than Al-PE. The results suggested that the amount of P removed by Al-PE-g-MA increased with pH in the range of 2.4 to 5.2. The removal of P was maximum in the pH interval between 5.2 and 7.8, decreasing abruptly for a pH value higher than 7.8. This behaviour can be explained by the different phosphate species present in solution at different pH values (Figure 3.6), which will affect the electrostatic interactions with aluminium oxide particles and consequently P removal.

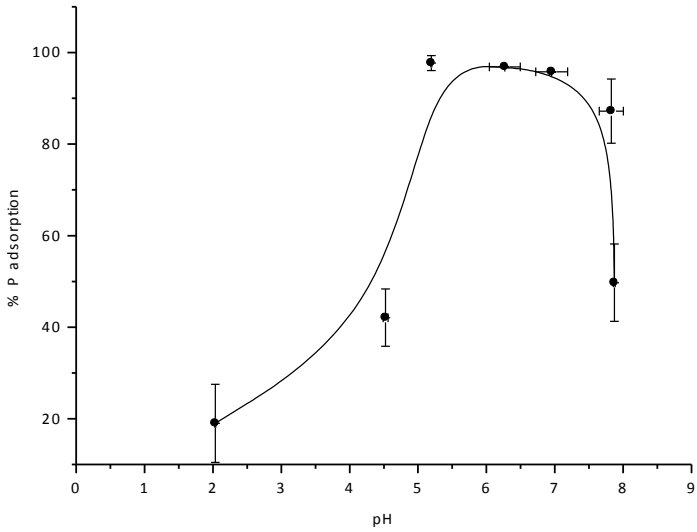


Figure 3.5 – Influence of pH on the amount of phosphorus removed by Al-PE-g-MA.

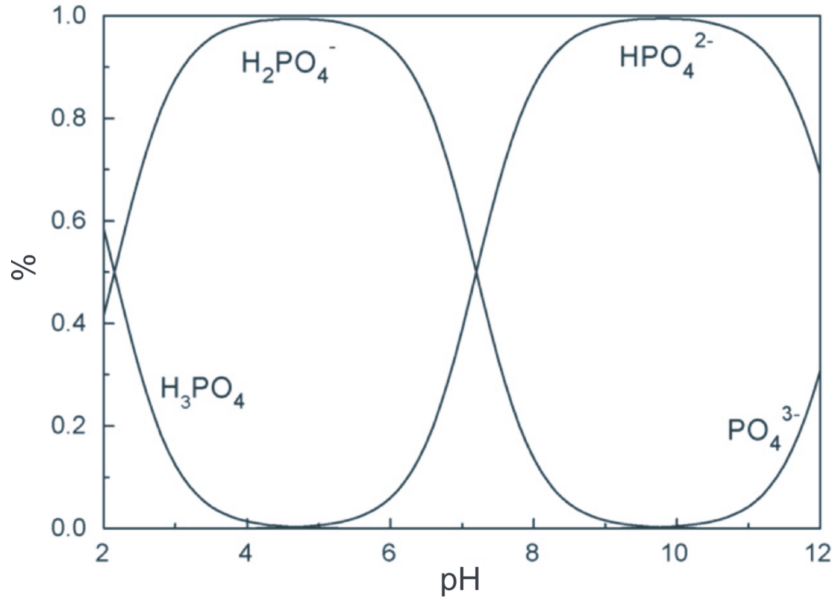


Figure 3.6 – Speciation of phosphoric acid at low ionic strength from Xiaofang et al., 2007 [24].

The maximum phosphate removal occurred for the ion pair $HPO_4^{2-}/H_2PO_4^-$ (pKa=7.21) and is the result of a strong electrostatic interaction of these two species with positive charges present on the aluminium oxide surface. As the pH decreases, the predominant species are $H_2PO_4^-/H_3PO_4$ (pKa=2.12) resulting in less P ions available to interact with the aluminium oxide. The decrease in phosphate removal at pH higher than 7.8 is probably due to the accumulation of a net negative charge on the aluminium oxide surface (most Al oxides have zero point of charge around pH 7 or 8). A limited number of studies investigated the effect of pH on phosphate removal by reactive materials. As examples, Tanada et al. (2003) reported a maximum phosphate removal

at pH 4 using aluminium oxide hydroxide [22]. Huang et al. (2008) and Zeng et al. (2004) reported that red mud and iron oxide tailings presented a maximum phosphate removal at pH 2.0 and 3.2, respectively [12,19]. The reactive barrier developed in the present work, Al-PE-g-MA, is very compatible to an application *in situ* because its maximum phosphate removal capacity occurs in a range of pH values that encompasses the ones characteristic of aquatic ecosystems, as opposed to the studies above mentioned.

Compared to accepted or previously explored strategies to sequester phosphorus and thus to control eutrophication in natural ecosystems, this new approach prevents the dispersion of materials into aquatic systems with the consequent increase of water turbidity, avoids water contamination with other ions and metals, and eliminates the formation of flocks that settle to the sediment at the bottom of the aquatic system. Further work is required to evaluate possible interferences coming from other substances present in the water before the *in situ* implementation of the active barriers developed in the present study

## 3.4 CONCLUSIONS

The present study suggested that active barriers composed of aluminium oxide immobilized onto polyolefins are an attractive alternative technology to remove P from water. The removal of P from aqueous solutions by aluminium oxide was described by a Freundlich adsorption isotherm. The maximum P removal capacity of active barriers was 11.1 μg/cm$^2$. The extent of P removal depended on pH and the best results were obtained at a pH interval from 5 and 8. A considerable decrease in the concentration of P, from 100 μg/L to 10 μg/L (90 % of removal), was achieved in long term experiments under static conditions simulating a natural system (e.g. lake). The major advantages of active barriers proposed in the present study to remove P from natural ecosystems compared to previously explored strategies are that they prevent the dispersion of materials with the consequent increase of water turbidity, avoid water contamination with other ions and metals, and eliminate the formation sediments.

## 3.5 BIBLIOGRAPHY

[1] Martins, G. Ribeiro, D. Pacheco, D. Cruz, J.V. Cunha, R. Gonçalves, V. Nogueira, R. Brito, A.G. 2008. Prospective scenarios for water quality and ecological status in Lake Sete Cidades (Portugal): the integration of mathematical modelling in decision processes. *Applied Geochemistry* 23(8):2171–2181.

[2] Ribeiro, D. Martins, G. Nogueira, R. Cruz, J.V. Brito, A.G. 2008. Phosphorus Fractionation in lake volcanic sediments (Azores – Portugal). *Chemosphere* 70(7):1256–1263.

[3] Hano, T. Takanashi, H. Hirata, M. Urano, K. Eto, S. 1997. Removal of phosphorus from wastewater by activated alumina adsorbent. *Water Science Technology* 35(7):39–46.

[4] Donnert, D. Salecker, M. 1999. Elimination of phosphorus from municipal and industrial waste water. *Water Science Technology* 40(4-5):195–202.

[5] Shin, E.W. Han, J.S. 2004. Phosphate adsorption on aluminium-impregnated mesoporous silicates: surface structure and behaviour of adsorbents. *Environmental Science Technology* 38(3):912–917.

[6] Thibodeaux, L.J. Bierman, V.J. 2003. The bioturbation-driven chemical release process. *Environmental Science Technology* 37(13):252A–258A.

[7] Drizo, A. Frost, C.A. Grace, J. Smith, K.A. 1999. Physical-chemical screening of phosphate removing substrates for use in constructed wetland systems. *Water Research* 33(17):3595–3602.

[8] Miller, N. 2005. Locally available adsorbing materials, sediment sealing and flocculants for chemical remediation of lake and stream. *Analytical and Environmental Consultants Report*:15–32.

[9] Westholm, L.J. 2006. Substrates for phosphorus removal – Potential benefits for on-site wastewater treatment. *Water Research* 40(1):23–36.

[10] Ann, Y. Reddy, K.R. Delfino, J.J. 2000. Influence of chemical amendments on phosphorus immobilization in soils from a constructed wetland. *Ecological Engineering* 14(1-2):157–167.

[11] Zhang, H.C. Cao, Z.H. Shen, Q.R. Wong, M.H. 2003. Effect of phosphate fertilizer application on phosphorus (P) losses from soil in Taihu Lake Region. I. Effect of phosphate fertilizer rate on P losses from paddy soil. *Chemosphere* 50(6):695–701.

[12] Zeng, L. Li, X. Liu, J. 2004. Adsorptive removal of phosphate from aqueous solutions using iron oxide tailings. *Water Research* 38(5):1318–1326.

[13] Boujelben, N. Bouzid, J. Elouear, Z. Feki, M. Jamoussi, F. Montiel, A. 2008. Phosphorus removal from aqueous solution using iron coated natural and engineered sorbents. *Journal Hazardous Materials* 151(1):103–110.

[14] Yuan, G. Wu, L. 2007. Allophane nanoclay for the removal of phosphorus in water and wastewater. *Science Technology Advanced Materials* 8(1-2):60–62.

[15] Sakadevan, K. Bavor, H.J. 1998. Phosphate adsorption characteristics of soils, slags and zeolite to be used as substrate in constructed wetland systems. *Water Research* 32(2):393–399.

[16] Hedström, A. 2006. Reactive filter materials for ammonium and phosphorus sorption in small scale wastewater treatment. PhD disses, Luleå University of Technology:12–31.

[17] Pant, K. Reddy, K.R. Lemon, E. 2001. Phosphorus retention capacity of root bed media of sub-surface flow constructed wetlands. *Ecological Engineering* 17(4):345–355.

[18] Pradas, E.G. Sanches, M.V. Campo, A.G. 1992. Effects of experimental variables on phosphate adsorption on bentonite. *Journal Chemical Technology Biotechnology* 54(3):291–295.

[19] Huang, W. Wang, S. Zhu, Z. Yao, L.X. Rudolph, V. Haghseresht, F. 2008. Phosphate removal from wastewater using red mud. *Journal Hazardous Materials* 158(1):35–42.

[20] Xu, D. Xu, J. Wu, J. Muhammad, A. 2006. Studies on the phosphorus sorption capacity of substrates used in constructed wetland systems. *Chemosphere* 63(2):344–352.

[21] Eaton, A.D. Clesceri, L.S. Greenberg, A.E. 1995. *Standard Methods for the Examination of Water and Wastewater*, 19th ed, American Public Health Association, Washington DC, 4-113–4-114.

[22] Tanada, S. Kabayama, M. Kawasaki, N. Sakiyama, T. Nakamura, T. Araki, M. Tamura, T. 2003. Removal of phosphate by aluminum oxide hydroxide. *Journal Colloid Interface Science* 257(1):135–140.

[23] Stack, A.G. Higgins, S.R. Eggleston, C.M. 2001. Point of zero charge of a corundum-water interface probed with optical second harmonic generation (SHG) and atomic force microscopy (AFM): New approaches to oxide surface charge. *Geochimica et Cosmochimica Acta* 65(18):3055–3063.

[24] Xiaofang, Y. Dongsheng, W. Zhongxi, S. Hongxiao, T. 2007. Adsorption of phosphate at the aluminium (hydr)oxides interface: Role of the surface acid-base properties. *Colloids and Surface A* 297(1-3):84–90.

CHAPTER

# 4 SYNTHESIS OF ALUMINIUM NANOPARTICLES IN A PP MATRIX DURING MELT PROCESSING: EFFECT OF THE ALKOXIDE ORGANIC CHAIN

The synthesis of aluminium nanoparticles in a polypropylene (PP) matrix by a sol-gel process in the melt was investigated. The study was performed using two aluminium precursors, aluminium isopropoxide and aluminium acetylacetonate, to assess the effect of the stereochemical hindrance of the precursor organic groups on reactivity. The hybrid nanocomposites were prepared in a batch mixer under constant processing conditions and characterized by several techniques. Chemical and morphological characterization proved that aluminium formed covalent bonds with polypropylene modified with maleic anhydride and the presence of aluminium nanoparticles. Moreover, TEM micrographs of both nanocomposites synthesised revealed a lower amount of nanoparticles when aluminium acetylacetonate was used. The values of the activation energy determined explained the higher reactivity of aluminium isopropoxide. The reaction mechanisms were proposed for both precursors.

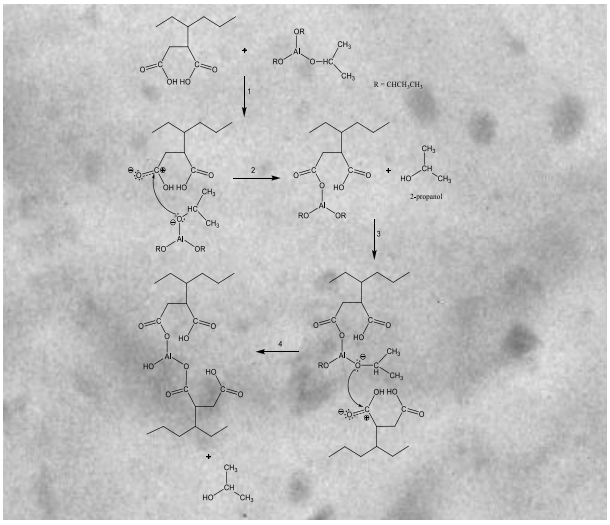

Oliveira, M. Nogueira, R. Machado, A.V. 2012. Synthesis of aluminium nanoparticles in a PP matrix during melt processing: effect of the alkoxide organic chain. *Reactive & Functional Polymers, DOI: 10.1007/s11270-012-1239-9*

## 4.1 INTRODUCTION

Polymer nanocomposites are a new class of materials, in which at least one of the components has dimensions at the nanometric scale. These materials have drawn considerable attention, in recent years, due to the significant improvements in several properties, such as, thermal stability, flame retardancy, dielectrical properties, heat distortion temperature, barrier properties and thermal expansion coefficient [1-4]. This remarkable change of the physical and mechanical macroscopic properties can be achieved by the addition of inorganic solid nanoparticles (typically in form of fibres, flakes, spheres or fine particles) with huge surface area, which increases the interaction with the polymer.

Even though a lot of research has been done on the preparation of these materials [3-5], the homogeneous dispersion of the nanoparticles in polymeric matrices, especially in non-polar, still a difficult task. In most cases the van der Waals attraction between nanoparticles promotes the formation of clusters and agglomerates. In addition, hydrophilic nanoparticles and hydrophobic polymers are not compatible in nature, which results in poor interfacial bonding and therefore bad dispersion. Thus, frequently nanocomposites exhibited worst properties than conventional polymers, which limits their effective application [6-8]. Therefore, further research is necessary to improve nanoparticles/polymer interaction and to develop materials with higher performance.

Three principal approaches have been used to disperse nanoparticles in a polymeric matrix: solution dispersion, melting dispersion and in situ nanoparticles formation by a sol–gel process. Solution dispersion is a direct route, which is a convenient way to study and understand, at laboratory scale, the interaction between polymer and inorganic nanoparticles. Even though, it is a simple process, it can not be used at industrial scale due to solvent elimination. Melt dispersion seems to be the most suitable and environmental friendly, as well as is solvent free method and it is compatible with current industrial process likes extrusion or injection moulding. Nevertheless, due to poor compatibility between polymeric matrices and nanoparticles, mainly with non-polar matrices, agglomerates are often obtained. A way to improve the dispersion is by using an in situ sol-gel method, which is based on a reaction between a precursor, containing the inorganic particle, and a polymer, followed by hydrolysis-condensation reaction. In classic sol-gel reaction, hydrolysis-condensation step is performed under acid or basic conditions in solution, which is not appropriated for industrial processes [2,9,10]. Consequently, the use of this type of reactions in the melt became a challenge.

The use of a sol-gel method to prepare nanocomposites of polypropylene (PP) and metal oxides is described in the literature for a few systems [2,11,12]. The most common system studied is PP/silica nanocomposite using different silica precursors [13-16]. For example, Dou et al. prepared a PP/silica nanocomposite by solvent free sol-gel reaction, using a pre-prepared polymer, hyperbranched polyethoxysilane (PEOS) [2]. More recently, Bahloul and co-workers developed PP/$TiO_2$ nanocomposites by reactive extrusion, where titanium n-butoxide ($Ti(OR)_4$) was used as precursor [17].

Therefore, the present work aims to prepare well dispersed aluminium nanoparticles in a PP matrix using a sol-gel process in the melt. Since PP does not have reactive groups to form covalent bonds with the precursor, PP modified with maleic anhydride (PP-g-MA) was used. Moreover, two precursors with different organic chain, aluminium isopropoxide ($Al(Pr\text{-}i\text{-}O)_3$) and aluminium acetylacetonate ($Al(acac)_3$), were selected to investigate the effect of the precursor organic chain in the sol-gel reaction. The hybrid nanocomposites were prepared in a batch mixer and were characterized using several analytical techniques.

## 4.2 MATERIALS AND METHODS

### 4.2.1 MATERIALS

Polypropylene modified with maleic anhydride (PP-g-MA, Polybond 3200) with a melting temperature around 160 °C and a MA content of 1 wt.%, was supplied by Crompton. Aluminium isopropoxide ($Al(Pr\text{-}i\text{-}O)_3$) and aluminium acetylacetonate ($Al(acac)_3$), both in powder state, were used as received and were supplied by Sigma Aldrich and Acros Organics, respectively.

### 4.2.2 SYNTHESIS

PP containing aluminium nanoparticles was prepared in the melt, in a Haake batch mixer (Rheocord 90; volume 60 mL), equipped with two rotors running in a counter-rotating way. The rotor speed was 50 rpm and the set temperature was 180 °C. The following procedure was adopted to prepare the nanocomposites, first pellets of PP-g-MA were introduced into the hot mixer, after melting, the aluminium precursor was added in a ratio 1:1 (maleic

anhydride/precursor). The total sample was removed after 10 minutes mixing. The hybrid polymer nanocomposite (HPN) synthesized with $Al(Pr\text{-}i\text{-}O)_3$ was called *HPN-Pr* and the HPN synthesized with $Al(acac)_3$ was called *HPN-acac*.

Sheets of 1 mm thickness were prepared by compression moulding from the sample collected from the mixer. These sheets were placed in an acidic solution (HCl 1M) and the hydrolysis-condensation reaction was carried out at 80 °C according to the Sioplast process [9].

### 4.2.3 STRUCTURAL CHARACTERIZATION

#### *4.2.3.1 FT-IR*

Infrared spectra of all HPNs were recorded in transmission mode between 400 $cm^{-1}$ and 4000 $cm^{-1}$ using a Perkin Elmer 1610, with 32 scans and resolution of 4 $cm^{-1}$. Thin films were previously prepared by compression moulding in a hot press at 180 °C and analyzed directly using a solid film support.

#### *4.2.3.2 XRD*

X-ray diffraction (XRD) spectra of the samples were obtained at room temperature using a Bruker D8 Discover X-ray equipment with Ni-filter. The applied current and accelerating voltage were 40 mA and 40 kV, respectively.

#### *4.2.3.3 XPS*

X-ray photoelectron spectroscopy (XPS) was performed using a Thermo Scientific K-Alpha ESCA instrument equipped with aluminium $K_\alpha 1.2$ monochromatized radiation at 1486.6 eV X-ray source. Due to the insulating nature of the samples it was necessary to use an electron flood gun in order to minimize surface charging. Neutralization of the surface charge was achieved using both a low energy flood gun, in the range of 0 to 14 eV, and a low energy Argon ions gun. The XPS measurements were carried out using monochromatic Al-K$\alpha$ radiation ($h\upsilon$ = 1486.6 eV). Photoelectrons were collected from a 90° take-off angle relative to the sample surface. The measurement was done in the Constant Analyzer Energy mode (CAE) with 100 eV pass energy

for survey spectra and 20 eV pass energy for high-resolution spectra. Charge reference was done by setting the lower binding energy C1s peak at 285.0 eV for the C1s hydrocarbon peak.

#### *4.2.3.4 SEM and EDS*

Scanning electron microscopy (SEM) analysis was performed in a Leica Cambridge S360 microscope. The samples were previously fractured in liquid nitrogen and coated with a gold thin film. X-ray microanalysis mapping was performed with an energy dispersive X-ray Spectrometer (EDS) from Link eXL II from Oxford Instruments attached to the SEM.

#### *4.2.3.5 TEM*

Samples of 100 nm thickness were cut using a diamond knife, in a Leica ultramicrotome at -40 °C. The cut sections were transferred onto copper grids and then analysed in a Philips CM120 transmission electron microscope (TEM).

#### *4.2.3.6 Rheological properties*

The rheological behaviour of the initial polymer and prepared HPNs was determined by oscillatory rheological measurements carried out in a Paar Physica MCR300 rheometer at 180 °C. The gap and diameter of the plates was 1 mm and 25 mm, respectively. A frequency sweep from 0.1 Hz to 100 Hz under constant strain in the linear viscoelastic region was performed for each sample. Nitrogen atmosphere was used to prevent thermo-oxidative degradation.

#### *4.2.3.7 Gel content*

Around 150 mg of the HPNs were used to determine the gel content. HPNs previously weight were place in a 125-mesh stainless steel basket. All cages were weight and then immersed in hot xylene at 140 °C until weigh equilibrium. The final weight was determined after drying the samples in a vacuum oven at 105 °C during the night. The gel content was calculated as the

weight of non-extractable material divided by the total weight of the original sample and was expressed as the percentage.

#### *4.2.3.8 TGA and DSC*

Thermogravimetric measurements for all HPNs were carried out using a TA Q500 termobalance. Samples were heated from 30 °C to 600 °C at 10 °C/min under a nitrogen flow (50 mL/min).

Thermal properties of HPNs were measured using a Perkin Elmer Diamond DSC 131 apparatus, equipped with an LNCS (Liquid Nitrogen Cooling System) accessory. Samples (about 10 mg) are placed in Al pans and heated at 10 °C/min from 30 °C to 220 °C under nitrogen flow. The crystallinity degree ($X_c$) was calculated by the ratio of $\Delta H_f$ (the apparent melt enthalpy calculated from DSC curves as the melting enthalpy per gram) of the component and $\Delta H_f^i$ (the theoretically melt enthalpy component in its completely crystalline state).

#### *4.2.3.9 Activation energy*

The activation energy ($E_a$) of the HPNs synthesized using the two inorganic precursors was determined using gel content values. For each precursor the HPNs were prepared at three different temperatures (170, 180 and 200 °C) according to the procedure described above and samples were collected after 0.5, 2 and 5 min of mixing. For all the samples, the gel content was measured as according to the method described previously. For each temperature, the crosslinking rate was determined as the slope of gel content vs time reaction, as described by Shieh [18]. Then, the $E_a$ was calculated from the plot of the crosslinking reaction rate at the three different temperatures as a function of the reciprocal absolute temperature, according to the Arrehenius equation:

$$\ln(k) = \ln A - \frac{E_a}{R}\frac{1}{T} \qquad \text{Equation 4.1}$$

where $k$ is the crosslinking rate, $E_a$ is the activation energy, $R$ is the gas constant, and $T$ is the absolute temperature.

## 4.3 RESULTS AND DISCUSSION

### 4.3.1 STRUCTURAL CHARACTERIZATION

The FT-IR spectra of PP-g-MA, HPN-Pr and HPN-acac are presented in Figure 4.1. Analysing the FT-IR spectra, there are two spectral ranges that are important to take into consideration, one between 3000 – 3500 $cm^{-1}$ and the other 400 – 1000 $cm^{-1}$, where the OH and Al-O stretching modes occur, respectively. In HPN-Pr spectrum, depicted in Figure 4.1a, a very board band appears around 3450 $cm^{-1}$, this band corresponds to the stretching mode of Al-OH, which is confirmed by the respective bending mode band at 1627 $cm^{-1}$ with medium intensity.

In the HPNs structure, aluminium can exist in two different coordination states, octahedral and tetrahedral [19, 20]. While a broad band of stretching mode between 500 – 750 $cm^{-1}$ confirms the tetrahedral coordination, the stretching mode band in the region of 640 – 500 $cm^{-1}$ evidences the octahedral coordination. However, giving the broad bands in the HPN-Pr spectrum, the tetrahedral Al-O coordination seems to prevail.

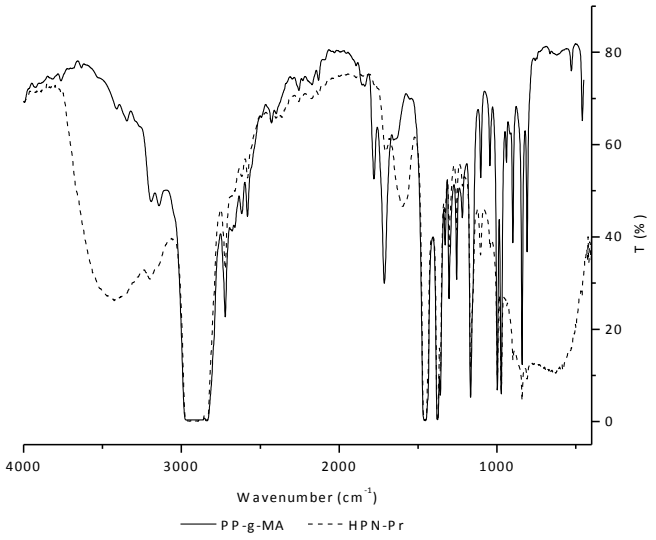


(a)

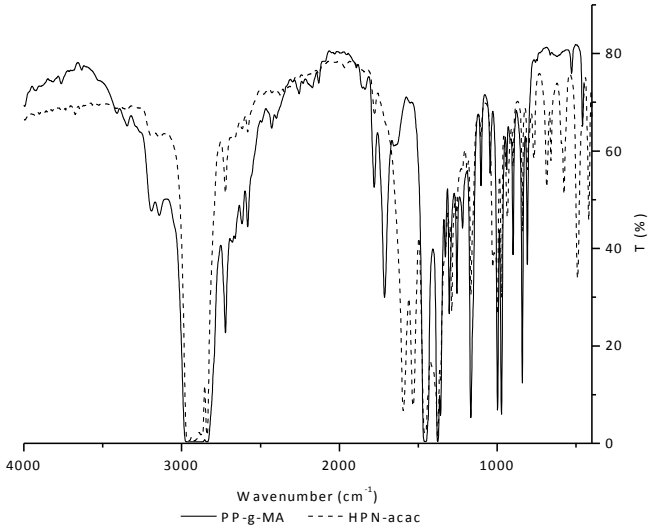


(b)

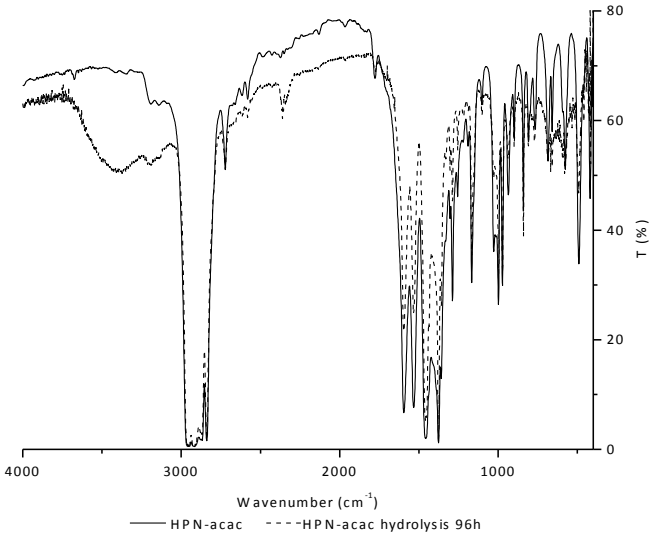


(c)

Figure 4.1 – FT-IR spectra of a) PP-g-MA and HPN-Pr; b) PP-g-MA and HPN-acac and c) HPN-acac before and after hydrolysis.

The spectrum of HPN-acac sample collected from the mixer (Figure 4.1b) does not show any evidence of Al-O formation. Moreover, two bands at 1520 $cm^{-1}$ and 1580 $cm^{-1}$ characteristics of acetylacetonate (acac) group, which should come out during the synthesis as secondary reaction product, still present. This means that the hydrolysis reaction did not take place in the mixer. This could be associated to the difference between $Al(acac)_3$ melting temperature (190 °C) and the set temperature (180 °C). Since the melt temperature increased during mixing and a

constant value of 193 °C was reached after 5 min, the precursor was sufficiently melted to react with the polymer. Therefore, to overcome the low reactivity, HPN-acac was subject to a hydrolysis treatment during 96 h to promote the reaction between $Al(acac)_3$ and MA group of PP-g-MA. The spectrum recorded after this treatment (Figure 4.1c) shows a decrease of the acac bands and the appearance of the Al-OH band between 3000 – 3500 $cm^{-1}$. However, in the range of 400 – 1000 $cm^{-1}$, where the stretching mode of Al-O occurs, no significant peak can be detected.

The XRD spectra of PP-g-MA, HPN-Pr and HPN-acac are shown in Figure 4.2. The crystalline peaks at 14°, 16.8°, 18.4° and 21° in XRD pattern corresponding to (110), (040), (130) and (041) planes, respectively, confirm the monoclinic form of the PP-g-MA [21].

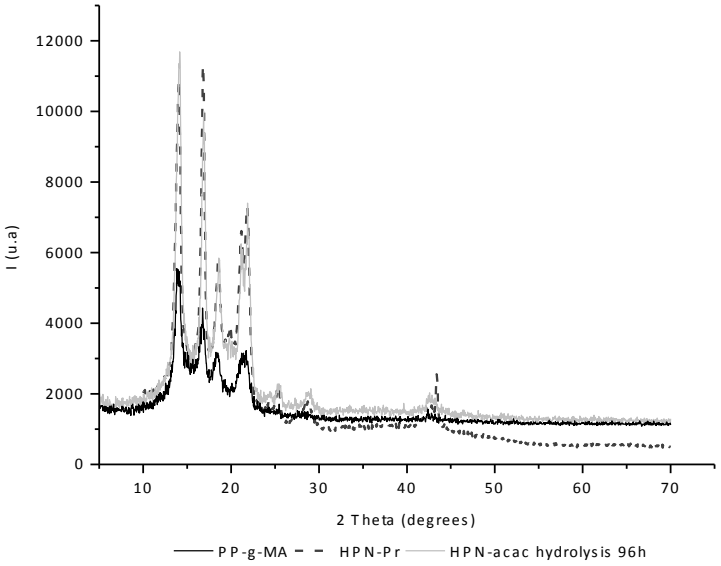


(a)

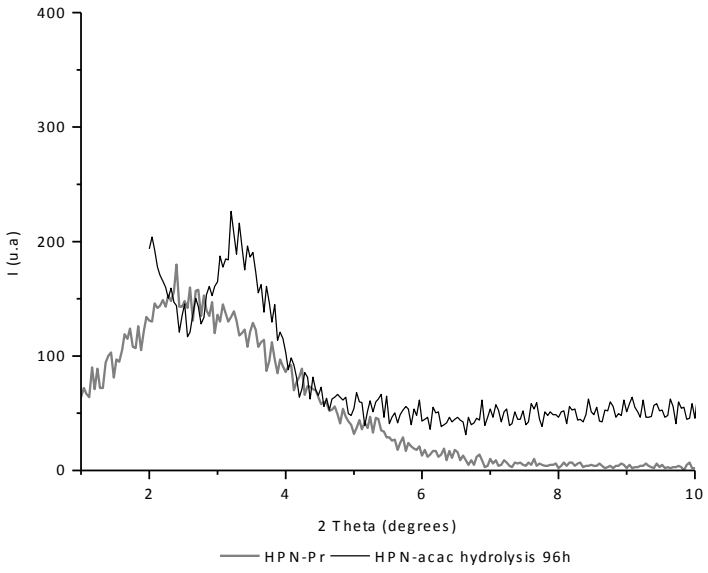

(b)

Figure 4.2 – XRD pattern for a) PP-g-MA, HPN-Pr and HPN-acac after hydrolysis; b) HPN-Pr and HPN-acac after hydrolysis.

The comparison of the PP-g-MA and HPN-Pr spectra reveals new peaks at 19.8°, 20.9°, 23.9°, and 44.23° (Figure 4.2a). The new peaks might be due to the presence of aluminium oxide hydroxide (AlOOH) and aluminium hydroxide ($Al(OH)_3$), as observed by FT-IR. As indicated by Ervin and Osborn, the formation of aluminium oxy-hydroxide phase is thermodynamic favoured in a temperature range of 130 °C and 350 °C [22]. However, the total number of peaks characteristics of either AlOOH or $Al(OH)_3$ are not present in the spectra or are hindered by others more intense, which makes difficult to conclude if these two species are really present [23-25].

Contrarily to HPN-Pr XRD result, HPN-acac after 96 h hydrolysis shows less peaks corresponding to aluminium oxide formation, which is in agreement with previous FT-IR analysis.

The comparison the HPN-Pr and HPN-acac after hydrolysis patterns at low angles (Figure 4.2b) reveals a shift between the peaks of the two nanocomposites. While the peak of the HPN-Pr is at 2.2°, the peak of HPN-acac is at 3.2°. This can be an indication that the aluminium nanoparticles are better dispersed in the PP-g-MA matrix in HPN-Pr. Similar observation was made by Wu in the study of PCL/$TiO_2$ and PCL-g-AA/$TiO_2$ composites [26]. He observed two peaks at 2.9° and 2.6° for PCL/$TiO_2$ and PCL-g-AA/$TiO_2$, respectively. The peak at low angle was associated to a well and homogeneous dispersion of $TiO_2$ in the PCL matrix.

The X-ray photoelectron spectroscopy analysis (XPS) was preformed only for HPN-Pr and the values of binding energies and areas for all peaks are summarized in Table 4.1. The Al 2p peak of the aluminium isopropoxide (Al(Pr-i-O)3) appears at 74.477 eV and it was shifted to 75.075 eV in the HPN-Pr. According to the literature, the binding energy of Al 2p for $Al_2O_3$ appears in the range of 74.4 – 75.8 eV (27). The shift observed for Al 2p signal can be due to a complex formation (-C(=O)-O-Al-) between PP-g-MA and $Al(Pr\text{-}i\text{-}O)_3$, which changed the aluminium neighbour groups and therefore its binding energy.

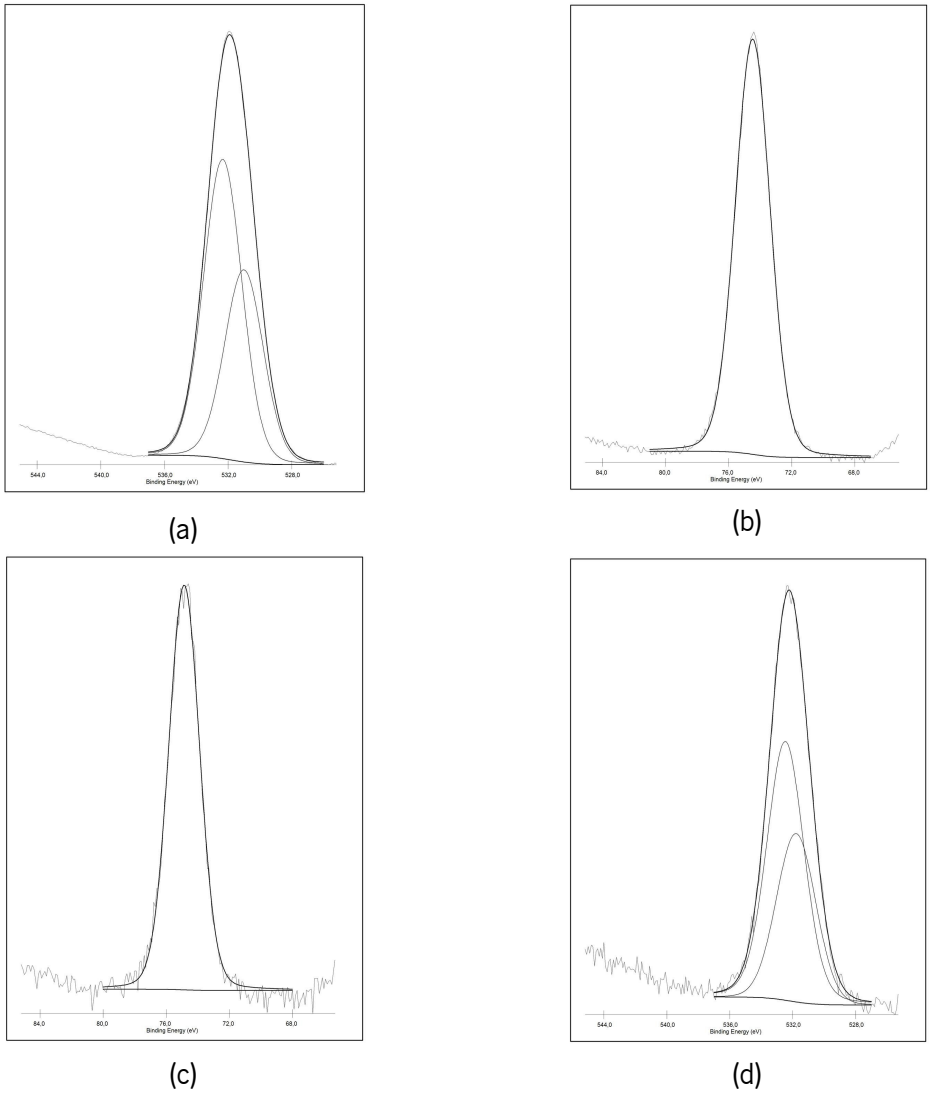


Figure 4.3 – The XPS for Al 2p: a) $Al(Pr\text{-}i\text{-}O)_3$ precursor, b) HPN-Pr and for O 1s, c) $Al(Pr\text{-}i\text{-}O)_3$ precursor, d) HPN-Pr.

For O 1s peak of $Al(Pr\text{-}i\text{-}O)_3$ and HPN-Pr a large peak can be observed between 527 eV and 538 eV, respectively. After peak deconvolution two oxygen species (531.462 and 532.590 eV) can be detected (Table 4.1). In general, peaks around ≈ 530 eV are attributed to oxides ($O_o$) whereas peaks around ≈ 532 eV are considered to adsorbed oxygen ($O_a$) [21]. The Oa with higher binding energy corresponds to strongly adsorb oxygen as -OH or $H_2O$. The O 1s peak of HPN-Pr has similar binding energy to $Al(Pr\text{-}i\text{-}O)_3$. Although crosslinking took place, the sol-gel reaction did not change significantly the oxygen atoms neighbourhood.

The O/Al atomic ratio of the HPN-Pr is much lower than for the precursor. This value is related with the hydroxyl fraction present in the HPN-Pr and gives information on the oxidation evolution [27,28]. Brand and co-workers indicated in their study that for a completely anhydrous

amorphous oxide layer ($Al_2O_3$ with a hydroxyl fraction of zero) the value of the O/Al atomic ratio corresponds to 1.5, while for crystalline AlOOH (with a hydroxyl fraction of 0.5) the ratio is 2.0 [29]. The atomic ratio obtained for HPN-Pr was 1.8, which is in agreement with the FT-IR and XRD results and confirms that AlOOH groups are presented in nanocomposite prepared.

Table 4.1 – XPS peaks values obtained for $Al(Pr\text{-}i\text{-}O)_3$ and HPN-Pr.

| | Al 2p | | O 1s | | | | Atomic ratio $O_o/Al$ |
|---|---|---|---|---|---|---|---|
| | | | $O_o$ | | $O_a$ | | |
| | Binding energy (eV) | Area | Binding energy (eV) | Area | Binding energy (eV) | Area | |
| $Al(Pr\text{-}i\text{-}O)_3$ | 74.477 | 37478.3 | 531.137 | 158472.6 | 532.250 | 244428.8 | 4.034 |
| HPN-Pr | 75.075 | 5158.9 | 531.462 | 10630.6 | 532.590 | 16500.6 | 1.808 |

Microscopic techniques were used to characterize the morphology of HPNs as well as its chemical composition. SEM micrographs presented in Figure 4.4a show that HPN-Pr has a homogeneous and rough surface. The presence of aluminium agglomerates cannot be observed in the micrographs, which indicates a good dispersion and interaction between organic and inorganic components. Figure 4.4b and c depict the surface morphology for HPN-acac before and after hydrolysis, respectively. Comparing the surface of HPN-acac and HPN-Pr, it is clear that the former is smoother. The hydrolysis treatment of HPN-acac provokes a strong change on the surface morphology, the presence of holes can be observed in Figure 4.4c. These holes can be due to the lost of $Al(acac)_3$ particles during the hydrolysis treatment, as it will be explained below.

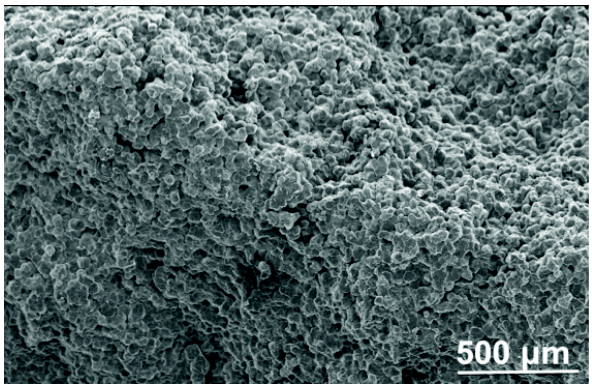


(a)

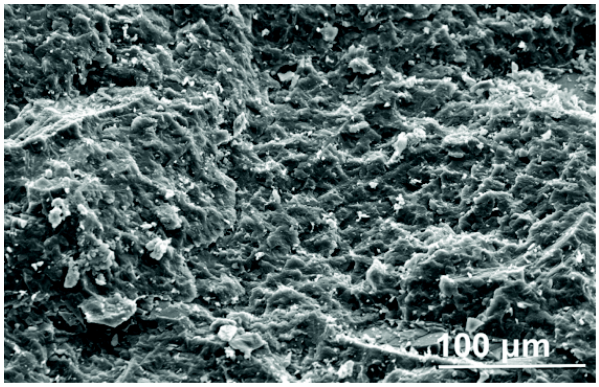


(b)

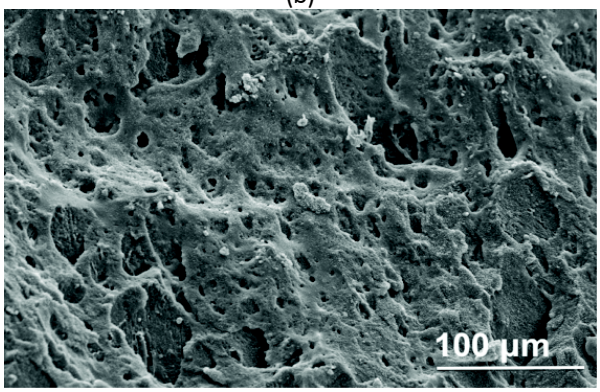


(c)

Figure 4.4 – SEM micrographs of a) HPN-Pr surface, b) HPN-acac surface before hydrolysis and c) HPN-acac surface after hydrolysis.

Since agglomerates were not observed by SEM analysis and in order to have more detail on particle size and its distribution, the samples were analysed by TEM and the results are presented in Figure 4.5. The morphology of HPN-Pr (Figure 4.5a) evidence well dispersed aluminium nanoparticles (± 200 nm) in the PP matrix. Even though a good dispersion is observed for HPN-acac (Figure 4.5b), the number of aluminium nanoparticles is lower than for HPN-Pr. In agreement with the previous results, this difference can be explained by the lower extension of the chemical reaction.

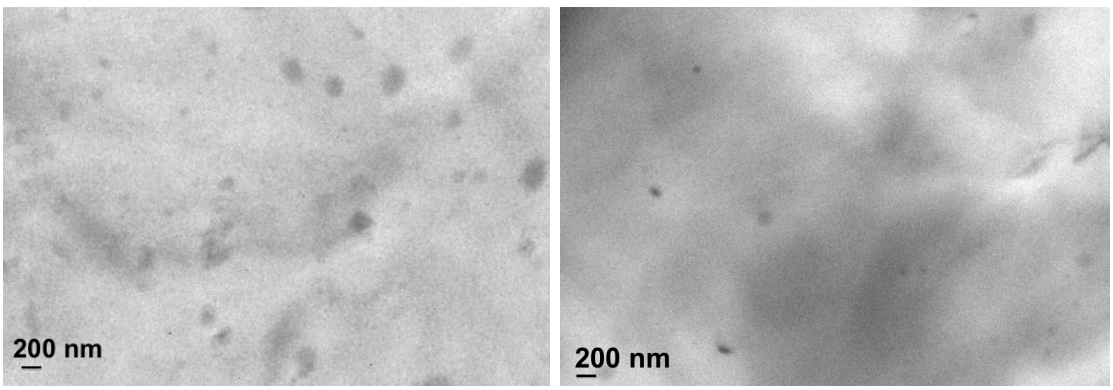


(a) (b)

Figure 4.5 – TEM micrographs of a) HPN-Pr and b) HPN-acac.

Figure 4.6 shows the EDS analysis preformed on the HPNs surfaces. The presence of aluminium is confirmed for both materials. However, a clear decrease of the aluminium peak intensity was observed for HPN-acac after hydrolysis treatment. This can explain the holes observed by SEM, part of the $Al(acac)_3$ was lost during hydrolysis treatment from PP-g-MA matrix. In order to confirm this, both HPNs were immersed in acidic water solution during 5 days, then the aluminium concentration in the solution was analysed by atomic absorption. The results revealed that $6.9x10^{-3}\pm1.9x10^{-3}$ mg/L and 5.5±0.4 mg/L of Al were presented in the solution of the HPN-Pr and HPN-acac, respectively.

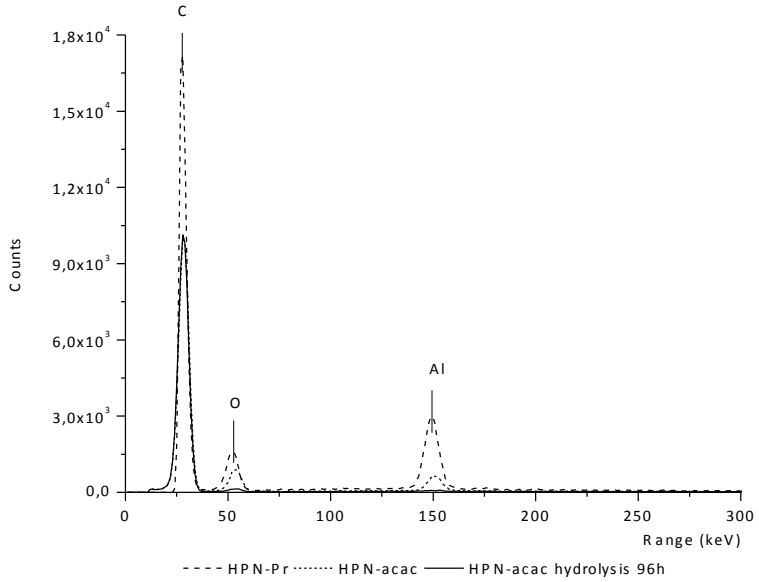


Figure 4.6 – EDS spectrum of HPN-Pr and HPN-acac.

The rheological behaviour of the prepared HPN gives important information about its molecular structure. The results presented in Figure 4.7a show a significant difference between the viscoelastic behaviour of HPN-Pr and PP-g-MA. A strong increase in complex viscosity and storage modulus can be observed for HPN-Pr. This change can be associated with a transition from a liquid-like behaviour to a solid-like behaviour, where the storage modulus is independent of the frequency value. This type of behaviour is characteristic of the crosslinking materials, which unlike the linear ones do not show a plateau at low frequencies in complex viscosity and have in the limit a slope of -1 (solid materials). The slope of the complex viscosity of the HPN-Pr is -0.95, which evidences that HPN-Pr has a crosslinking structure. The value of the gel content obtained (70 wt.%) corroborates the rheological data.

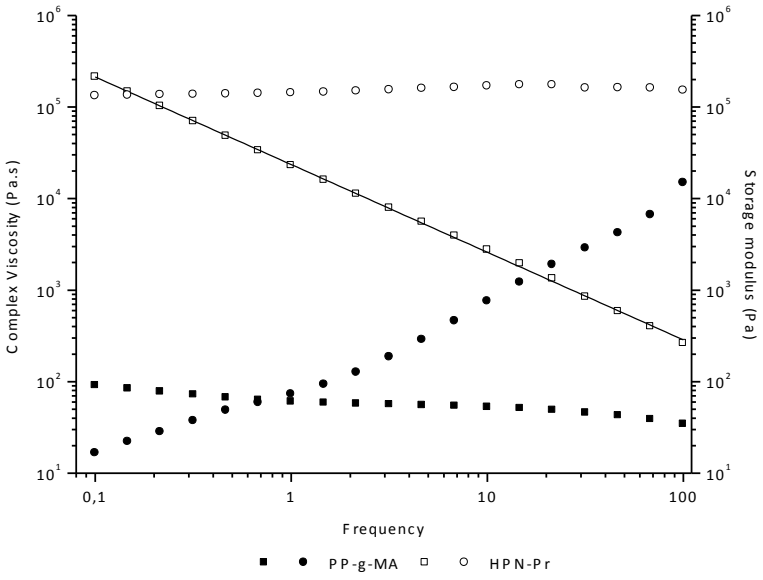


(a)

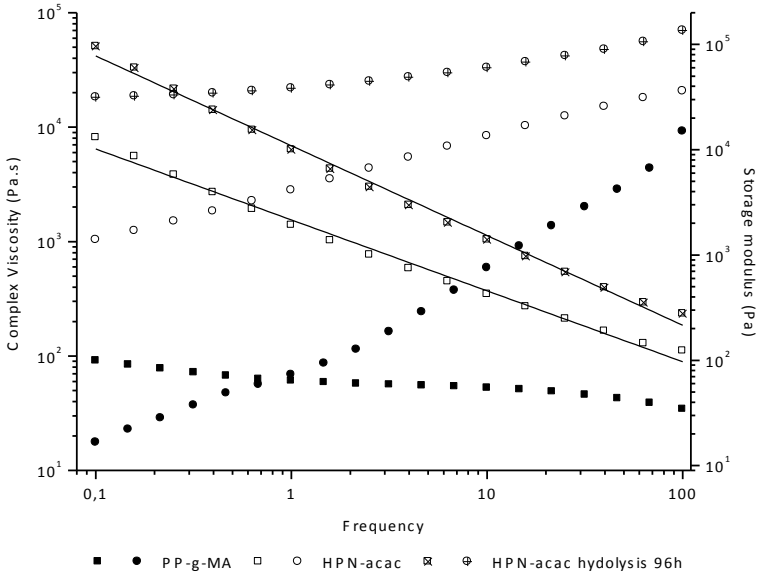


(b)

Figure 4.7 – Rheological behaviour of a) PP-g-MA and HPN-Pr and b) PP-g-MA and HPN-acac before and after hydrolysis.

The rheological behaviour of HPN-acac before and after hydrolysis is depicted in Figure 4.7b. Although FT-IR and XRD results did not show any evidence that the reaction took place in the mixer, an increase in complex viscosity and storage modulus can be observed for the samples before hydrolysis. The increase in viscosity and storage modulus cannot be only explained by the presence of inorganic filler in the PP-g-MA matrix but also by the formation of a branched/crosslinking molecular structure. As expected, the hydrolysis treatment promotes the

reaction and the values of viscosity and storage modulus increase. The slope of complex viscosity curves increases from -0.5 to -0.75. The values of the gel content before (31.4 wt.%) and after hydrolysis (37.6 wt.%) are in line with the rheological results.

A power law relationship (Equation 4.2) can be used to analyse qualitatively the effect of hydrolysis treatment on the crosslinking degree:

$$\eta^* = p[\omega]^{n-1} \qquad \text{Equation 4.2}$$

where $\eta^*$ is the complex viscosity, $\omega$ the angular frequency and *p* and *n* the fitting parameters. The parameter *n-1* corresponds to the slope of the curve $\log(\eta^*)$ vs $\log(\omega)$, which reflects the shear thinning behaviour. Decrease on *n* value represents an increase of crosslinking. The *n* values obtained from Equation 4.2 for HPN-acac before and after hydrolysis were 0.38 and 0.22, respectively.

Figure 4.8 shows the change of thermal behaviour determined by thermogravimetric analysis (TGA) and of melting temperature and crystallinity degree (Table 4.2), determined by differential scanning calorimetry (DSC).

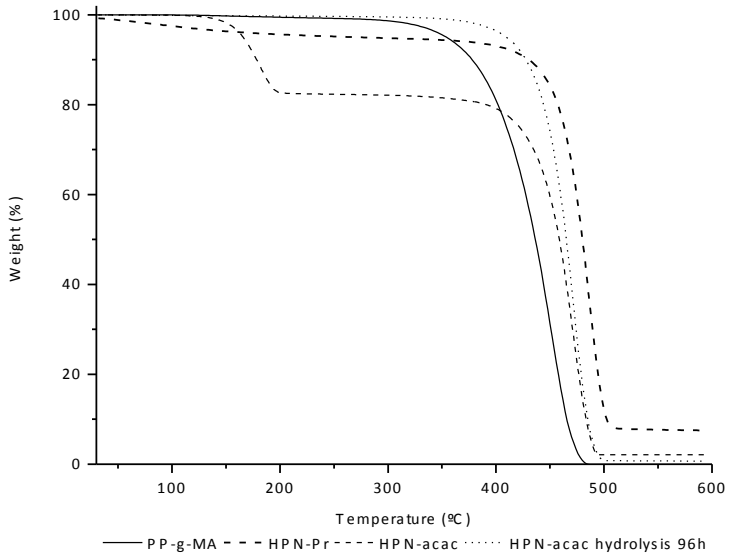


Figure 4.8 – Thermograms of PP-g-MA, HPN-Pr, HPN-acac and HPN-acac after hydrolysis.

The TGA results presented in Figure 4.8 show that HPN-Pr start to loose weight around 100 °C due to evaporation of some residual reactions sub-products. During the synthesis of HPN-Pr, 2-propanol ($C_3H_7OH$) is formed as a sub-product. This alcohol has a boiling point of 82.5 °C, which

explains the first weight variation. Comparing the curves of PP-g-MA and HPN-Pr, it can be observed that the latter has higher thermal stability. This behaviour can be due to the crosslinking bonds between organic and inorganic components. The residual value obtained (0.8592 mg) was a little higher than the one (0.6873 mg) that was calculated assuming that only $Al_2O_3$ species would be present at 550 °C.

As expected, HPN-acac has a different thermal behaviour before and after hydrolysis. Before, it shows a first step decomposition around 190 °C, which corresponds to the $Al(acac)_3$ melting temperature and then has a second one due to matrix degradation. After hydrolysis, degradation change for one-step process, indicating that all acac reacted during hydrolysis in agreement with FT-IR (Figure 4.1). Comparing the degradation curves of HPN-acac with and without hydrolysis treatment it can be seen that the final degradation temperature is the same. Moreover, it is clear that the residual weight is higher for the sample before hydrolysis (2.10 before and 0.36 wt.% after). This is in line with previous results that evidence that the amount of inorganic particles decreases after hydrolysis.

DSC data obtained for PP-g-MA and HPNs are presented in Table 4.2. The crystalline fraction ($X_c$) was calculated from melting enthalpy, using Equation 4.3.

$$X_c = \frac{\Delta H}{\Delta H^0} \times 100 \qquad \text{Equation 4.3}$$

where $\Delta H$ is the melting enthalpy of the material given by the area under the endothermic peak, and $\Delta H^0 \approx 165$ J/g is the melting enthalpy for 100 % isotactic PP [22].

The crosslinking structure of HPN-Pr influences the crystalline regions of PP-g-MA matrix. In fact, the melting temperature, melting enthalpy and crystallinity degree of HPN-Pr is lower than the matrix. This is explained by the effect of crosslinking on crystallinity regions, which inhibits the folding of macromolecules chains and decrease the lamellar crystals. The formation of crosslinking between organic and inorganic components of HPN-Pr, during sol-gel reaction, disturbs the reorganization and chain folding during crystallization process, which results imperfect crystallites formation with smaller size and also less content. All this parameters contributed for the observed decrease in melting temperature, enthalpy and crystallinity degree for HPN-Pr [26].

In case of HPN-acac before and after hydrolysis, a decrease on melting enthalpy and crystallinity degree was observed. This decrease was driven by a reduction on structural regularity and separation of chains by the presence of organic group (acac), which obstructs or disturbs the reorganization and the folding of macromolecular chains, decreasing in general the size and content of the crystals. After hydrolysis this effect was even higher due to the formation of more crosslinking bonds, resulting in new decrease of crystallinity degree and melting temperature.

Table 4.2 – DSC results obtained for HPNs.

| | $T_m$(C°) | ΔH (J/g) | Xc (%) |
|---|---|---|---|
| PP-g-MA | 162.50 | 96.07 | 58.23 |
| HPN-Pr | 155.80 | 76.61 | 46.43 |
| HPN-acac | 161.36 | 60.02 | 36.32 |
| HPN-acac hydrolysis 96 h | 159.80 | 46.62 | 28.21 |

### 4.3.2 GENERAL DISCUSSION

#### *4.3.2.1 Effect of the organic groups of the precursor on reaction*

In order to explain better and understand the results obtained with each aluminium precursor used in the present work, the activation energy ($E_a$) involved in the synthesis of the HPNs was determined. Figure 4.9 depicts the Arrhenius plots obtained for HPN-Pr and HPN-acac. A linear relationship was found for the reactions with both precursors. The $E_a$ was 52.9 kJ/mol and 113.9 kJ/mol for HPN-Pr and HPN-acac, respectively. According to the results shown above, the $Al(acac)_3$ precursor has a higher $E_a$ value. This can be attributed to the volume of its organic groups ($O_2C_5H_7$), which may prevent the chemical reaction with the maleic anhydride group of the PP. Thus, to promote the reaction between $Al(acac)_3$ and PP-g-MA it is necessary to provide more energy to the system to overcome the effect of the stereochemical hindrance. Contrarily, since the $Al(Pr\text{-}i\text{-}O)_3$ has a linear organic chain ($OC_3H_7$), the reaction is easier with this precursor and the $E_a$ is lower. Bahloul and co-workers obtained similar $E_a$ value (66 kJ/mol) using titanium n-butoxide for the synthesis of $TiO_2$ nanoparticles in PP matrix by reactive extrusion [12].

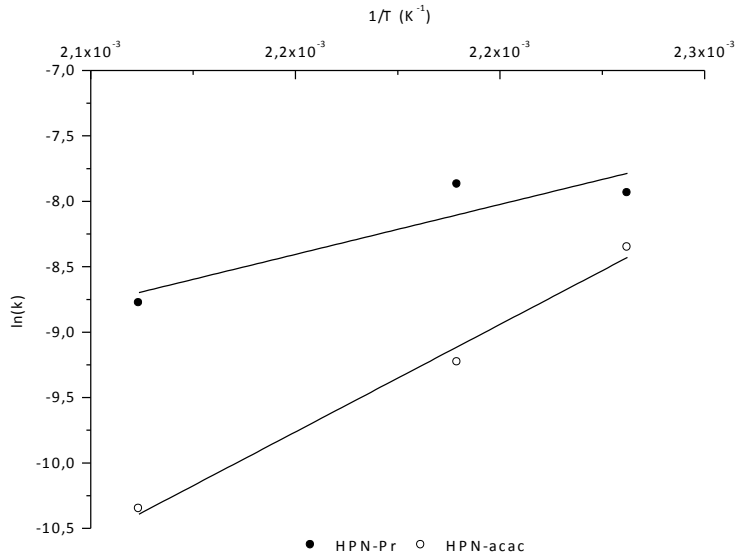


Figure 4.9 – Arrhenius plots for the synthesis reactions of HPN-Pr and HPN-acac.

These results are in agreement with theory, as the extent of the sol-gel reaction, when aluminium alkoxides are used as inorganic precursor, depends mainly on the steric hindrance of the alkoxide ligand [30]. This group is bonded to the metal by hydrolytically stable way. Metal with alkoxide ligands type –O-$CH_2$-R, where R is: n-$C_4H_9$; i-$C_4H_9$; n-$C_5H_{11}$, etc., has lower steric hindrance as a result of molecules symmetry. However, if the alkoxide groups has a OR as secondary or tertiary, the conversion of tetrahedral Al atoms to penta or octahedral coordination, results in the formation of less species, like dimers or trimers and consequently lower reactivity [31]. Schubert et al. (1995), outlined the general equation for hydrolysis-condensation reaction of metal alkoxides, Equation 4.4 [32]. If the M(OR') group changes by other more hydrolytacally stable, the degree of crosslinking during the sol-gel process decreases [32,33]. This explains the behaviour of the precursors used in the present work.

$$xRM(OR')_n + yM(OR')_m + zH_2O \rightarrow R_qMO_p + wR'OH \qquad \text{Equation 4.4}$$

*4.3.2.2 Reaction mechanism*

Metal alkoxides are widely used as inorganic precursors due to their great reactivity resulting from the lower electronegativity of the metal and its ability to exhibit several coordination states. When the metal is in its saturated coordination state and in the absence of catalyst, the hydrolysis and condensation mechanism of the alkoxide occurs by nucleophilic substitution

involving nucleophilic addition followed by a proton transfer from the attacking group to an alkoxide or hydroxo-ligand and the removal of the protonated species as, either, alcohol (alcoxolation) or water (oxolation) [30].

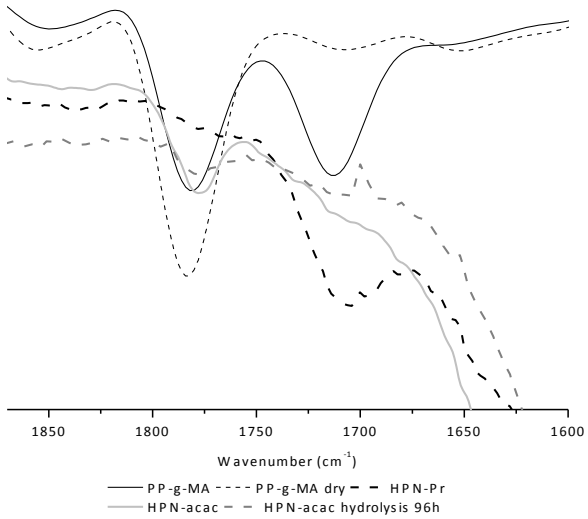


Figure 4.10 – FT-IR of maleic anhydride ring for HPN-Pr and HPN-acac.

It is well known that during hydrolysis reaction, a decrease of anhydride absorbance at 1780 $cm^{-1}$ and an increase of the carboxylic acid absorbance at 1710 $cm^{-1}$ occur. The FT-IR results (Figure 4.10) clearly show the ring open form of MA in the HPN-Pr. Therefore, for the synthesis of HPN-Pr hydrolysis treatment was not necessary, the open form of the MA group was provoked by the formation of covalent bond between aluminium and PP-g-MA backbone. In case of HPN-acac, the close form of MA ring still predominant both before and after hydrolysis. This seems to indicated the absence or lower level of reaction between $Al(acac)_3$ precursor and MA groups of the PP-g-MA. Nevertheless, a decrease on acetylacetonate (acac) group bands at 1520 $cm^{-1}$ and 1580 $cm^{-1}$ together with the appearance of Al-OH stretching mode can be observed, as depicted in FT-IR results.

Taking this data into consideration and all the results obtained by the several techniques used, a reaction mechanism for each precursor is proposed in Figure 4.11a and b.

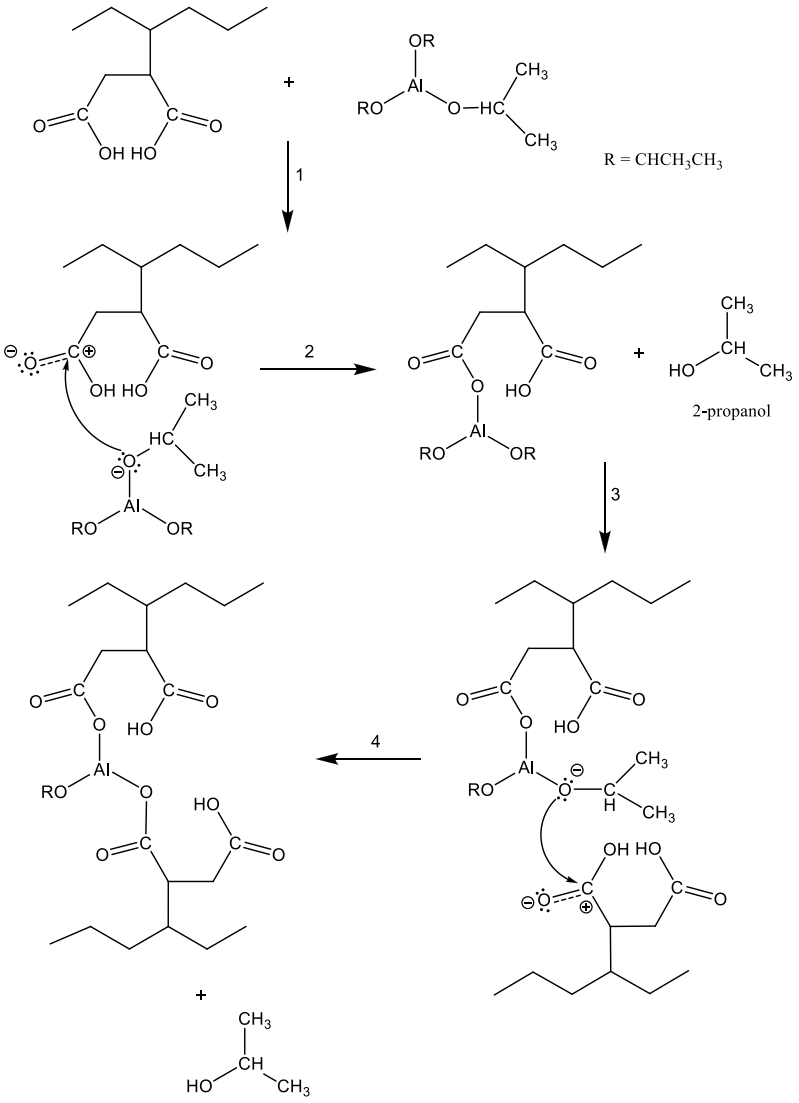


(a)

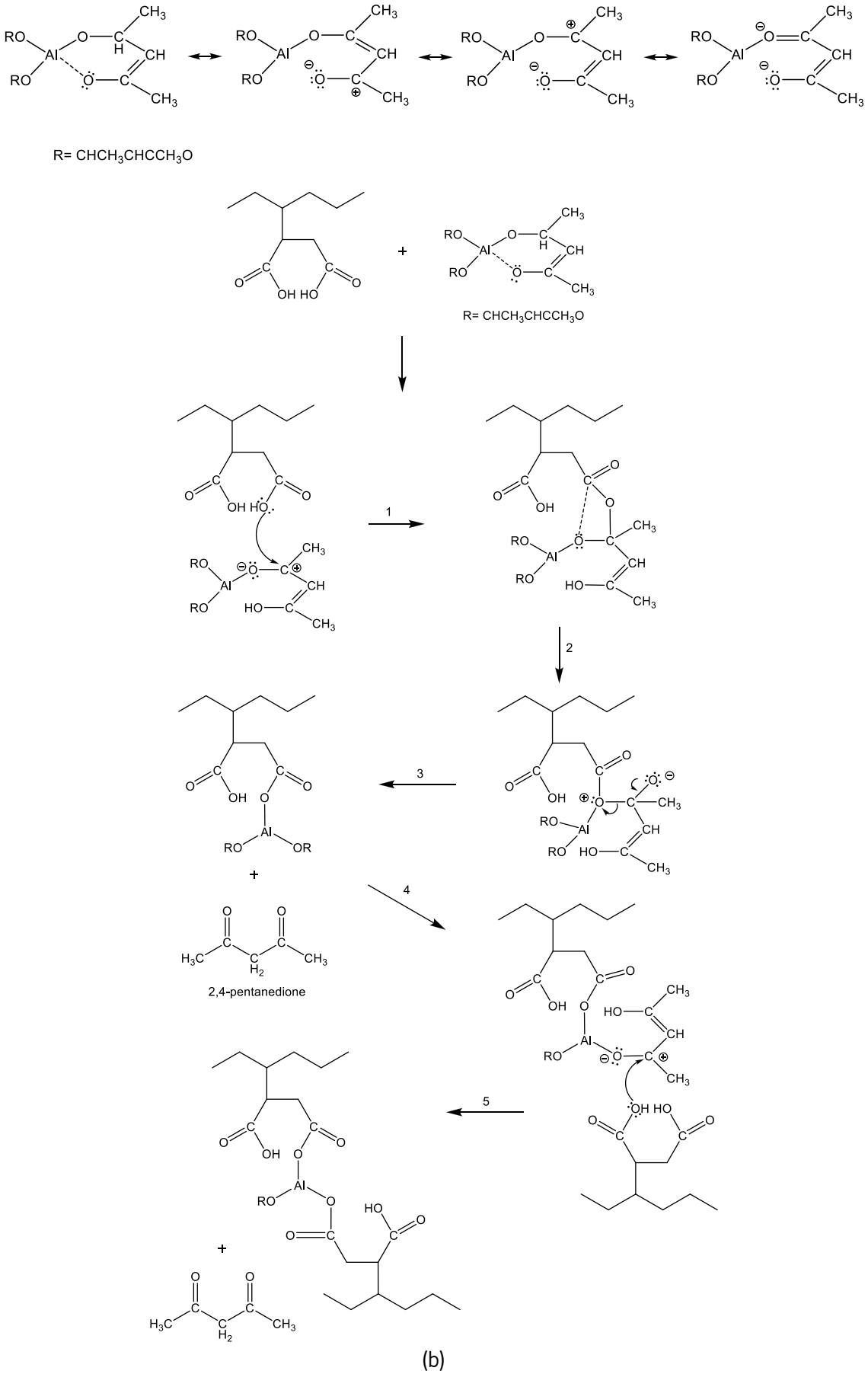


Figure 4.11 – Reaction mechanism of a) HPN-Pr and b) HPN-acac.

The crosslinking structure obtained during HPN-Pr synthesis occurs by nucleophilic attack of oxygen bonded to aluminium to the carboxylic acid formed when the acid form of maleic anhydride is present (reaction 1). After nucleophilic attack the hydroxyl group of carboxylic acid comes out, reacting with organic group of aluminium isopropoxide ($C_3H_7$), resulting in the formation of 2-propanol ($C_3H_7OH$) and polymeric species containing aluminium (reaction 2). Then the crosslinking proceeds by the reaction between the polymeric specie formed in the previous step with another maleic anhydride group (reaction 3 and 4).

In the case of HPN-acac synthesis, the carboxylic group from the maleic anhydride reacts with aluminium acetylacetonate as describe in first reaction of Figure 4.11b. In this case, due to the mesomeric form of the acetylacetonate group, the oxygen of hydroxyl group attacks the carbon of the precursor (reaction 1) [34]. In the second step, the carbocation suffers a rearrangement due to the interaction between the oxygen atom that has free electron pairs and the cationic centre of the carbon atom (reaction 2). Since the specie formed is unstable, further rearrangement occurs resulting in PP containing aluminium and 2,4-pentanedione formation (reaction 3). After, the reaction continues between the previous polymeric formed specie and a new PP-g-MA molecule (reaction 4) forming crosslinking (reaction 5).

## 4.4 CONCLUSION

This study confirms that it is possible to produce inorganic nanoparticles in a polymeric matrix by reaction in the molten state without solvents. Whereas the chemical reaction occurred in only one step process for $Al(Pr\text{-}i\text{-}O)_3$, for $Al(acac)_3$ a post step treatment by hydrolysis was necessary. FT-IR spectroscopy, rheology, TGA, DSC analysis and gel content determination proved that aluminium formed covalent bonds with PP-g-MA. Thermal behaviour was also enhanced comparing with PP-g-MA, where the degradation temperature increased, being the onset around 450 °C.

The reactions extend and the amount of aluminium depends on the precursor used. This was explained by the determination of the activation energy, which showed a lower value when precursor $Al(Pr\text{-}i\text{-}O)_3$ was used.

Taking into account all the results obtained, the reaction mechanisms for both precursor were proposed.

## 4.5 BIBLIOGRAPHY

[1] Turova, N.Y. Turevskaya, E.P. Kessles, V.G. Yanovskaya, M.I. 2002. The chemistry of metal alkoxides. *Kluwer Academic Publisher*, editor:149–157.

[2] Dou, Q. Zhu, X. Peter, K. Demco, D.E. Möller, M. Melian, C. 2008. Preparation of polypropylene/silica composites by in-situ sol-gel processing using hyperbranched polyethoxysiloxane. *Journal of Sol-Gel Science Technology* 48(1-2):51–60.

[3] Wang, K.H. Choi, M.H. Koo, C.M. Choi, Y.S. Chung, I.J. 2001. Synthesis and characterization of maleated polyethylene/clay nanocomposites. *Polymer* 42(24):9819–9826.

[4] Taylor, L.J. 1975. Direct synthesis of composites materials. US Patent 3891594.

[5] Judeinstein, P. Sanchez, C. 1996. Hybrid organic-inorganic materials: a land of multidisciplinarity. *Journal Materials Chemistry* 6(4):511–525.

[6] Xu, C. Ohno, K. Ladmiral, V. Composto, R. 2008. Dispersion of polymer-grafted magnetic nanoparticles in homopolymers and block copolymers. *Polymer* 49(16):3568–3577.

[7] Rong, M.Z. Zhang, M.Q. Zheng, Y.X. Zeng, H.M. Walter, R. Frieddrich, K. 2001. Structure-propertiy relationships of irradiation grafted nano-inorganic particle filled polypropylene composites. *Polymer* 42(1):167–183.

[8] Liua, X. Wu, Q. 2001. PP/clay nanocomposites prepared by grafting-melt intercalation. *Polymer* 42(25):10013–10019.

[9] Bounor-Legaré, V. Angelloz, C. Blanc, P. Cassagnau, P. Michel, A. 2004. A new route for organic–inorganic hybrid material synthesis through reactive processing without solvent. *Polymer* 45(5):1485–1493.

[10] Rong, M.Z. Zhang, M.Q. Pan, S.L. Friedrich, K. 2003. Interfacial effects in polypropylene–silica nanocomposites. *Journal of Applied Polymer Science* 92(3):1771–1781.

[11] Kruenate, J. Tongpool, R. Panyathanmaporn, T. Kongrat, P. 2004. Optical and mechanical properties of polypropylene modified by metal oxides. *Surface Interface Analysis* 36(8):1044–1047.

[12] Bahloul, W. Oddes, O. Bounor-Legaré, V. Mélis, F. Cassagnau, P. Vergnes, B. 2011. Reactive extrusion processing of polypropylene/$TiO_2$ nanocomposites by in situ synthesis of the nanofillers: Experiments and modeling. *American Institute of Chemical Engineeris* 57(8):2174–2184.

[13] Jain, S. Goossensa, H. van Duinb, M. Lemstra, P. 2005. Effect of in situ prepared silica nano-particles on non-isothermal crystallization of polypropylene. *Polymer* 46(20):8805–8818.

[14] Jain, S. Goossensa, H. Picchionia, F. Magusinb, P. Mezarib, B. van Duin, M. 2005. Synthetic aspects and characterization of polypropylene–silica nanocomposites prepared via solid-state modification and sol–gel reactions. *Polymer* 46(17):6666–6681.

[15] Zou, H. Wu, S. Shen, J. 2008. Polymer/Silica Nanocomposites: Preparation, Characterization, Properties, and Applications. *Chemical Reviews* 108(9):3893–3957.

[16] Sun, D. Zhang, R. Liu, Z. Huang, Y. Wang, Y. He, J. Han, B. Yang, G. 2005. Polypropylene/Silica Nanocomposites Prepared by in-Situ Sol–Gel Reaction with the Aid of $CO_2$. *Macromolecules* 38(13):5617–5624.

[17] Bahloul, W. Bounor-Legaré, V. David, L. Cassagnau, P. 2010. Morphology and viscoelasticity of PP/$TiO_2$ nanocomposites prepared by *in situ* sol–gel method. *Journal Polymer Science part B: Polymer Physics* 48(11):1213–1222.

[18] Shieh, Y. Liau, J. Chen, T. 2001. An investigation of water crosslinking reactions of silane-grafted LDPE. *Journal Applied Polymer Science* 81(1):186–196.

[19] Joe, I.H. Vasudevan, A.K. Aruldhas, G. Damodaran, A.D. Warrier, K.G.K. 1997. FTIR as a Tool to Study High-Temperature Phase Formation in Sol–Gel Aluminium Titanate. *Journal of Solid State Chemistry* 131(1):181–184.

[20] Wengrovius, J.H. Garbauskas, M.F. Williams, E.A. Going, R.C. Donahue, P.E. Smith, J.F. 1986. Aluminum alkoxide chemistry revisited: synthesis, structures, and characterization of several aluminum alkoxide and siloxide complexes. *Journal of American Chemical Society* 108(5):982–989.

[21] Stojanovic, Z. Kacarevic-Popovic, Z. Galovic, S. Milicevic, D. Suljovrujic, E. 2005. Crystallinity changes and melting behavior of the uniaxially oriented iPP exposed to high doses of gamma radiation. *Polymer Degradation and Stability* 87(2):279–286.

[22] Sakka, S. 2004. Handbook of sol-gel science and technology: processing, characterization and applications. Volume III: Applications of sol-gel technology. *Kluwer Academic*, editor:193–200.

[23] Tonejc, A. Stubičar, M. Tonejc, A.M. Kasanović, K. Subotić, B. Smit, I. 1994. Transformation of γ-AlOOH (boehmite) and $Al(OH)_3$ (gibbsite) to α-$Al_2O_3$ (corundum) induced by high energy ball milling. *Journal Materials Science Letters* 13(7):519–520.

[24] Mishra, D. Anand, S. Panda, R.K. Das, R.P. 2000. Hydrothermal preparation and characterization of boehmites. *Materials Letters* 42(1-2):38–45.

[25] Khalil, K.M.S. 2008. Formation of mesoporous alumina via hydrolysis of modified aluminum isopropoxide in presence of CTAB cationic surfactant. *Applied Surface Science* 255(5 – Part 2):2874–2878.

[26] Wu, C. 2004. In Situ Polymerization of Titanium Isopropoxide in Polycaprolactone: Properties and Characterization of the Hybrid Nanocomposites. *Journal of Applied Polymer Science* 92(3):1749–1757.

[27] Yang, C. Kim, J. Choi, J. Kwon, M. Kim, Y. Choi, J. Kim, G. 2000. XPS study of aluminium oxides deposited on PET thin film. *Journal of Industrial and Engineering Chemistry* 6(3):149–156.

[28] Khonakdara, H.A. Morshediana, J. Wagenknechtb, U. Jafari, S.H. 2003. An investigation of chemical crosslinking effect on properties of high-density polyethylene. *Polymer* 44(15):4301–4309.

[29] Brand, J. Sloof, W.G. Terryn, H. Wit, J.H.W. 2004. Correlation between hydroxyl fraction and O/Al atomic ration as determined from XPS spectra of aluminium oxide layers. *Surface and Interface Analysis* 36(1):81–88.

[30] Brinker, C.J. Scherer, G.W. 1989. Sol-gel Science. The physics and chemistry of sol-gel processing. *Academic Press*, editor:43–59.

[31] Maneeratana, V. 2007. Alkoxide-based precursor for direct electrospinning of aluminum fibers. *PhD Thesis* 49–52.

[32] Schubert, U. Husing, N. Lorenz, A. 1995. Hybrid inorganic-organic materials by sol-gel processing of organofunctional metal alkoxides. *Chemical Materials* 7(11):2010–2027.

[33] Wengrovius, J.H. Carbauskas, M.F. Williams, E.A. Going, R.C. Donahue, P.E. Smitb, J.F. 1986. Aluminium alkoxide chemistry revisited: Synthesis, structures, and characterization of several aluminium alkoxide and siloxide complexes. *Journal of American Chemical Society* 108(108):982–989.

[34] Czech, Z. Wojciechowicz, M. 2006. The crosslinking reaction of acrylic PSA using chelate metal acetylacetonates. *European Polymer Journal* 42(9):2153–2160.

CHAPTER

# 5 PREPARATION OF EVA CONTAINING ALUMINIUM NANOPARTICLES IN THE MELT

The synthesis of aluminium nanoparticles in a EVA matrix, by sol-gel process in the melt, was investigated. Two EVA with different vinyl acetate (VA) content and aluminium isopropoxide were used as organic and inorganic phases. The nanocomposites were prepared in a batch mixer under constant processing conditions and were analysed by several characterization techniques. Even though aluminium nanoparticles were synthesised with both EVAs, smaller and better dispersed nanoparticles were achieved with EVA with higher VA content. Aluminium isopropoxide presented a low activation energy allowing the synthesis of the nanoparticles without a post step treatment. The reaction mechanism was proposed.

The nanocomposites prepared exhibited higher stability than EVA and improved fire resistance.

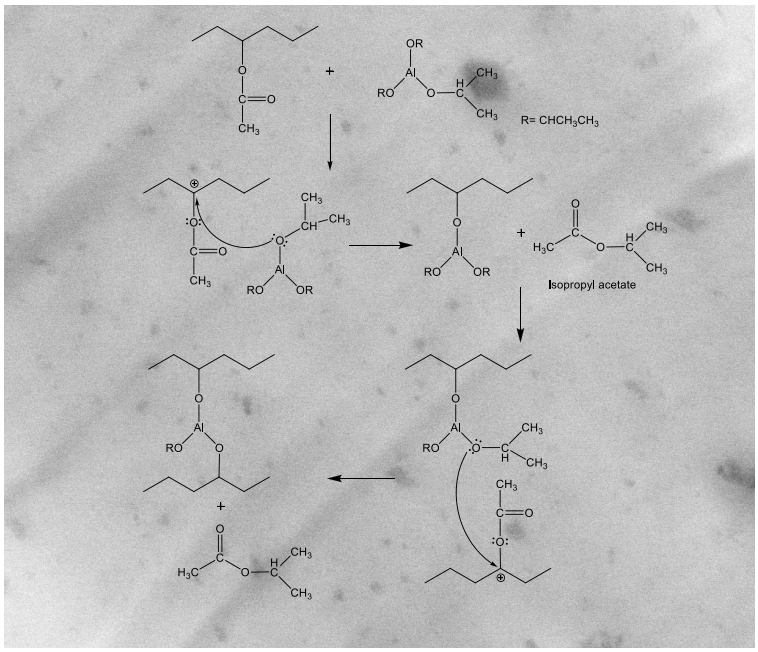


Oliveira, M. Nogueira, R. Machado, A.V. 2012. Preparation of EVA containing aluminium nanoparticles in the melt. Submitted to *Polymer Advanced Technologies*

## 5.1 INTRODUCTION

Since 1940's organic inorganic materials have had attracted considerable attention both from academic and industry since they combine the properties of organic and inorganic components. A small amount of well dispersed inorganic filler can improve significantly the material properties, such as, gas permeability, thermal stability, flame retardance, mechanical performance or chemical resistance [1-3].

Despite a lot of research have been performed concerning nanocomposites preparation, homogeneous dispersion of nanofillers in a polymeric matrix still a difficult task. The main disadvantages resulting from fillers incorporation in polymeric matrix are particle agglomeration and voids formation at the interface of the particles and the polymer matrix [4]. Aiming to improve this, the research for new methods led to the use of sol-gel reactions to synthetize inorganic fillers in a polymeric matrix [5,6]. The sol-gel method is based on a hydrolysis-condensation reaction of a metal alkoxide, which allow the synthesis of nanoparticles well dispersed in the polymer matrix. Metal alkoxide are the precursors most widely used in this method [7], since they can react rapidly with water to form hydroxyl compounds, which, in turn, allow fast reactions [8].

Using sol-gel method to synthesise organic inorganic hybrid, two different types of materials can be obtained. One containing only weak bonds between the two phases, without restriction of the molecular motion of the polymer matrix. Other, comprising covalent bounds between the polymer and metal, which were formed during the hydrolysis condensation reaction of metal alkoxide. In this case the dispersion of inorganic filler increases due to the network formation. Therefore, the molecular motion of the polymer is restricted and the material properties are improved [6,9].

The preparation of nanocomposites of ethylene-vinyl acetate (EVA) and inorganic compounds like, clays or metal hydroxides is a common practice and is well describe in the literature [10]. For applications like, wire and cables, fillers are frequently added to improve fire retardancy and thermal stability, among them aluminium trihydrate [11]. Therefore, this work aims to incorporate aluminium nanoparticles into ethylene-vinyl acetate (EVA) by sol-gel reaction in molten state without the presence of solvent and to investigate the effect of aluminium bonded to the EVA backbone on the nanocomposite properties.

Nanocomposites of two EVAs (different VA content and viscosity) and aluminium isopropoxide were prepared in a batch mixer under constant processing conditions. The prepared materials were characterized by rheology, FT-IR, TGA, crosslinking density measurement and SEM/TEM/EDS analysis.

## 5.2 MATERIALS AND METHODS

### 5.2.1 MATERIALS AND REAGENTS

Ethylene-vinyl acetate (EVA) with 12 wt.% (EVA12, Escorene Ultra UL 00112, melting temperature of 96 °C) and 27 wt.% (EVA27, Escorene Ultra UL 00328, melting temperature of 71 °C) of vinyl acetate, were supplied by Exxon Mobil. Aluminium isopropoxide ($Al(Pr\text{-}i\text{-}O)_3$), used as received in powder state, was supplied by Sigma Aldrich.

### 5.2.2 SYNTHESIS

The aluminium alkoxide concentration was defined as 25 % (w/w), which correspond to the ratio between of vinyl acetate number (VA) and aluminium alkoxide (OR) of 0.36 and 0.81 for EVA12 and EVA27, respectively. The EVA containing aluminium nanoparticles was produced in the melt, in a Haake batch mixer (Rheocord 90; volume 60 $cm^3$), equipped with two rotors running in a counter-rotating way. The rotor speed was 50 rpm and the set temperature was 90 °C. The following procedure was implemented to produce the nanocomposites, first pellets of EVA were introduced into the hot mixer, after 3 min the aluminium precursor was added. The sol-gel reaction proceeded during 10 min and the total sample was removed. The hybrid polymer nanocomposite synthesized with EVA12 was called HPNEVA12 and the one synthesized with EVA27 was HPNEVA27.

## 5.2.3 CHARACTERIZATION

### *5.2.3.1 Rheological properties*

The rheological behaviour of the initial polymers and prepared materials were determined by oscillatory rheological measurements using a Paar Physica MCR300 rheometer at 90 °C. The gap and diameter of the plates was 1 mm and 25 mm, respectively. Nitrogen atmosphere was used to prevent thermo-oxidative degradation. A frequency sweep from 0.1 Hz to 100 Hz under constant strain in the linear viscoelastic region was performed for each sample.

### *5.2.3.2 Crosslinking density*

The crosslinking density was assessed from the volume swelling degree determinate at equilibrium. Around 300 mg of samples were placed in hot xylene at 140 °C during 30 h until swelling equilibrium was reached. Then, the polymer volume fraction at swelling equilibrium, $v_r$, was calculated as follows:

$$\nu_r = \frac{1}{1+\left(\frac{m_1}{m_2}\right)\times\left(\frac{\rho_2}{\rho_1}\right)} \qquad \text{Equation 5.1}$$

where $m_1$ and $m_2$ are, respectively, the weight of swelled sample and the weight of dried sample and $\rho_1$ and $\rho_2$ are, respectively, the polymer and solvent densities (g/cm³).

The Flory-Rehner model was used to determine the crosslinking density. This model coupled with the phantom network assumption gives a correlation between the swelling results and the number of elastic strands, $\nu$:

$$\nu = -\left[\frac{\ln(1-\nu_r) + \nu_r + \chi\nu_r^2}{V\left(\nu_r^{1/3} - 0.5\nu_r\right)}\right] \qquad \text{Equation 5.2}$$

where $\chi$ is the polymer/solvent interaction parameter, $V$ the molar volume of solvent and $v_r$ is the polymer volume fraction at swelling equilibrium. The polymer/solvent interaction parameter ($\chi$) was calculated as followed:

$$\chi = \frac{V(\delta_1 - \delta_2)^2}{RT + 0.34} \qquad \text{Equation 5.3}$$

where $\delta_1$ and $\delta_2$ are the solubility parameters of polymer and solvent, respectively, $V$ is the molar volume; $R$ is the universal gas constant and $T$ is the absolute temperature.

#### *5.2.3.3 FT-IR*

Infrared spectra were recorded in transmission mode between 400 $cm^{-1}$ and 4000 $cm^{-1}$ using a Perkin Elmer 1610, with 32 scans and resolution of 4 $cm^{-1}$. Thin films were previously prepared by compression moulding in a hot press at 90 °C.

#### *5.2.3.4 Activation energy*

The activation energy ($E_a$) of the HPNEVA27 hybrid was determined using gel content values. The nanocomposite was prepared at three different temperatures (90, 100 and 110 °C) according to the procedure described above and samples were collected after 3, 7 and 10 min of mixing. For all samples, the gel content was measured according to the method described previously. For each temperature, the crosslinking rate was determined as the slope of gel content *vs* time reaction, as described by Shieh [12]. Then, the $E_a$ was calculated from the plot of the crosslinking reaction rate at the three different temperatures as a function of the reciprocal absolute temperature, according to the Arrhenius equation:

$$\ln(k) = \ln A - \frac{E_a}{R}\frac{1}{T} \qquad \text{Equation 5.4}$$

where $k$ is the crosslinking rate, $E_a$ is the activation energy, $R$ is the gas constant and $T$ is the absolute temperature.

#### *5.2.3.5 SEM and EDS*

Scanning electron microscopy (SEM) analysis was performed in a Leica Cambridge S360 microscope in back-scatter mode. The samples were previously fractured in liquid nitrogen and coated with a gold thin film. X-ray microanalysis mapping was performed in 300 $\mu m^2$, in the same place where SEM analysis was made, with an energy dispersive X-ray Spectrometer (EDS) from Link eXL II from Oxford Instruments attached to the SEM.

#### *5.2.3.6 TEM*

Samples of 70 nm thickness were cut using a diamond knife, in a Leica ultramicrotome at -60 °C. The cut sections were transferred onto copper grids and then analysed without stain in a Philips CM120 transmission electron microscope (TEM).

#### *5.2.3.7 Thermal stability*

The EVA hybrids thermal stability was assessed by thermogravimetric measurements (TGA) carried out in a TA Q500 thermobalance. Samples were heated from 30 °C to 600 °C at 10 °C/min under a nitrogen flow (50 mL/min).

#### *5.2.3.8 UL94 test*

The flammability behaviour of the EVA nanocomposites was investigated according to UL-94 test using 2 mm thick specimens ignited from the bottom in the vertical configuration [13].

## 5.3 RESULTS AND DISCUSSION

Figure 5.1 shows the torque evolution along mixing time for HPNEVA12 and HPNEVA27. The first peak is associated to EVA melting followed by the addition of the aluminium precursor. The effect of aluminium precursor on both EVAs chemical structure is clear, in both cases after the addition of the aluminium precursor the torque increased. This is due to the crosslinking reaction between vinyl acetate groups and aluminium precursor. Since EVA27 has more vinyl acetate groups, a more crosslinked structure would be anticipated and consequently higher torque. However, EVA27 (71 °C) has lower melting temperature than EVA12 (96 °C), which results in a decrease of viscosity and consequently lower torque for HPNEVA27. Thus, the nanocomposite torque value was always under HPNEVA12. Moreover, as shown by Antunes et al. [14], the decrease of the torque values observed for HPNEVA27 at around eleven minutes can be attributed to the network degradation. This phenomenon occurs for materials with very high crosslinking contents.

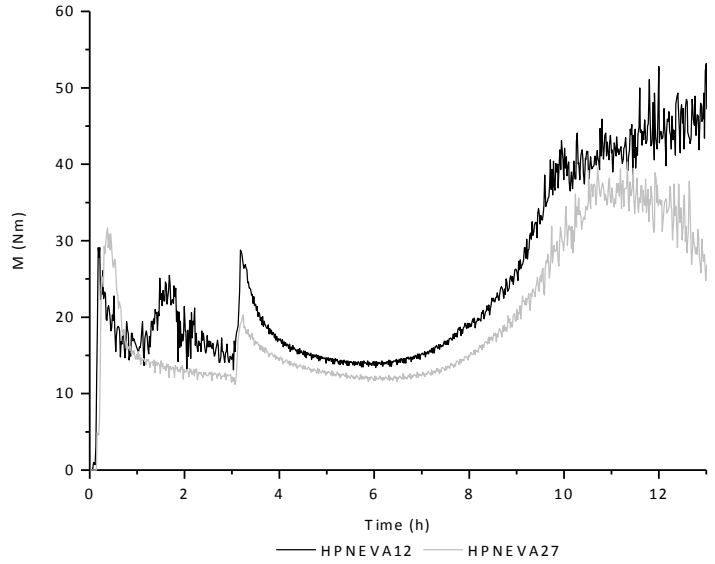


Figure 5.1 – Torque evolution during HPNEVA12 and HPNEVA27 preparation.

As shown in Figure 5.2, for both EVAs, the storage modulus and complex viscosity increase along reaction time, which is due to the crosslinking reaction. Crosslinking affects the molecular motion and has a significant effect on rheological behaviour [10]. As the reaction takes place the material changes from liquid-like to solid-like material. The nanocomposites prepared do not show a plateau at low frequencies and the complex viscosity has, in the limit, a slope of minus one [5].

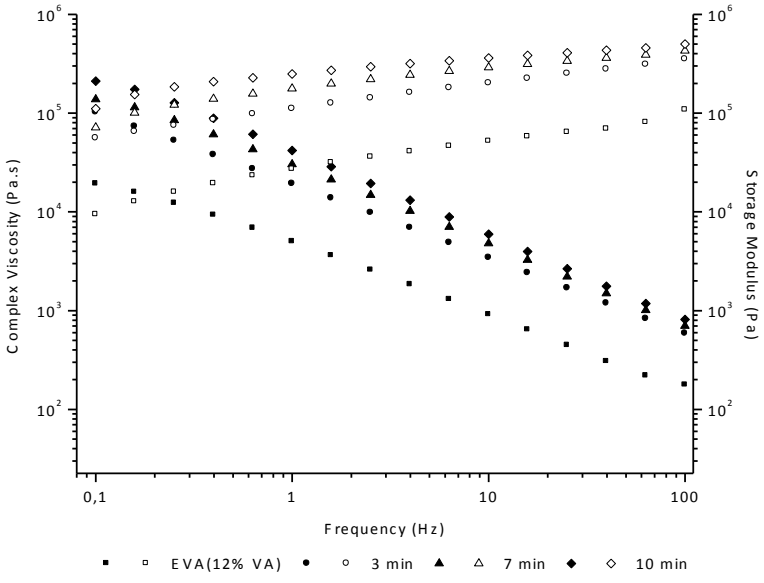


(a)

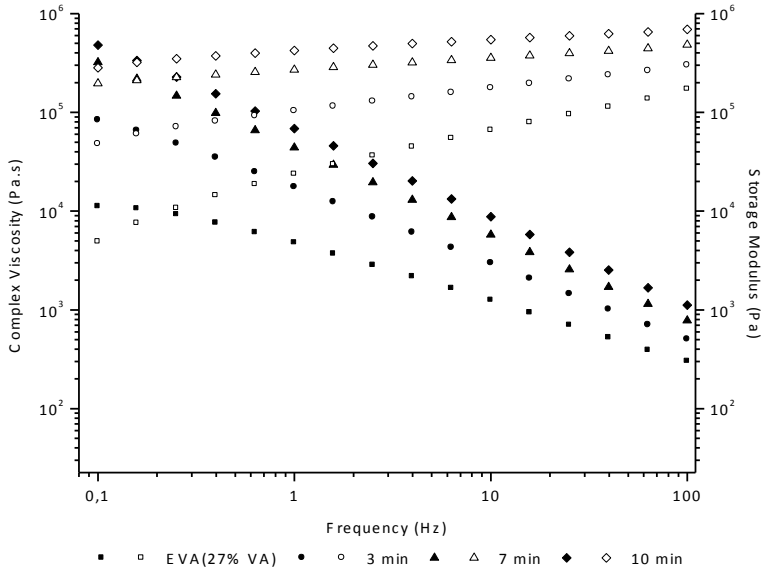


(b)

Figure 5.2 – Rheological behaviour of a) HPNEVA12 and b) HPNEVA27.

Table 5.1 describes the curves slope evolution for both EVAs at different reaction times. For both HPNEVAs it is clear the evolution of the crosslinking structure based on the curves slope values. Moreover, and spite the lower torque values, rheological measurements confirm that HPNEVA27 as higher crosslinking level.

Table 5.1 – Complex viscosity curves slope for HPNEVA12 and HPNEVA27.

| | 3 min | 7 min | 10 min |
|---|---|---|---|
| HPNEVA12 | - 0.75 | - 0.78 | - 0.83 |
| HPNEVA27 | - 0.76 | - 0.88 | - 0.89 |

The storage modulus of the nanocomposites appears to be constant over a very broad range of frequencies. From the theory of the rubber elasticity, the equilibrium shear elasticity modulus ($G_e$) can be determined based on the slop of the tangent curve to G' at low frequencies [10,14]. Using $G_e$ and the Flory-Rehner model coupled with the phantom network it is possible to predict the swelling results of a imperfect network:

$$\nu = \frac{G_e}{RT} \qquad \text{Equation 5.5}$$

where $v$ is the crosslinking density, $R$ is the universal gas constant and $T$ is the absolute temperature. $G_e$ was taken as the asymptotic value of G' at low frequency. Figure 5.3 depicts the theoretical values of ν determined using Equation 5.5 and the experimental data measured by the swelling degree experiments.

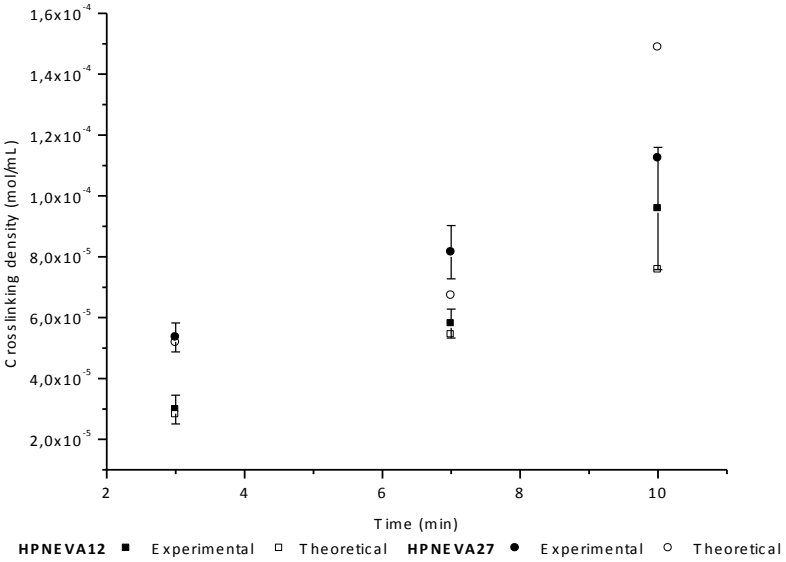


Figure 5.3 – Crosslinking density evolution along the reaction time for HPNEVA12 and HPNEVA27.

Both EVAs show the same trend, the crosslinking density increases along the time. Nevertheless, as expected HPNEVA27 exhibits higher crosslinking density values as a result of the higher amount of vinyl acetate groups that react to form covalent bounds with aluminium particles. A different result was observed by Bounor-Legaré and co-workers, the crosslinking density decreased along the time during the reaction between EVA and tetrapropoxysilane (TPOS) [10]. However, in their study the sol-gel reaction occurred during a post step treatment to promote the hydrolysis condensation reaction. They explained the decrease due to side reactions.

The theoretical crosslinking density values determined using Equation 5.5 are in good agreement with the experimental results for reaction times of 3 and 7 min. A slightly different between theoretical and experimental values was observed for 10 min of reaction. This can be explained by the fact that at 10 min the G' values remained almost constant in a very broad range of frequencies, in this case the $G_e$ corresponds to the constant value of G' [15].

FT-IR analysis of initial EVAs and nanocomposites are shown in Figure 5.4. For both prepared hybrids the appearance of OH band between 3000 – 3500 $cm^{-1}$ confirms that aluminium precursor suffer hydrolysis reactions with respective bending mode band at 1627 $cm^{-1}$ with medium intensity. Moreover, the Al-O stretching mode band between 400 – 1000 $cm^{-1}$ can also be observed, which confirms that the sol-gel reaction has been successfully carried out. Differences can also be noticed in the peak of the C=O stretching mode of the acetate group (Figure 5.4b). After reaction, for both EVAs, the peak becomes less wide. This corroborates the reaction between the acetate groups and the precursor.

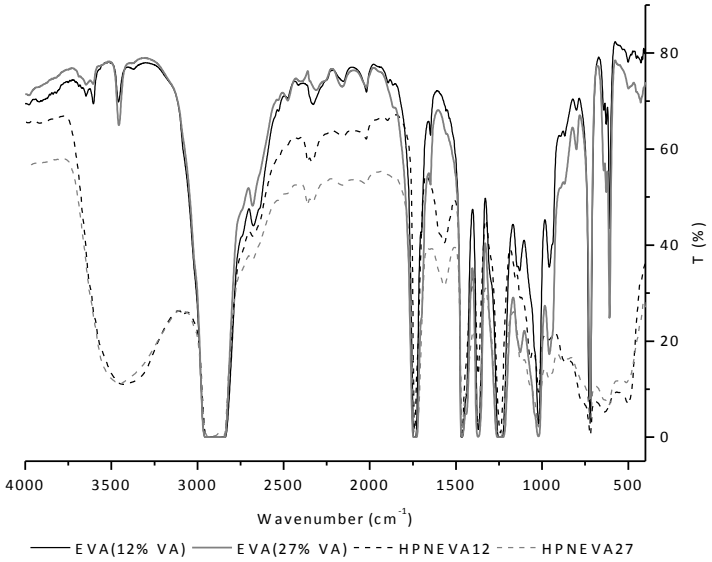


(a)

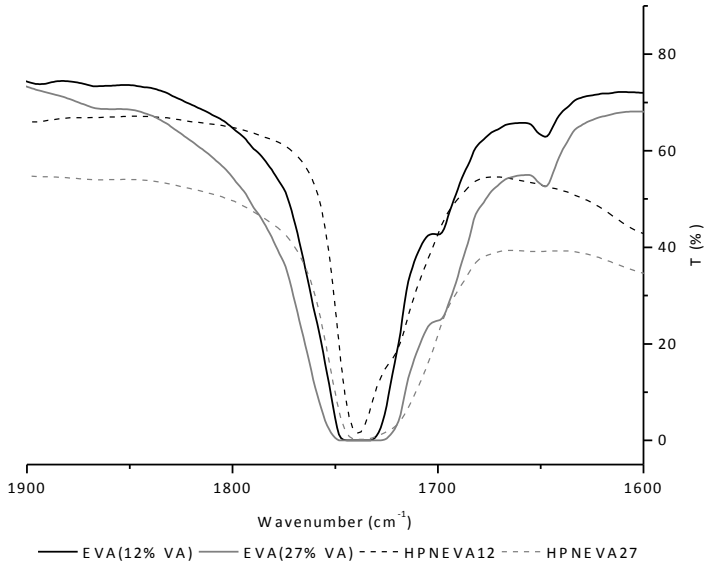


(b)

Figure 5.4 – FT-IR spectra a) EVA polymers and nanocomposites and b) zoom of carbonyl band.

The reactivity of the system was assesses by the determination of the activation energy ($E_a$) involved in the synthesis of HPNEVA27. Figure 5.5 depicts the Arrhenius plots obtained for HPNEVA27. A linear relationship was found corresponding to a $E_a$ of 36.3 kJ/mol. Bounor-Legaré and co-workers obtained similar Ea value (47 kJ/mol) for the synthesis of EVA (28 % of VA) with tetraethoxysilane (TEOS) using as catalyst dibutyltin oxide (DBTO) [10]. The precursor $Al(Pr\text{-}i\text{-}O)_3$ reveals to be very reactive, which can be explained by the linear organic chain ($\text{-}OC_3H_7$) with low the stereochemical hindrance.

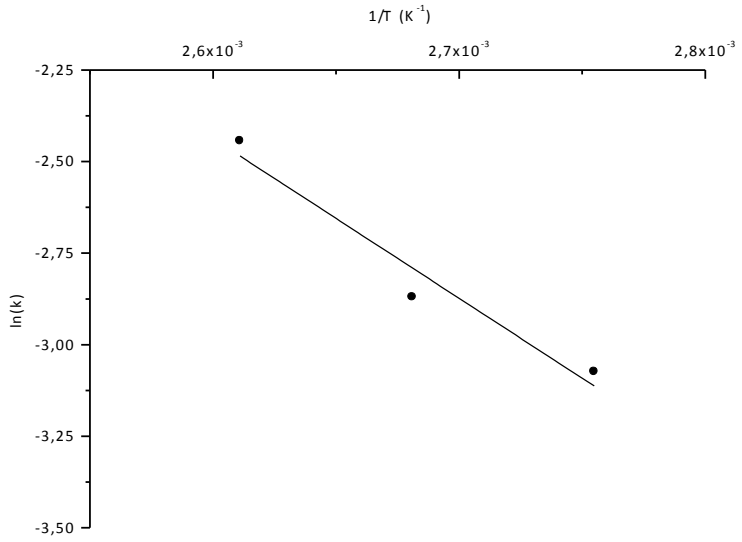


Figure 5.5 – Arrhenius plots for the synthesis reactions of HPNEVA27.

Taking into account the previous results a reaction mechanism can be proposed (Figure 5.6). According to this chemical scheme, one alkoxide group from $Al(Pr\text{-}i\text{-}O)_3$ reacts with vinyl acetate and the acetate group leaves as isopropyl acetate. As $Al(Pr\text{-}i\text{-}O)_3$ is a trifunctional compound, two and three exchanges can take place leading to a crosslinking structure.

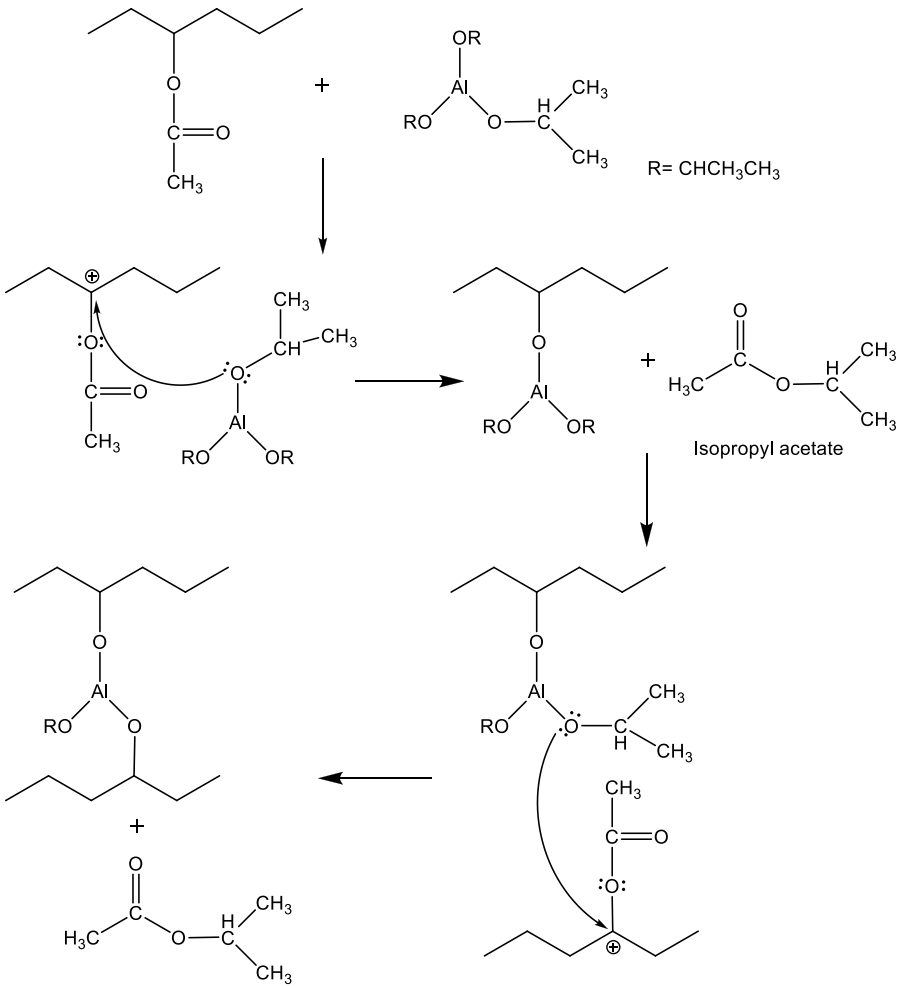


Figure 5.6 – Reaction mechanism for the synthesis of EVA hybrids.

The back-scattered electrons (BSE) SEM was used to analyse the aluminium particles dispersion on EVA matrices. BSE micrographs presented in Figure 5.7 shows that HPNEVA12 and HPNEVA27 have homogeneous and smoother surfaces without presence of aluminium agglomerates. In Figure 5.7a it can be observed the presence of small white shining dots well dispersed on EVA surface. These dots, were analysed by EDS as aluminium nanoparticles. In the case of HPNEVA27 (Figure 5.7b) only a few white dots could be seen, which could indicate a better dispersion and interaction between organic and inorganic components. As confirmed by rheology and crosslinking density results, the reaction was more extensive with this polymer. TEM micrographs (Figure 5.8) confirm that even though the aluminium particles are well dispersed in both EVAs matrices, it seems better in EVA27. The average particle size is 130 and 120 nm for HPNEVA12 and HPNEVA27, respectively.

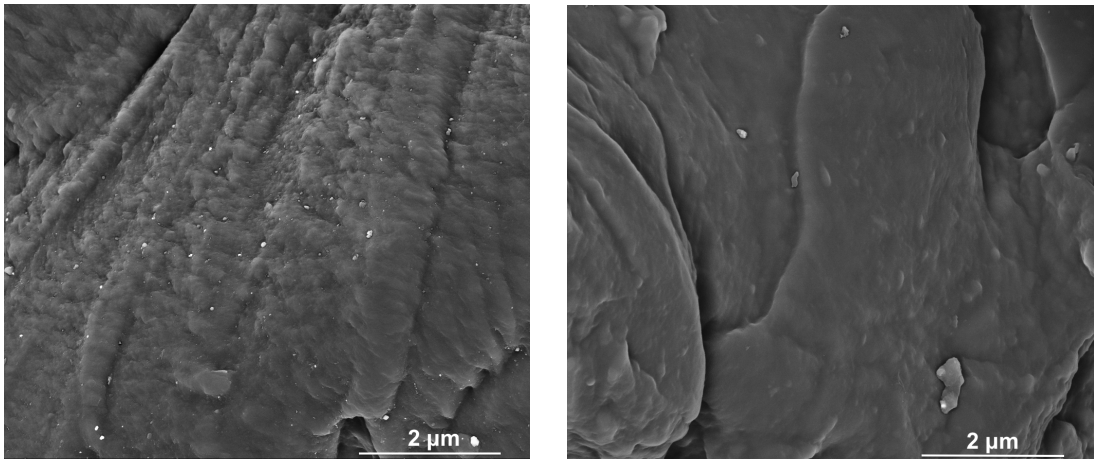


(a) (b)

Figure 5.7 – SEM micrographs of a) HPNEVA12 surface and b) HPNEVA27 surface.

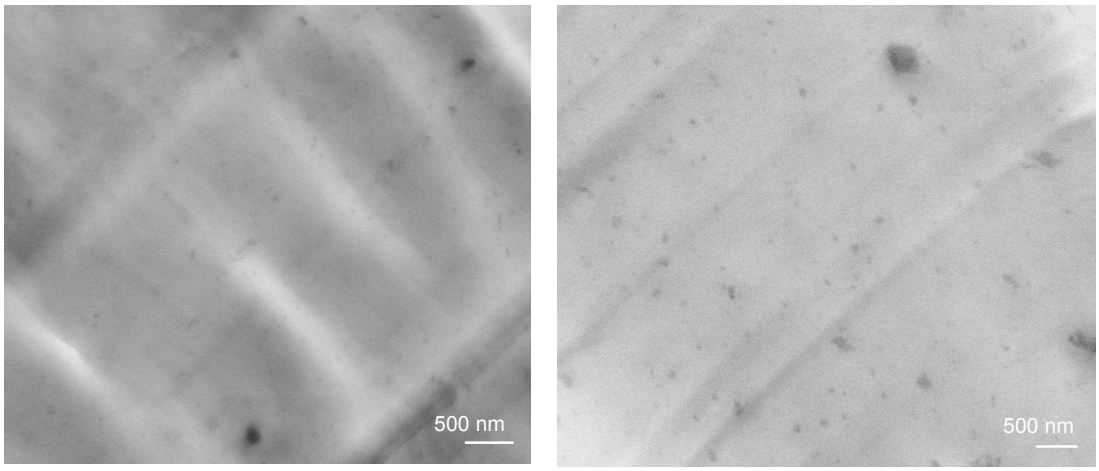


(a) (b)

Figure 5.8 – TEM micrographs of a) HPNEVA12 and b) HPNEVA27.

The presence of aluminium at the material surface was analysed by EDS. The spectra of Figure 5.9 indicate the presence of aluminium in both nanocomposites. The quantification of the spectra peaks gave the values of 5.07 % and 3.49 % of aluminium content for HPNEVA12 and HPNEVA27, respectively.

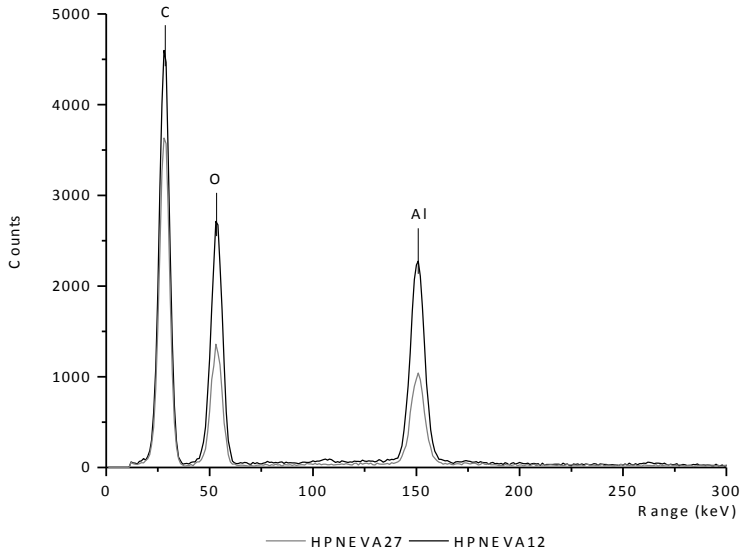


Figure 5.9 – EDS spectrum of EVA12 and EVA27.

The thermal properties of EVA matrices and nanocomposites were tested under nitrogen atmosphere and the data is presented in Figure 5.10. TGA results show that thermal degradation occurred in two distinct regions. The first around 300 °C degrees have been assigned to the loss of acetic acid and the second around 400 °C to the degradation of resulting unsaturated material poly(ethylene-co-acetylene) [16]. The HPNEVA12 and HPNEVA27 start to lose weight around 100 °C due to evaporation of some residual reaction sub-product. During EVA hybrids synthesis, isopropyl acetate ($C_5H_7O_2$) is formed (Figure 5.6), having a boiling point at 89 °C, this explained the first weight variation. Comparing the curves of EVA matrices and nanocomposites, it can be observed that the prepared materials have higher thermal stability. The crosslinking bonds between organic and inorganic components explain this behaviour. As expected, the residuals weight obtained for both materials is similar.

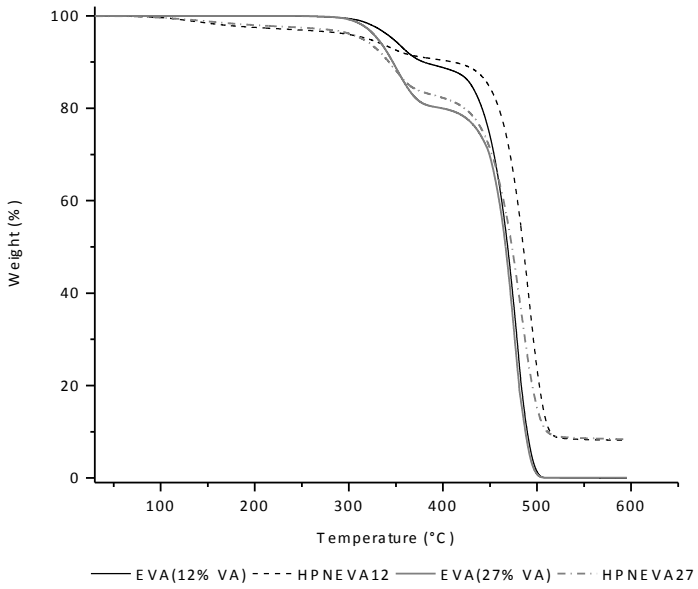


Figure 5.10 – Evaluation of thermal degradation of EVA matrixes and hybrids.

Preliminary fire retardant tests were performed to study the effect of aluminium nanoparticles on burning behaviour of HPNEVA12 and HPNEVA27. While specimens of EVAs matrices burned very quickly (10 s) and dripping at the same time, EVA nanocomposites exhibited higher resistance to flame propagation, increasing the combustion time (15 s), and the dripping effect was not observed.

## 5.4 CONCLUSION

This study show that is possible to incorporate aluminium nanoparticles well dispersed in a EVA matrix, by a method suitable to be used by the polymer processing industry. Since $Al(Pr\text{-}i\text{-}O)_3$ has a low activation energy, post step treatment to promote the formation of aluminium nanoparticles was not necessary.

The rheology and crosslinking density values demonstrate that aluminium is covalently bond to EVA structure forming a crosslinking structure. Morphological analysis corroborate that aluminium nanoparticles are well dispersed.

Taking into account all the results obtained, the reaction mechanism was proposed.

The thermal stability and fire retardancy of the EVA matrices was enhanced.

## 5.5 BIBLIOGRAPHY

[1] Sanchez, C. Shea, K. Kitagawa, S. 2011. Applications of advanced hybrid organic-inorganic nanomaterials: from laboratory to market. *Chemical Society Reviews* 40:696–753.

[2] Sadeghi, M. Khanbabaei, G. Dehaghani, A. Sadeghi, M. Aravand, M. Akbarzade, M. Khatti, S. 2008. Gas permeation properties of ethylene vinyl acetate-silica nanocomposite membranes. *Journal Membrane Science* 322(2):423–428.

[3] Bahloul, W. Bounor-Lagaré, V. David, L. Cassagnau, P. 2010. Morphology and viscosity of PP/$TiO_2$ nanocomposite prepared by *in situ* sol-gel method. *Journal Polymer Science, Part B: Polymer Physics* 48(11):1213–1222.

[4] Cong, H. Radosz, M. Towler, B. Shen, Y. 2008. Polymer–inorganic nanocomposite membranes for gas separation. *Separation Purification Technology* 55(3):281–291.

[5] Oliveira, M. Nogueira, R. Machado, A.V. 2012. Synthesis of aluminum nanoparticles into PP matrix: Effect of the alkoxide organic chain. *Reactive & Functional Polymers DOI: 10.1016/j.reactfunctpolym.2012.06.022*.

[6] Bounor-Legaré, V. Angelloz, C. Blanc, P. Cassagnau, P. Michel, A. 2004. A new route for organic-inorganic hybrid material synthesis through reactive processing without solvent. *Polymer* 45(5):1485–1493.

[7] Turova, N. Turevskaya, E. Kessler, E. Yanovskaya, M. 2002. The chemistry of metal alkoxides. *Kluwer Academic*, editor:1–6.

[8] Brinker, C. Scherer, G. 1989. Sol-gel science. The physics and chemistry of sol-gel processing. *Academic Press*, editor:2–12.

[9] Schottner, G. 2001. Hybrid sol-gel derived polymers: Aplications of multifunctional materials. *Chemical Materials* 13(10):3422–3435.

[10] Bounor-Legaré, V. Ferreira, I. Verbois, A. Cassagnau, P. Michel, A. 2002. New transesterification between ester and alkoxysilane groups: application to ethylene-co-vinyl acetate copolymer crosslinking. *Polymer* 43(23):6085–6092.

[11] Zhang, X. Guo, J. Chen, J. Wang, G. Liu, H. 2005. Investigation of interfacial modification for flame retardant ethylene acetate copolymer/alumina trihydrate nanocomposites. *Polymer Degradation Stability* 87(3):411–418.

[12] Shieh, Y. Liau, J. Chen, T. 2001. An investigation of water crosslinking reactions of silane grafted LDPE. *Journal Applied Polymer Science* 81(1):186–196.

[13] UL94, Test for flammability of plastic materials for parts in devices and applicances. (5th ed). Underwriters Laboratories, Inc.: Northbrook, IL, 1996.

[14] Antunes, C.F. Machado, A.V. Duin, M. 2009. Degradation of the rubber network during dynamic vulcanization of EPDM/PP blends using phenolic resol. *Rubber Chemical and Technology Journal* 82(5):492–505.

[15] Patel, S. Malone, S. Cohen, C. Gilmor, J. Colby, H. 1982. Elastic modulus and equilibrium swelling of poly(dimethylsiloxane) networks. *Macromolecules* 25(20):5241–5251.

[16] Costache, M. Jiang, D. Wilkie, C. 2005. Thermal degradation of ethylene–vinyl acetate coplymer nanocomposites. *Polymer* 46(18):6947–6958.

CHAPTER

# 6 HYBRID NANOCOMPOSITE PREPARATION IN A BATCH MIXER AND A TWIN-SCREW EXTRUDER

Hybrid polymer nanocomposite (HPN) with same composition were prepared in an internal mixer and in an extruder at the same temperature. Polypropylene grafted with maleic anhydride and aluminium isopropoxide were using as organic and inorganic components, respectively. Moreover, the chemical and morphological evolution along the extruder was followed. The HPNs were characterized by several techniques, such as, FT-IR, rheology, XRD, gel content, SEM/EDS and TEM.

Chemical and morphological characterization showed that the sol-gel reaction in the extruder was more extensive, the nanocomposite produced exhibited higher crosslinking level, smaller and more homogeneous nanoparticles. Along the extruder the nanoparticles size decreases as the reaction occurs.

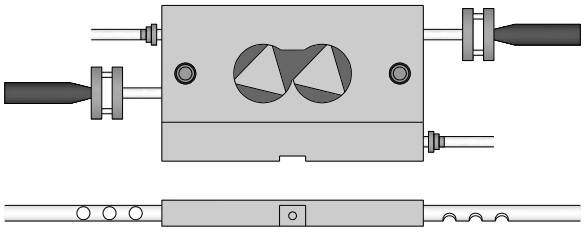

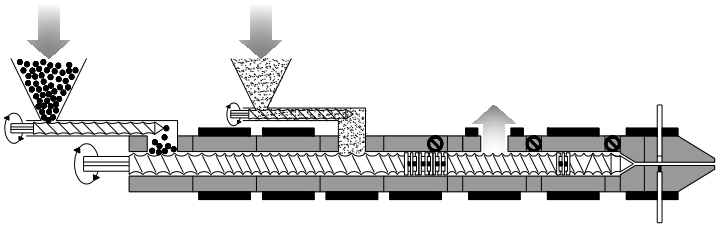

Oliveira, M. Nogueira, R. Machado, A.V. 2012. Hybrid nanocomposite preparation in a batch mixer and a twin-screw extruder. Submitted to *Advances in Polymer Technologies*

## 6.1 INTRODUCTION

Polymer systems, since early-to-middle of 20th century, started to receive considerable attention due to its unique properties, such as, easy to produce, light weight and often ductile nature [1,2]. Nevertheless, polymers have lower modulus, strength and fire resistance when compared to classic materials, like metals or ceramics [1]. Therefore, to overcome these disadvantages, the properties can be improved by addition of inorganic compounds (fibres, whiskers, platelets or particles) to polymers [1,3,4], which initiated a new field on polymer research, the *polymer nanocomposites* [5]. Polymeric/inorganic nanocomposites result from nano-size particles inclusions in a polymer matrix leading to new properties that could not be achieved by the polymer [6], keeping, at the same time, their light weight and ductile nature [1]. In fact, small amount of inorganic fillers, when well dispersed, can improve significantly the material properties, such as, gas permeability, thermal stability, flame retardance, mechanical performance and chemical resistance [7].

Since nanocomposites result from the combination of at least two phases and the degree of mixing between the two phases has great influence on final nanocomposite properties, the main challenge is to obtain homogenous nanofiller dispersion in the polymeric matrix [3,8]. Even though a variety of methods to produce polymer nanocomposite have been studied, the most used are melt mixing, in situ polymerization and in situ sol-gel reactions [1,6,9,10]. According to literature, in situ sol-gel reactions in the melt is one of the most suitable method to produce dispersed nanoparticles in a polymer matrix without solvent and it can be applied to industrial processes like extrusion [4,6,11]. This approach, applies the classic sol-gel method to extrusion, the hydrolysis-condensation reaction of metal alkoxide precursor can occur directly in the polymer melt [6,12]. The extruder and internal mixer act as a continuous or batch chemical reactor, respectively.

It is known that reactive extrusion is a complex process with many variables that can change during the process. Residence time, pressure, temperature, mixing and diffusion are parameters that govern the material final properties [11]. Therefore, sometimes for research work, an internal mixer, with fewer variables to consider, is used to developed materials. Nevertheless, at the same time, internal mixers are used to simulate the extrusion process. Thus, the main objective of this work is to compare the preparation of hybrid nanocomposites in an internal batch mixer and a twin-screw extruder. Moreover, the chemical reaction evolution and

nanoparticle dispersion along the extruder was also assessed. Nanocomposites with the same composition were prepared in an internal mixer and twin-screw extruder at the same temperature. The materials were characterized by several techniques, such as, FT-IR, rheology, XRD, gel content, SEM/EDS and TEM.

## 6.2 MATERIALS AND METHODS

### 6.2.1 MATERIALS AND REAGENTS

Polypropylene modified with maleic anhydride (PP-g-MA, Polybond 3200) with a melting temperature around 160 °C and a MA content of 1 wt.%, was supplied by Crompton. Aluminium isopropoxide ($Al(Pr\text{-}i\text{-}O)_3$) was used as received and was supplied by Sigma Aldrich.

### 6.2.2 NANOCOMPOSITES PREPARATION

#### *6.2.2.1 Internal mixer*

PP containing aluminium nanoparticles was prepared in the melt, in a Haake batch mixer (Rheocord 90; volume 60 mL), equipped with two rotors running in a counter-rotating way. The rotor speed was 50 rpm and the set temperature was 180 °C. The following procedure was adopted to prepare the nanocomposites, first pellets of PP-g-MA were introduced into the hot mixer, after melting, the aluminium precursor was added (15 and 25 wt.%). The total sample was removed after 10 min mixing. The hybrid nanocomposites (HPN) synthesized in the internal mixer was called *HPN-int*.

#### *6.2.2.2 Extruder*

A modular co-rotating twin-screw extruder, Leistritz LSM 30.34, was used (Figure 6.1). As in the internal mixer, 15 wt.% of aluminium precursor was added using a side feeder to PP-g-MA after melting. The barrel set temperature was 180 °C, the screw speed 200 rpm and the throughput 3.8 kg/h. The average residence time at the various sampling locations along the extruder, under the selected operating conditions, estimated using a tracer impulse technique, was 65, 105, 139 and 160 seconds for V1, V2, V3 and extrudate, respectively.

The molten polymer samples were collected along the screw axis and from the extrudate, and then quenched in liquid nitrogen in order to avoid further reaction (about 3 g sample in 300 mL liquid nitrogen) [13]. The hybrid nanocomposite (HPN) synthesized in the extruder was called HPN-ext.

The hybrid nanocomposite (HPN) synthesized in the extruder was called *HPN-ext*.

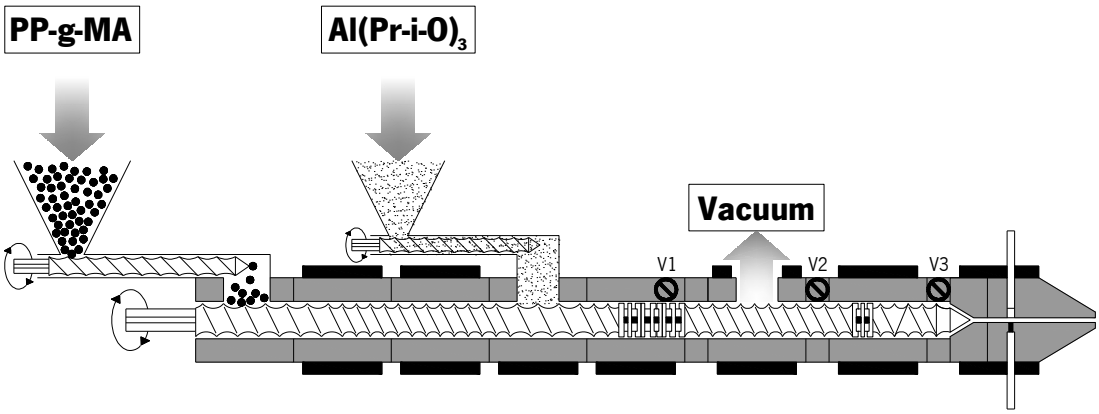


Figure 6.1 – Extruder layout.

### 6.2.3 CHARACTERIZATION

#### *6.2.3.1 FT-IR*

Infrared spectra of all HPNs were recorded in transmission mode between 400 $cm^{-1}$ and 4000 $cm^{-1}$ using a Perkin Elmer 1610 spectrometer, with 32 scans and a resolution of 4 $cm^{-1}$. Thin films were previously prepared by compression moulding in a hot press at 180 °C and analysed directly using a solid film support.

#### *6.2.3.2 XRD*

X-ray diffraction (XRD) spectra of the samples were obtained at room temperature using a Bruker D8 Discover X-ray equipment with Ni-filter. The applied current and accelerating voltage were 40 mA and 40 kV, respectively.

#### *6.2.3.3 Rheological properties*

The rheological behaviour of the initial polymers and prepared HPNs were determined by oscillatory rheological measurements carried out in a Paar Physica MCR300 rheometer at 180 °C. The gap and diameter of the plates was 1 mm and 25 mm, respectively. Nitrogen atmosphere was used to prevent thermo-oxidative degradation. A frequency sweep from 0.1 Hz to 100 Hz under constant strain in the linear viscoelastic region was performed for each sample.

#### *6.2.3.4 Gel content and crosslinking density*

Around 150 mg of samples were used to determine the gel content. The materials, previously weighted, were place in a 125-mesh stainless steel basket and immersed in hot xylene at 140 °C during 30 h. The final weight was determined after drying the samples in a vacuum oven at 105 °C during the night. The gel content was calculated as the weight of non-extractable material divided by the total weight of the original sample and was expressed as a percentage.

The crosslinking density was assessed from the volume swelling degree determination at equilibrium, as described by Oliveira [14].

#### *6.2.3.5 Morphological characterizationand*

Scanning electron microscopy (SEM) analysis was performed in a Leica Cambridge S360 microscope. The samples were previously fractured in liquid nitrogen and coated with a gold thin film. X-ray microanalysis mapping was performed on 300 μm2 in the same place where SEM micrographs were recorded, with an energy dispersive X-ray Spectrometer (EDS) from Link eXL II from Oxford Instruments attached to the SEM.

Transmission electronic microscope (TEM) pictures were taken from samples of 70 nm thickness cut using a diamond knife, in a Leica ultramicrotome at -40 °C. The cut sections were transferred onto copper grids and then analysed without staining in a Philips CM120, TEM.

## 6.3 RESULTS

### 6.3.1 COMPARISON BETWEEN INTERNAL MIXER AND EXTRUDER PREPARATION

The FT-IR spectra of PP-g-MA, HPN-int and HPN-ext are shown in Figure 6.2a. Nanocomposites prepared in the internal mixer and in the extruder present two new bands between 1000 – 400 $cm^{-1}$ and 3500 – 3000 $cm^{-1}$, corresponding to Al-O and OH stretching modes, respectively. The OH band, with respective bending mode band at 1627 $cm^{-1}$, confirms that the precursor has undergone hydrolysis. The presence of Al-O band indicates that sol-gel reaction was successfully carried out.

Comparing the spectra of HPN-int and HPN-ext it is clear that the OH band is smaller for the latter even though with less reaction time. This can be associated to higher reaction extension in extruder and to high efficient removal of the reaction by-product (2-propanol, $C_3H_7OH$) [9] due to devolatilization applied on the extruder barrel (Figure 6.1).

A more detailed inspection of the region 850 – 400 $cm^{-1}$ evidences more differences between the two prepared materials (Figure 6.2b). In the HPNs structure, aluminium oxide can exist in two different coordination states, tetrahedral and octahedral [15,16]. A broad band extending from 500 to 750 $cm^{-1}$ confirms the presence of tetrahedral Al-O coordination and bands at 500 and 640 $cm^{-1}$ are assigned to octahedral coordination. While these two bands can be clearly seen for HPN-ext indicating octahedral coordination, only a broad band is presented in HPN-int, suggesting tetrahedral Al-O coordination. This difference is directly related with the extension of the sol-gel reaction and consequently, with crosslinking density. Extensive sol-gel reactions result in higher levels of crosslinking density and different distribution of the inorganic domains.

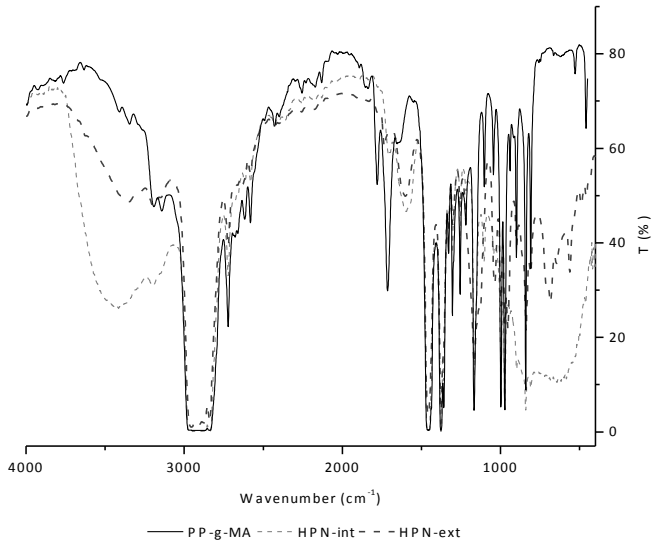


(a)

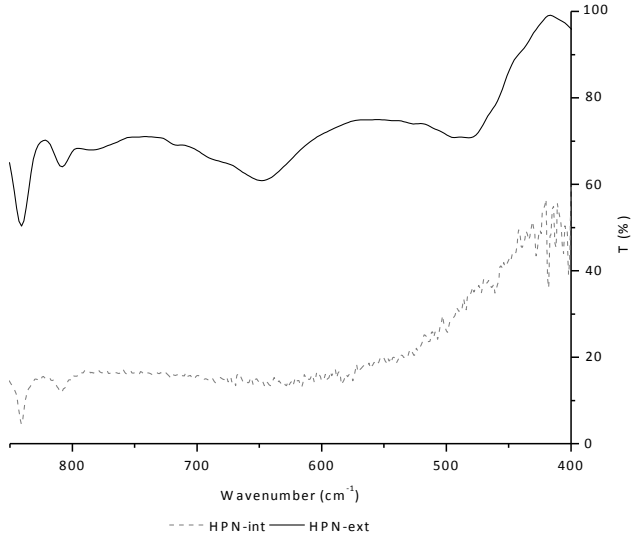


(b)

Figure 6.2 – a) FT-IR spectra of PP-g-MA, HPN-int and HPN-ext and b) FT-IR spectra of PP-g-MA, HPN-int and HPN-ext between 500 and 850 $cm^{-1}$.

The XRD spectra of PP-g-MA, HPN-int and HPN-ext are shown in Figure 6.3. The comparison of HPN-int and HPN-ext with PP-g-MA reveals new peaks at 19.8º, 20.9º, 23.9º, and 44.2º, which are in agreement with another work describe by Oliveira et al. [9]. Moreover, the results reveal

that the two methods used to prepare the nanocomposites do not affect the final microstructure of obtained nanocomposites. Then, the new peaks might be due to the presence of aluminium oxide hydroxide (AlOOH) and aluminium hydroxide ($Al(OH)_3$), as it was observed in FT-IR spectra. Nevertheless, the total number of peaks characteristics of either AlOOH or $Al(OH)_3$ are not present in the spectra, which makes difficult to conclude if these two species are really present.

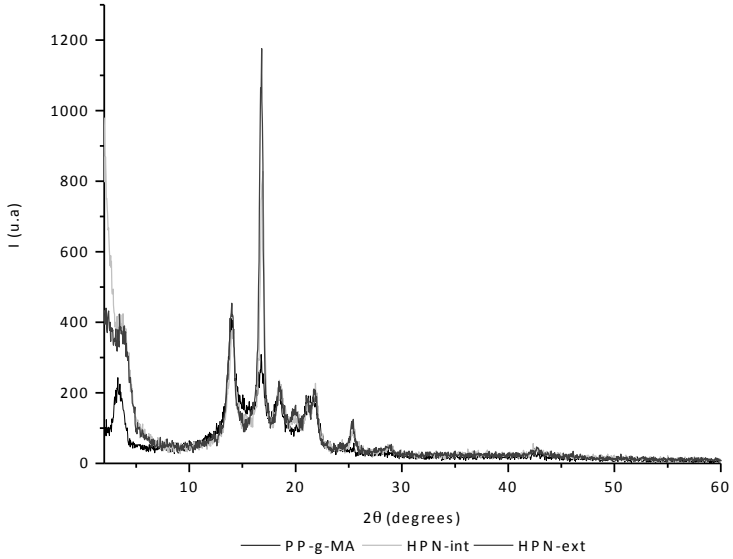


Figure 6.3 – XRD pattern for PP-g-MA, HPN-int and HPN-ext.

As shown by FTIR, $Al(Pr\text{-}i\text{-}O)_3$ reacts with PP-g-MA to form covalent bonds with the polymer backbone. Since the precursor has three reactive groups it can create three covalent bonds with PP, maximum. Therefore, depending on the reaction extension a polymer with different crosslinking degrees can be produced. The rheological behaviour of HPN-int and HPN-ext with different composition is depicted in Figure 6.4. The results obtained show a significant difference in viscosity and storage modulus between HPN-int and HPN-ext. Moreover, is possible to observe that HPN-ext has the same viscosity values as the nanocomposite produced in the internal mixer with 25 wt.% of precursor. This significant improvement in viscosity of the HPN-ext can be associated to the mixing efficiency in the extruder, which resulted in a more efficient sol-gel reaction and consequently more crosslinking. The storage modulus also increases and has the same trend, for the same amount of precursor. This change can be associated to the transition from liquid-like behaviour to solid-like, where storage modulus is almost constant in all frequency range, as it can be observed for HPN-ext. This type of behaviour is characteristic of a material with high crosslinking level.

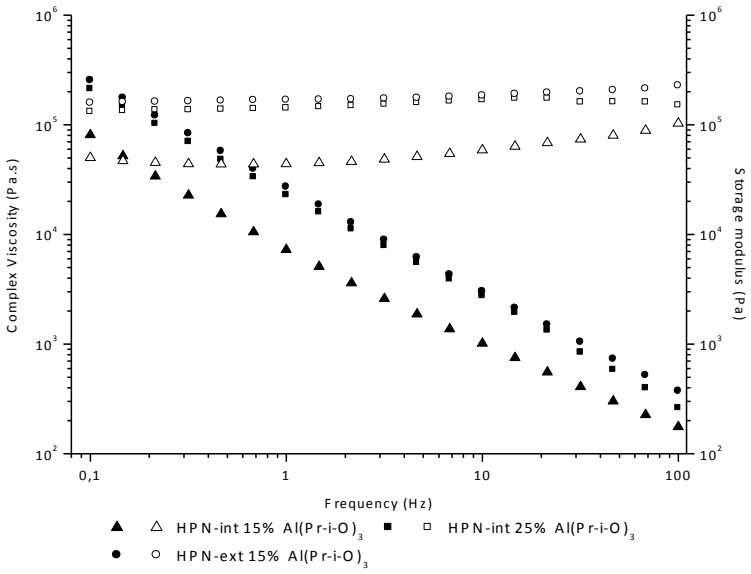


Figure 6.4 – Rheological behaviour of HPNs.

The gel content and crosslinking density values, depicted in Table 6.1, confirm the difference detected for viscosity and storage modulus, HPN-ext has similar gel content and crosslinking level to HPN-int produced with 25 wt.% of precursor. However, the gel content values obtained with the same composition are different, 48.7 and 69.6 % for HPN-int and HPN-ext, respectively. These results corroborate the FT-IR and rheological measurements that indicate that the sol-gel reaction was more extensive in the extruder.

Table 6.1 – Gel contente and crosslinking density values for HPNs.

| Samples | Gel content (%) | Crosslinking density (mol/mL) |
|---|---|---|
| HPN-int 15% wt. precursor | 48.7±3.2 | $7.77\times10^{-5} \pm 5.78\times10^{-6}$ |
| HPN-int 25% wt. precursor | 71.0±1.6 | $1.05\times10^{-4} \pm 2.08\times10^{-6}$ |
| HPN-ext 15% wt. precursor | 69.6±1.9 | $1.18\times10^{-4} \pm 9.99\times10^{-6}$ |

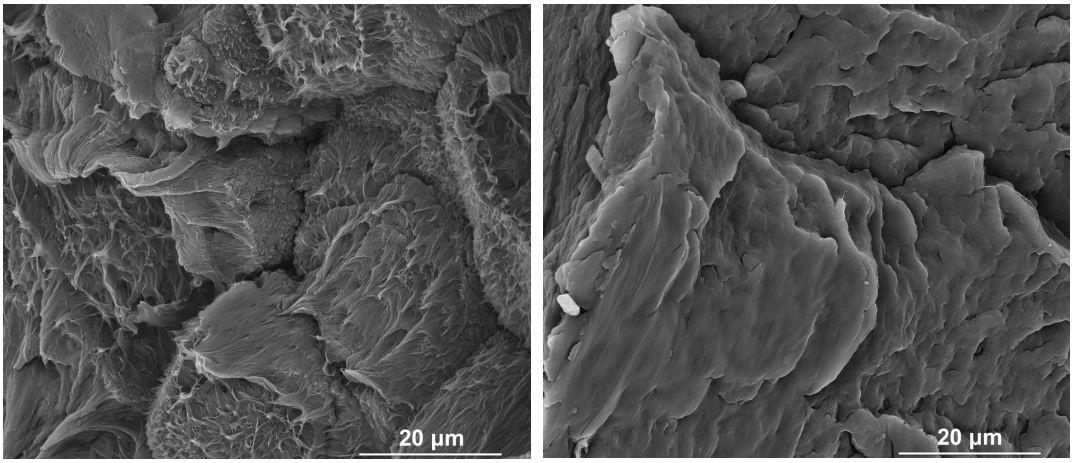


(a) (b)

Figure 6.5 – SEM micrographs of a) HPN-int and b) HPN-ext

The SEM micrographs, in back-scattered electrons (BSE) mode, of HPNs fracture surfaces are present in Figure 6.5. While HPN-int exhibits an heterogeneous surface (Figure 6.5a), HPN-ext micrograph (Figure 6.5b) shows a homogeneous and smooth surface, more cohesive and regular than HPN-int. Even though the micrographs were taken in the same area where EDS analysis was performed, due to a good dispersion it was not possible to detect any inorganic particles. Therefore, TEM analysis was accomplished to assess the nanoparticles dispersion achieved by the two preparation methods.

TEM micrographs depicted in Figure 6.6 clearly show that HPN-ext has a better particle dispersion with lower particle size, around 85 nm. HPN-int presents worst dispersion and bigger particles, about 155 nm. Since the reaction was more extensive in the extruder, which resulted in a higher crosslinking level, a better dispersion and smaller nanoparticle would be anticipated for HPN-ext.

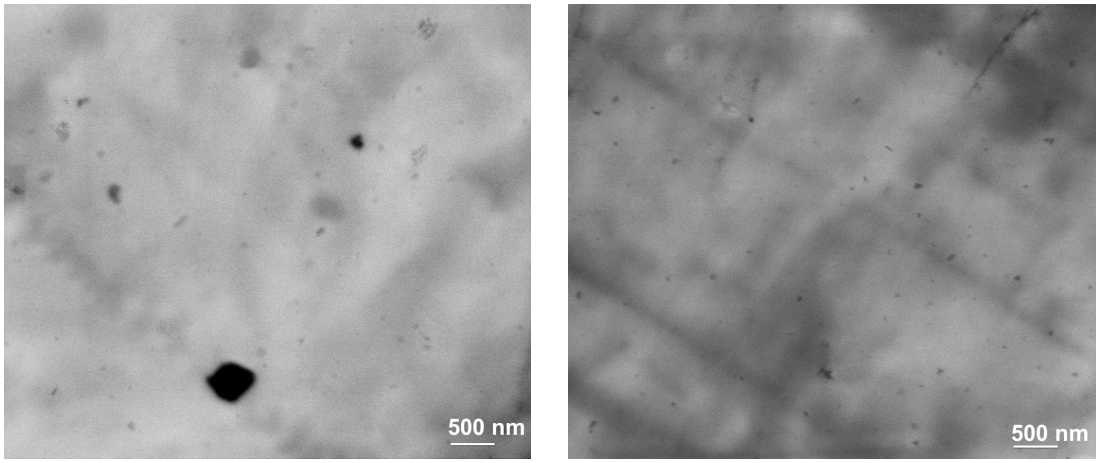


(a) (b)

Figure 6.6 – TEM micrographs of a) HPN-int and b) HPN-ext.

The EDS spectra of Figure 6.7 confirm that both HPNs contain aluminium. Moreover, similar value of aluminium content, for both nanocomposites, was obtained after quantification of the spectra peaks.

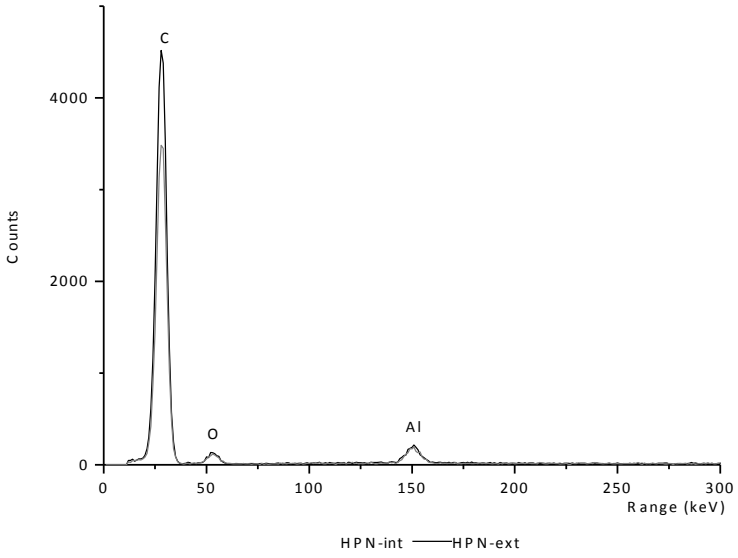


Figure 6.7 – EDS spectrum of HPNs surfaces.

### 6.3.2 EVOLUTION ALONG THE EXTRUDER

To follow the reaction evolution and morphology along the extruder during HPN-ext preparation, the samples collected at three different locations along the screw barrel (V1, V2, V3) and extrudate (Figure 6.1) were characterize by FTIR, gel content and TEM. Figure 6.8 depicted the

FTIR spectra of the samples collected along the extruder. The spectrum of the sample collected at V1 indicates that the reaction started very quickly, immediately after the precursor addition. However, along the extruder differences can be noticed at 3500 – 3000 $cm^{-1}$ and 1000 – 400 $cm^{-1}$ corresponding to OH and Al-O stretching modes, respectively. The decrease of intensity of the band between 3500 and 3000 $cm^{-1}$ along the extruder reveals that the reaction still going on until the extrudate. These results are in line with the gel content determination, at the first sampling location the gel content was already around 60 %, it increases along the barrel reaching a value of 70 % for the extrudate (Figure 6.9).

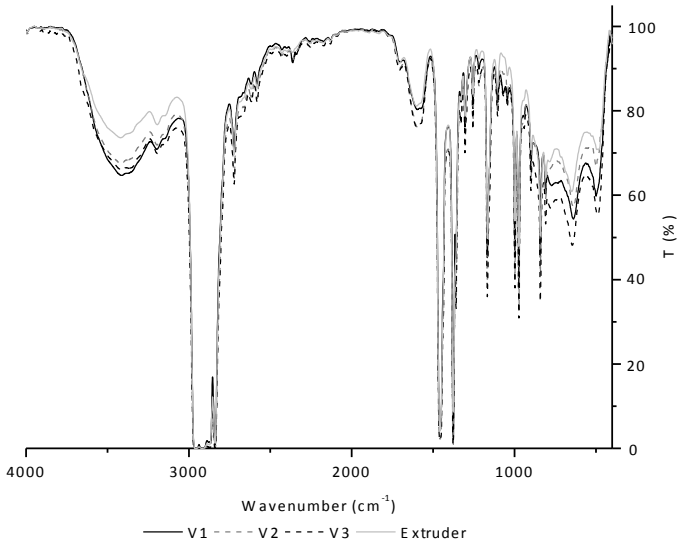


Figure 6.8 – FT-IR spectra evolution of HPN-ext along the extruder screw.

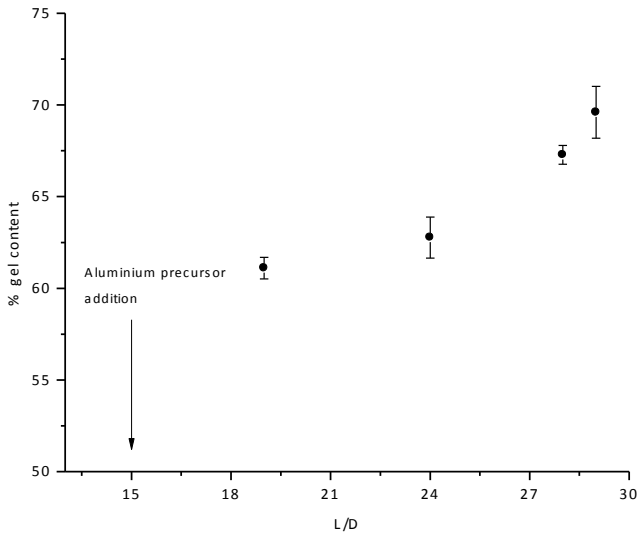


Figure 6.9 – Gel content evolution along the extruder screw.

TEM micrographs of the collected samples provide information the particles dispersion evolution along the extruder (Figure 6.10). At location L/D 19 a heterogeneous dispersion can be noticed with an average particle size of 150 nm. The particle size is 130 and 98 nm for L/D 24 and 28. A homogenous dispersion with small particles (85 nm) was achieved for the extrudate. Taking into account the FTIR, gel content results and TEM pictures, the particle size decreases as the reaction takes place.

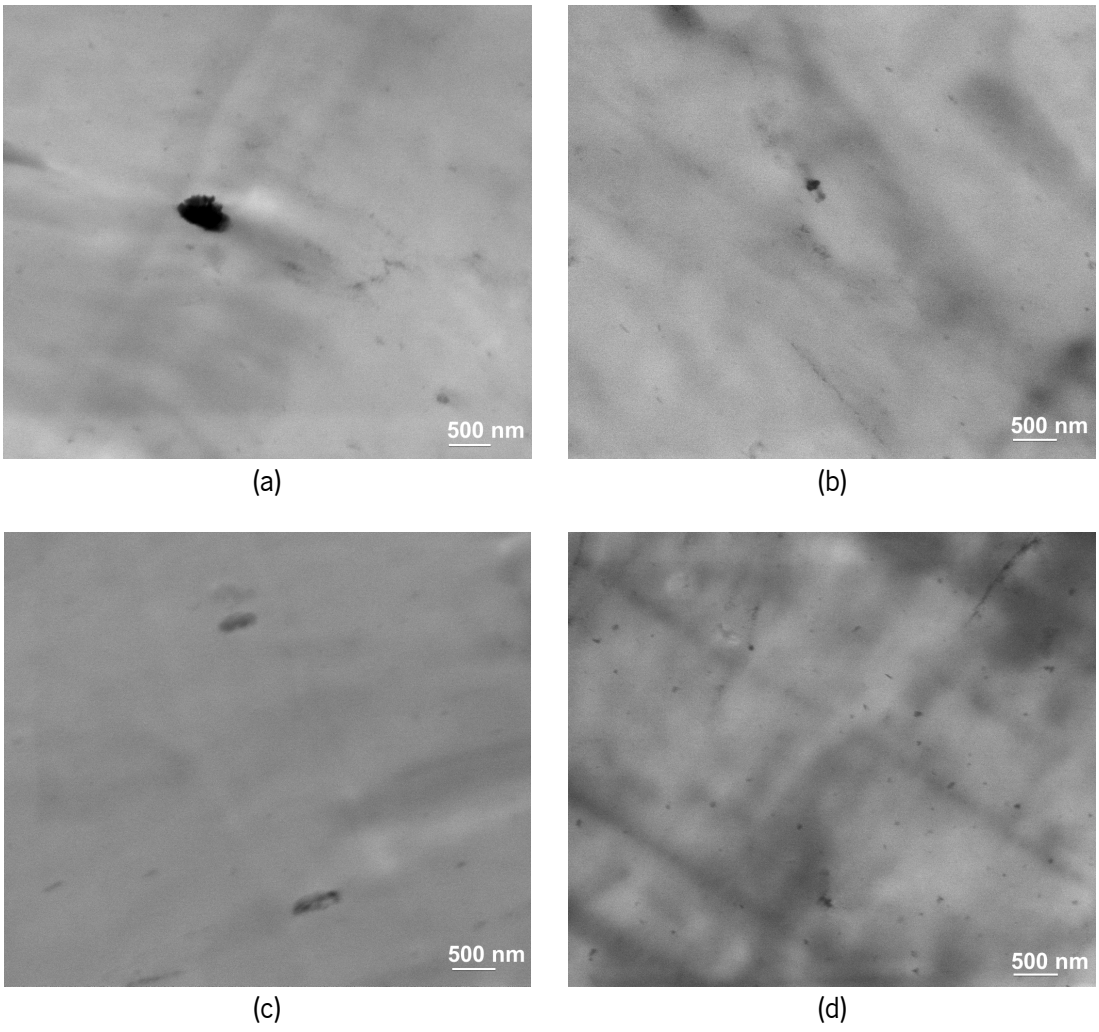


(a) (b)

(c) (d)

Figure 6.10 – TEM micrographs of HPN-ext at a) V1, b) V2, c) V3 and d) extrudate.

## 6.4 CONCLUSION

Hybrid polymer nanocomposites with the same composition were prepared in an internal mixer and in a twin-screw extruder at the same temperature.

Both FT-IR and rheological measurements showed that the sol-gel reaction was more extensive in the extruder. The nanocomposite prepared exhibited a more crosslinked structure. TEM micrographs evidenced that this nanocomposite presented smaller and well dispersed nanoparticles.

Both chemical reaction and morphology evolution occurs along the extruder. The particle size decreased as the chemical conversion increased.

## 6.5 BIBLIOGRAPHY

[1] Jordan, J. Jacob, K. Tannenbaum, R. Sharaf, M. Jasiuk, I. 2005. Experimental trends in polymer nanocomposites – a review. *Materials Science and Engineering A* 393(1-2):1–11.

[2] Schultz, J. 1974. Polymer materials science. *Prentice-Hall Inc. Englewood Cliffs*, editor:1–20.

[3] Ishida, H. Campbell, S. Blackwell, J. 2000. General approach to nanocomposite preparation. *Chemistry of Materials* 12(5):1260–1267.

[4] Di, Y. Iannace, S. Maio, E. Nicolais, L. 2003. Nanocomposites by melt intercalation based on polycaprolactone and organoclay. *Journal of Polymer Science Part B: Polymer Physics* 41(7):670–678.

[5] Krishnamoorti, R. Vaia, R. 2002. Polymer nanocomposites: synthesis, characterization and modelling. *American Chemical Society*, editor:1–6.

[6] Dou, D. Zhu, X. Peter, K. Demco, D. Möller, M. Melian, C. 2008. Preparation of polypropylene/silica composites by in-situ sol–gel processing using hyperbranched polyethoxysiloxane. *Journal of Sol-Gel Science and Technology* 48(1-2):51–60.

[7] Bahloul, W. Bounor-legaré, V. David, L. Cassagnau, P. 2010. Morphology and viscoelasticity of PP/$TiO_2$ nanocomposites prepared by in situ sol–gel method. *Journal of Polymer Science Part B: Polymer Physics* 48(11):1213–1222.

[8] Cong, H. Radosz, M. Towler, B. Shen, Y. 2008. Polymer–inorganic nanocomposite membranes for gas separation. *Separation Purification Technology* 55(3):281–291.

[9] Oliveira, M. Nogueira, R. Machado, A. 2012. Synthesis of aluminium nanoparticles in a PP matrix during melt processing: effect of the alkoxide organic chain. *Reactive & Functional Polymers DOI: 10.1016/j.reactfunctpolym.2012.06.022*.

[10] Rong, M. Zhang, M. Zheng, Y. Zeng, H. Walter, R. Friedrich, K. 2001. Structure–property relationships of irradiation grafted nano-inorganic particle filled polypropylene composites. *Polymer* 42(1):167–183.

[11] Bahloul, W. Oddes, O. Bounor-legaré, V. Mélis, F. Cassagnau, P. Vergnes, B. 2011. Reactive extrusion processing of polypropylene/$TiO_2$ nanocomposites by in situ synthesis of the nanofillers: experiments and modeling. *AIChE Journal* 57(8):2174–2184.

[12] Wanga, Y. Chena, F. Lib, Y. Wu, K. 2004. Melt processing of polypropylene/clay nanocomposites modified with maleated polypropylene compatibilizers. *Composites: Part B* 35(2):111–124.

[13] Machado, A.V. Covas, J.A. Duin, M. 1999. Evolution of Morphology in a Corotating Twin Screw Extruder. *Journal of Applied Polymer Science* 71(1):135–141.

[14] Oliveira, M. Nogueira, R. Machado, A.V. 2012. Preparation of EVA containing aluminium nanoparticles in the melt. *Submitted to Polymer Advanced Technologies.*

[15] Joe, I.H. Vasudevan, A.K. Aruldhas, G. Damodaran, A.D. Warrier, K.G.K. 1997. FT-IR as a Tool to Study High-Temperature Phase Formation in Sol–Gel Aluminium Titanate. *Journal of Solid State Chemistry* 131(1):181–184.

[16] Wengrovius, J.H. Garbauskas, M.F. Williams, E.A. Going, R.C. Donahue, P.E. Smith, J.F. 1986. Aluminum alkoxide chemistry revisited: synthesis, structures, and characterization of several aluminum alkoxide and siloxide complexes. *Journal of American Chemical Society* 108(5):982–989.

CHAPTER

# 7 PHOSPHORUS REMOVAL FROM EUTROPHIC WATERS WITH AN ALUMINIUM HYBRID NANOCOMPOSITE

An excess of phosphorus (P) is the most common cause of eutrophication of freshwater bodies. Thus, it is imperative to reduce the concentration of P to prevent harmful algal blooms. Moreover, recovery of P has been gaining importance because its natural source will be exhausted in the near future. Therefore, the present work investigated the removal and recovery of phosphate from water using a new developed hybrid nanocomposite containing aluminium nanoparticles (HPN).

The HPN-Pr removes 0.80±0.01 mgP/g in a pH interval between 2.0 and 6.5. The adsorption mechanism was described by a Freundlich adsorption model. The material presented a good selectivity for phosphate and could be regenerated using an HCl dilute solution.

The factors that contribute mostly to the attractiveness of HPN-Pr as a phosphate sorbent are its moderate removal capacity, feasible of production at industrial scale, reuse after regeneration and recovery of phosphate.

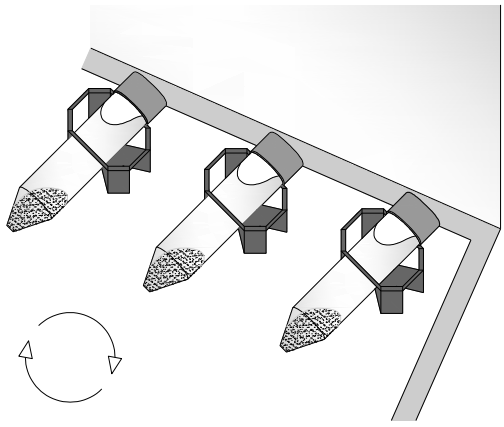

Oliveira, M. Machado, A.V. Nogueira, R. 2012. Phosphorus removal from eutrophic waters with an aluminium hybrid nanocomposite. *Water, Air, & Soil Pollution DOI: 10.1007/s11270-012-1239-9*

## 7.1 INTRODUCTION

Correll (1999) in his review work reported that the excess of phosphorus (P) is the most common cause of eutrophication in freshwater bodies: namely, lakes, reservoirs, streams, and headwaters of estuarine systems [1]. The high input of P to water bodies that has been observed in the last decades results from two main sources: namely, the growth of human population and inherent activities (point source of P) and the excessive use of fertilizers containing P to increase the production of crops (non point source of P). Nowadays, the classification of the trophic state of freshwater bodies used in most of the European countries is based on the concentration of P and algal density present in the water column. In fact, a concentration of P of 30 mg/L may be enough to provoke the excessive growth of aquatic plants and algal blooms [2-5]. Hickey and Gibbs (2009) reported that 51 % of the lakes in Great Britain with less than 1 ha required the implementation of P reduction measures to achieve the "good ecological status" prescribed by the Water Framework Directive until 2015 [5]. A study at global scale done by The Water Wheel reported that 54 % of the lakes and reservoirs in Asia are impaired by eutrophication, 53 % in Europe, 48 % in North America, 41 % in South America, and 28 % in Africa [6].

Several processes have been used to remove P from eutrophied freshwater bodies. Examples include chemical precipitation with aluminium, iron, calcium, and industrial by-products [7-10], and adsorption with clays [11]. Industrial by-products present a high removal capacity for P; however, they can contaminate the water with heavy metals. The use of aluminium and iron salts to precipitate P demands a tight control of the pH to avoid dissolution of the precipitates; in addition, the parallel reactions that occur consume part of the chemicals leading to the need of chemical overdose to guarantee the desired removal degree. Clay minerals have a tendency to disperse into very fine particles when applied to water bodies, which may cause an increase in turbidity for prolonged periods of time [12-16].

The present work investigated the removal of phosphate from water using a new developed hybrid nanocomposite containing aluminium nanoparticles (HPN). The HPN results from a reaction between an organic and an inorganic component, being the latter the removal agent for P. HPNs were obtained by a sol gel process, which took place during the mixing of a polymer in the molten state with an aluminium precursor. The chosen polymer was polypropylene grafted with maleic anhydride (PP-g-MA), and two aluminium precursors, aluminium isopropoxide ($Al(Pr\text{-}i\text{-}O)_3$) and aluminium acetylacetonate ($Al(acac)_3$) were used. The experiments done in the present

study comprised of short-term batch tests to compare the P removal rates of the HPN with that of other materials and column experiments to assess the long-term attenuation capacity of the HPN under conditions of continuous P loadings.

## 7.2 MATERIALS AND METHODS

### 7.2.1 MATERIALS AND HPN SYNTHESIS

Two different HPNs were synthesised based on a sol-gel reaction in the melt. This reaction allows a direct incorporation of aluminium nanoparticles into a polymeric matrix. The polypropylene grafted with maleic anhydride (PP-g-MA), supplied by Crompton, was the chosen polymer. Two distinct aluminium precursors, aluminium isopropoxide ($Al(Pr\text{-}i\text{-}O)_3$) and aluminium acetylacetonate ($Al(acac)_3$), supplied by Sigma Aldrich and Acros Organics, respectively, were used to produce aluminium nanoparticles into the HPN. The HPN synthesized with $Al(Pr\text{-}i\text{-}O)_3$ was named HPN-Pr, while the HPN synthesized with $Al(acac)_3$ was named HPN-acac. The HPN was produced in the melt, in a batch mixer (Haake Rheomix OS600; volume 60 mL), equipped with two rotors running in a counter-rotating way. The rotor speed was 50 rpm and the temperature was set to 180 °C. The following procedure was adopted: first the polymer pellets were introduced into the hot mixer and melted, then the aluminium precursor was added in a ratio 1:1 (maleic anhydride/precursor) and the mixing proceeded. After 10 min, the material was removed and crushed to a granular size between 100 – 300 μm. More detailed information on the synthesis and properties of HPN-Pr and HPN-acac can be found in Oliveira et al. 2012 [17].

The density and specific surface of HPN-Pr and HPN-acac were similar for both materials, 1.23 $g/cm^3$ and 2 $m^2/g$, respectively.

### 7.2.2 REACTION EXTENSION AND CHEMICAL PROPERTIES OF THE HPNS

#### *7.2.2.1 Reaction extension*

The incorporation of aluminium nanoparticles into the HPNs was determined by infrared analysis (FT-IR). Thin films were previously prepared by compression moulding of the HPNs in a hot press at 180 °C. FT-IR spectra of the materials were recorded using a Perkin Elmer 1610 in transmission mode between 400 $cm^{-1}$ and 4000 $cm^{-1}$, with 32 scans and resolution of 4 $cm^{-1}$.

#### *7.2.2.2 Chemical properties*

The zero point charge is usually defined as the pH value at which a solid submerged in an electrolyte exhibits zero net electrical charge on the surface [18,19]. To determine the zero point charge pH ($pH_{zpc}$) of the HPN-Pr and HPN-acac, 0.1 g of each material was placed in 50 mL of 0.1 M NaCl solution (used as an inert electrolyte) with initial pH in the range of 2.0 to 12.0. The pH was adjusted by either addition of chloridric acid or sodium hydroxide, using an ORION pH meter (model 420A). The experiments took place in sealed plastic Erlenmeyer flasks clamped into an orbital shaker at 100 rpm and 22 °C. Chemical equilibrium was attained after 24 h and the pH was then measured. Experiments were done in triplicate.

### 7.2.3 PHOSPHATE REMOVAL

#### *7.2.3.1 Effect of pH on phosphate removal by HPNs*

The effect of pH on phosphate removal by both HPNs, HPN-Pr and HPN-acac, was studied by a batch contacting method as follows: 0.04 g of each material was contacted with 50 mL solution containing 1000 µg/L P with initial pH in the range of 2.0 to 11.0. The tests were done in triplicate, at 100 rpm and 22 °C, for 5 d. The concentration of phosphate was measured in the beginning and at the end of the experiments by the ascorbic acid colorimetric method using a Shimadzu spectrophotometer (Method 4500P-E, Standard Methods, 1995) [20]. Potassium dihydrogenophosphate ($KH_2PO_4$, Merck) was used as the phosphate source.

#### *7.2.3.2 Removal capacity of P by HPNs*

The phosphate saturation potential of the HPNs was assessed by a batch contacting method. In this method, 0.04 g of each material was contacted with 50 mL solution containing 1000 µg/L P with initial pH of 6.0. The tests were done in triplicate, at 100 rpm and 22 °C, for 5 d. The concentration of phosphate was measured daily as previously described.

At the end of the tests, the aluminium concentration present in solution was determined by the electrothermal atomic absorption spectrometric method using a Shimadzu AA-6880F spectrometer (Method 3500Al-B, Standard Methods, 1995) [20]. The HPN that released the lowest amount of aluminium was selected for further studies.

The capacity of the HPN-Pr to remove polyphosphate was tested by the batch contacting method. In this method, 0.04 g the HPN-Pr was contacted with 50 mL solution containing 1000 µg/L of polyphosphate with initial pH of 6.0. The tests were done in triplicate, at 100 rpm and 22 °C, for 5 d. Pentasodiumtripolyphosphate ($Na_5P_3O_{10}.6H_2O$, Sigma Aldrich) was used as sources of polyphosphate. The concentration of phosphate was measured by ascorbic acid colorimetric method after a digestion process, as previously describe.

### *7.2.3.3 Phosphate adsorption isotherm on HPN-Pr*

The extent of P adsorption from solution was studied using a batch contacting method. The HPN that released the lowest amount of aluminium, HPN-Pr, was previously crushed to a granular size around 200 µm, and weighed in a range of 10 mg to 300 mg. The weighed materials were contacted with 50 mL solution containing 10 mgP/L with initial pH of 6.0. Adsorption took place in sealed plastic Erlenmeyer flasks clamped into an orbital shaker at 100 rpm and 22 °C, during 5 d. The tests were done in triplicate. At equilibrium, the concentration of phosphate in solution was measured as previously described. The amount of P adsorbed on the HPN-Pr at equilibrium was calculated according to Equation 7.1, where $X$ (g/kg) is the mass of P (g) removed per mass of HPN-Pr (kg), $C_{ini}$ is the initial concentration of P (g/L), $C_{eq}$ is the equilibrium concentration of P (g/L), $V$ is the solution volume (L), and $M$ is the mass of HPN-Pr (kg).

$$X = \left(C_{ini} - C_{eq}\right) \times \frac{V}{M} \qquad \text{Equation 7.1}$$

### *7.2.3.4 Column test*

A column test was preformed to assess the long-term attenuation capacity of the HPN-Pr, under a continuous P flow rate. A column of 90 mm and 35 mm of height and diameter, respectively, was packed with 17 g of HPN-Pr granules with size between 100 µm and 300 µm and the porosity of the bed was 0.19. A solution with 1000 µg/L P was continuously pumped through the column at a flow rate of 1 mL/min during 4 weeks. The time required for the solution to cross the column was calculated using Equation 7.2.

$$t = \frac{\pi \times r^2 \times h \times \theta}{Q} \qquad \text{Equation 7.2}$$

where $t$ is the residence time (h), $r$ is the radius of the column (cm), $h$ is the height of the HPN-Pr in the column (cm), $\theta$ is the porosity of the HPN-Pr bed inside the column, and $Q$ is the flow rate (mL/h).

#### *7.2.3.5 Regeneration and recovery study*

The HPN-Pr was cut in small squares of 2 x 2 mm and saturated with phosphate. For that, 0.2 g of HPN-Pr was contacted with 50 mL solution containing 1000 µg/L P with initial pH of 6.0. Experiments were done in triplicate, at 100 rpm and 22 °C, for 5 d. The concentration of phosphate was measured at the beginning and at the end of the batch tests. To recover the adsorbed phosphate and regenerate the HPN-Pr, the material was washed with 0.5 M NaOH or 0.5 M HCl during 10 s. The saturation and washing steps were repeated cyclically and in between the material was washed with deionized water. As a comparison, the same procedure was done without the regeneration step. Finally, X-ray microanalysis mapping was performed on the HPN-Pr surface to evaluate its chemical composition. An energy dispersive X-ray Spectrometer (EDS) from Link eXL II attached to an electronic microscope Oxford Instruments was used.

## 7.3 RESULTS AND DISCUSSION

### 7.3.1 CHEMICAL PROPERTIES

The synthesis of HPN was based in a sol-gel reaction consisting in the incorporation of aluminium nanoparticles into a polymeric matrix via a hydrolysis condensation reaction, as illustrated in Equation 7.3:

$$\text{PP-g-MA} + \text{Al}\left(\text{Pr-i-O}\right)_3 + 2\text{H}_2\text{O} \rightarrow \text{PP-g-MAAl}(\text{OH})_2 + 3\text{Pr-i-OH} \qquad \text{Equation 7.3}$$

where PP-g-MA is the organic compound, $Al(Pr\text{-}i\text{-}O)_3$ the aluminium precursor, $PP\text{-}g\text{-}MAAl(OH)_2$ the final HPN-Pr, and Pr-i-OH a by-product of the reaction.

The FT-IR spectra gave information about the hydrolysis condensation of the aluminium precursor and thus the new bonds formed. The spectra obtained for both HPNs are shown in Figure 7.1. To evaluate the extension of PP-g-MAAl(OH)$_2$ formation, it is important to analyse two spectral ranges: 3500 – 3000 cm$^{-1}$ where the OH stretching mode appears, and 1000 – 400 cm$^{-1}$ where the Al-O stretching mode occurs. In the spectra of HPN-Pr, a very broad band appeared around 3450 cm$^{-1}$ and another between 1000 – 400 cm$^{-1}$. Conversely, the OH or Al-O stretching modes were not observed in the spectra of HPN-acac. These results suggested that the precursor Al(Pr-i-O)$_3$, which has smaller organic groups, promoted the formation of aluminium nanoparticles chemically bond to the polymer backbone. On the contrary, Al(acac)$_3$ did not react with the polymer, as it can be concluded by the presence of two bands at 1520 cm$^{-1}$ and 1580 cm$^{-1}$ characteristic of the organic group (acac) connected to the aluminium. After being removed from the mixer, the HPN-acac consists in a physical mixture of polymer and aluminium precursor. A more detailed description of the synthesis and characterization of HPNs can be found in Oliveira et al. (2012) dedicated to the development of these materials [17].

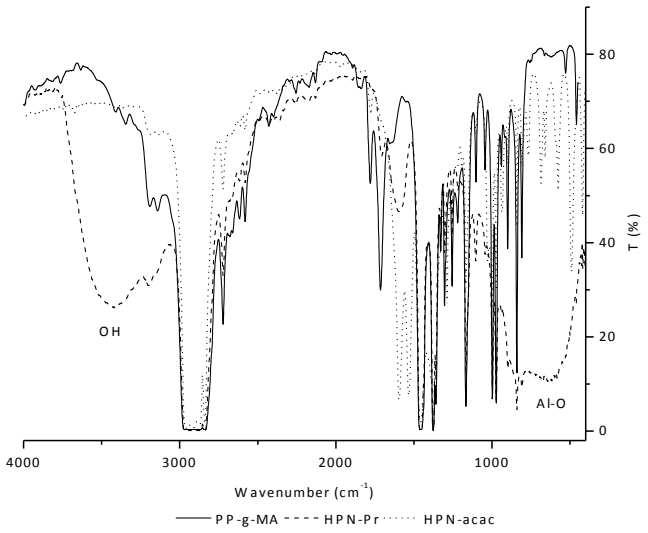


Figure 7.1 – FT-IR spectra of HPN-Pr and HPN-acac.

The pH of zero point charge (pH$_{ZPC}$) of the HPNs studied in the present work was derived from Figure 7.2. In the pH interval from 5.0 to 9.0, the pH at equilibrium was similar to the pH$_{ZPC}$ suggesting that the surface of both HPNs exhibited amphoteric properties acting as a buffer in this pH interval. No significant differences in charge density were observed between both HPNs and the pH$_{ZPC}$ values obtained ranged from 7.0 to 8.0.

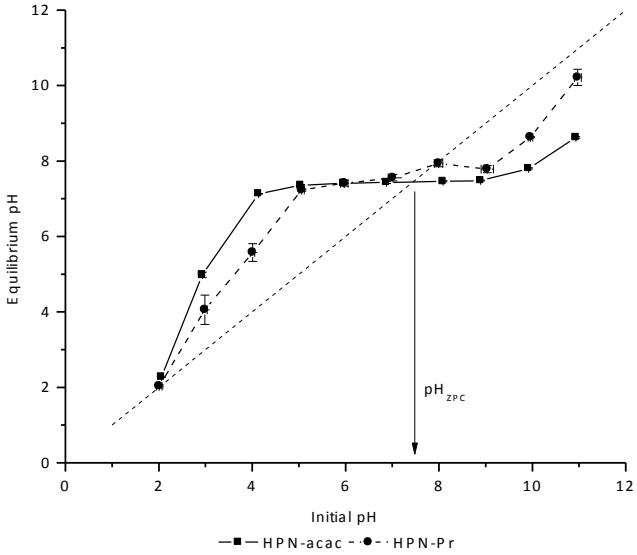


Figure 7.2 – Point of zero charge of HPNs.

## 7.3.2 P REMOVAL

### *7.3.2.1 Effect of pH on phosphate removal*

The effect of pH in the removal capacity of phosphate by both HPNs is shown in Figure 7.3. The HPN-Pr presented a maximum removal capacity in the pH interval of 2.0 to 6.5. For pH values near its $pH_{zpc}$ (7.0 – 8.0), a drastic reduction in the phosphate removal capacity was observed, due to the change of the surface charge from positive (+) to negative (–). Also, at high pH values, it was expected a decrease in the phosphate removal capacity due to $OH^-$ competition. HPN-acac depicted a maximum phosphate removal capacity in a narrower pH range, between 6.0 and 8.5. Moreover, for pH values above the $pH_{zpc}$ a reduction in the phosphate removal capacity was detected. A similar behaviour was described for $Al(OH)_3$ by [21]. Since HPN-acac consists in a physical mixture of polymer and aluminium precursor, the latter when immersed in water rapidly hydrolysed forming $Al(OH)_3$. This might explain the different behaviour.

Taking into account that the pH values found in freshwater bodies range from 2.5 to 8.2 [22-25], the HPN-Pr (7.22% oxide composition) has a broader application to remove phosphate compared to that of HPN-acac (2.84 % oxide composition).

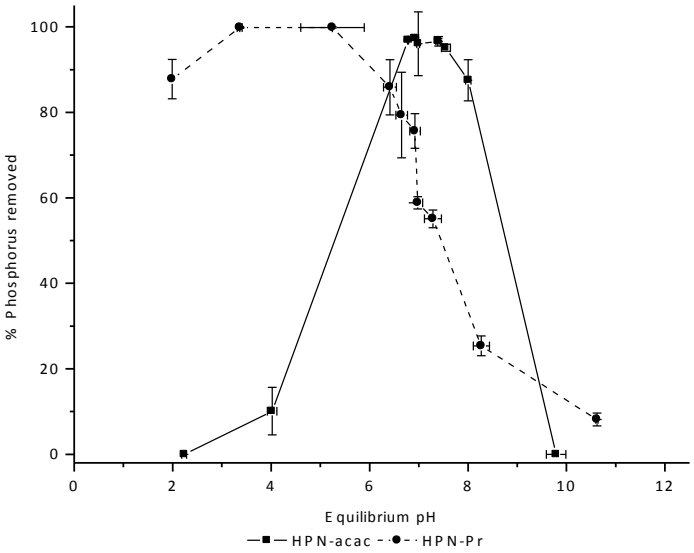


Figure 7.3 – Influence of pH on the phosphate removal capacity of HPNs.

### *7.3.2.2 Removal of P by HPNs*

The kinetic curves of P removal by both HPNs are depicted in Figure 7.4. A clear difference can be observed between both materials, the HPN-acac removed all phosphate in less than 24 h, while the HPN-Pr only lowered the phosphate concentration from 1000 µg/L P to 400 µg/L P in 5 d. The phosphate removal capacity was 0.80±0.01 mg/g for HPN-Pr and 1.27±0.02 mg/g for HPN-acac.

Bauxite and shale, both argillaceous rocks, presented a phosphate removal capacity of the same order of magnitude of HPN-Pr, 0.36 mg/g and 0.73 mg/g respectively. Previous studies showed that activated alumina, which is pure $Al_2O_3$, presented a phosphate removal capacity of 7 mg/g, which is almost 10 times higher than that of HPN-Pr [26,27]. Xiong and Peng (2011) using ferrihydrite-modified diatomite (89.2% $SiO_2$ and 4% $Al_2O_3$) achieved a total phosphorus removal efficiency of 85 % under anoxic conditions with an initial phosphorus concentration of 113 µg/L [28]. However, when comparing the phosphate removal capacity of HPN-Pr with other aluminium based materials described in literature (Table 7.1), we need to keep in mind that only a fraction of the HPN is active in removing phosphate (8 %). Clipnotiolite, a zeolite based on $SiO_2$ (65.90 %) and $Al_2O_3$ (12.97 %), presented a phosphate removal capacity of 2.15 mg/g that is higher than that of both HPNs developed in the present study (6.2% for HPN-Pr and 3.9% for HPN-acac) [27].

This fact might be due to the very high porosity and consequently internal surface area of zeolites. Also, a mesoporous silica has been functionalized with Cu and Fe to remove phosphate from water [29]. The removal capacity of these sorbents is much higher than that of both HPNs, which is due to, again, their huge internal area (169 $m^2/g$). Although it is very advantageous to use sorbents containing very small pores to maximize the removal capacity; on the other hand, the tiny pores with a size of angstroms might be immediately blocked, when used in natural systems where solid particles are present that have higher dimensions than the pores (for example bacteria have in average 1 μm), resulting in a fast decrease of the removal capacity. The approach followed in the present work was to produce a polymeric sorbent with a rough surface but without internal pores, whose surface area can be improved and optimized via a 3D structure. Future studies will be dedicated to improve the design of the HPN-Pr.

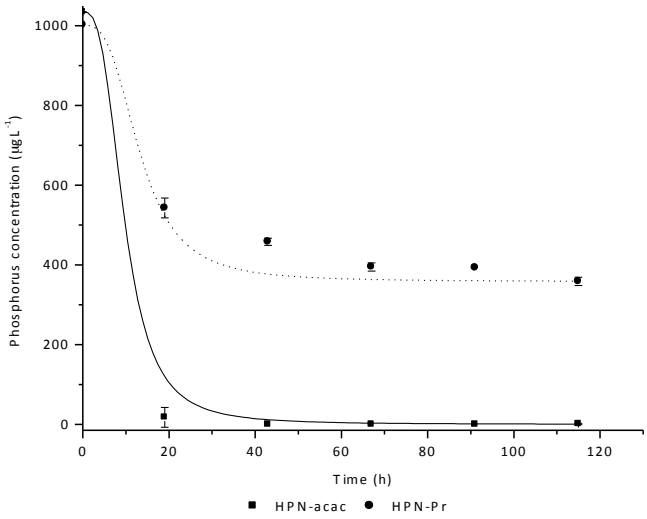


Figure 7.4 – Phosphate concentration profile for both HPNs at initial pH of 6.0.

Table 7.1 – Comparison of phosphate removal capacity of HPNs with other materials describe in the literature.

| | Phosphate removed (mg/g) |
|---|---|
| HPN-Pr | 0.80 |
| HPN-acac | 1.27 |
| Bauxite | 0.36 |
| Shale | 0.73 |
| Alumina | 7.00 |
| Clipnotiolite | 2.15 |

To assess the feasibility of both HPNs to remediate eutrophic freshwater bodies without further contamination, the concentration of aluminium was assessed after a batch contacting test. The results revealed that $6.9x10^{-3}\pm1.9x10^{-3}$ mg/L Al and 5.5±0.4 mg/L Al were obtained with HPN-Pr and HPN-acac, respectively. As expected by the FT-IR analysis and the pH test, the $Al(acac)_3$ precursor did not form covalent bonds with the polymer backbone and can easily hydrolyse into $Al(OH)_3$ provoking contamination of the water with aluminium. Therefore, the application of HPN-acac in freshwater bodies to remove phosphate is not recommended due to the water contamination with aluminium. Therefore, the HPN-Pr seems to be an interesting solution to remediate eutrophic freshwater bodies due to its stability and reasonable capacity to remove phosphate.

Besides phosphate, polyphosphate is also present in water bodies and gradually hydrolyses into phosphate contributing to the excessive growth of algae [30,31]. For this reason, the polyphosphate removal capacity of HPN-Pr was assessed from its concentration profile (data not shown). The amount of polyphosphate removed was 0.52±0.01 mgP/g and occurred mainly in the first 71 h. This value was slightly lower compared to that of phosphate. This fact might be related to the size of the anions, being orthophosphate ($H_2PO_4^-$, $HPO_4^{2-}$ and $PO_4^{3-}$) smaller and less complex than polyphosphate ($P_2O_7^{1-}$) thus orthophosphate can more easily be adsorbed [32]. Razali et al. (2007) reported a polyphosphate removal capacity of 7.4 mg/g for a by-product generated during the production of drinking water [33]. This was to be expected because this sludge was mainly constituted of aluminium (46 % as $Al_2O_3$).

### *7.3.2.3 P adsorption isotherm on HPN-Pr*

The adsorption isotherm of phosphate on the HPN-Pr was determined to assess the adsorption mechanism. The experimental data was fitted using the Freundlich model (Figure 7.5 and Equation 7.4) with a correlation coefficient of 0.986.

$$S = 0.76\times[C]^{0.56} \qquad \text{Equation 7.4}$$

where $S$ is the amount of P adsorbed (mg/g), and $C$ the equilibrium concentration (mg/L). The values of the equation constants $K$ and $n$ calculated were 0.76 $mg^{1-n}.g^{-1}.L^n$ and 1.79, respectively. In general, it is considered that the adsorption capacity of the adsorbent improves with the increase of the $K$ value [34]. The $K$ value obtained in the present study was higher than that reported by Kuroda for the adsorption of phosphate onto aluminium oxide (0.2). The $n$ value

obtained was higher than 1, indicating that P adsorption on HPN-Pr was a favourable process [35].

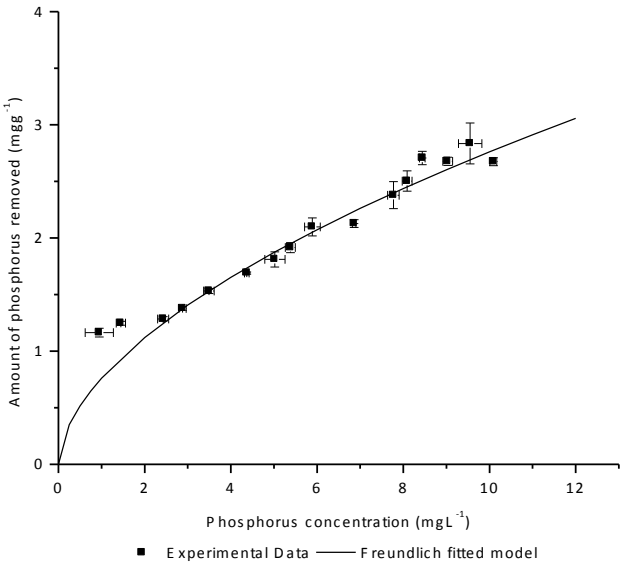


Figure 7.5 – Adsorption isotherm of phosphate onto HPN-Pr at initial pH of 6.0.

### *7.3.2.4 Column test*

The removal of phosphate in a packed bed column with HPN-Pr along 30 d is depicted in Figure 7.6. The residence time (t) determined was around 29 min. The removal efficiency of phosphate was 100 % during the first 40 h of operation. It decreased to 50 % at the end of 134 h, and the column reached complete saturation at 500 h. The removal capacity determined in the column test was 0.67 mgP/g, which was lower than that obtained in batch essays. This result might be explained by the low porosity of the particles, 0.19, and the very small HPN-Pr particles (100-300 μm). Since they are very small they can easily compacted, this would decrease the contact between the material and the solution resulting in lower remover capacity. Future studies will test higher granulometry of the material. In a similar study with alum residues, 0.48 mgP/g were removed from an aquaculture process water at pH 7.0 [36].

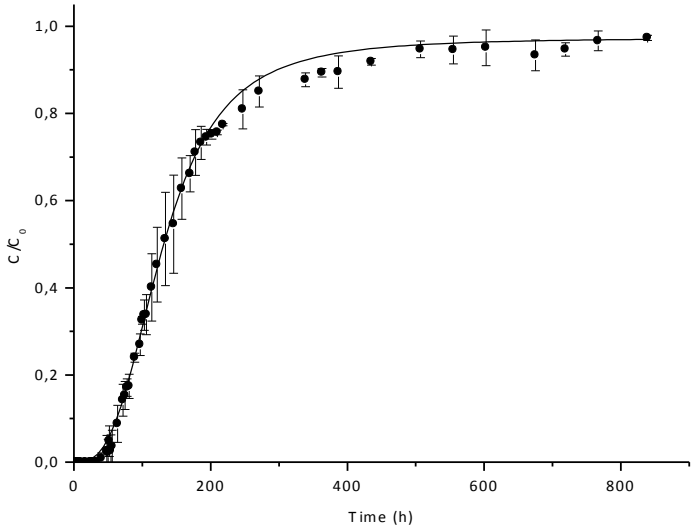


Figure 7.6 – Relative phosphate concentration ($C/C_0$) at the effluent of a column as a function of time for HPN-Pr.

### 7.3.3 REGENERATION STUDY

The regeneration of HPN-Pr and recovery of phosphate after the removal step is very important from economical and environmental points of view. This process should be simple, fast and not expensive. The removal capacity of HPN-Pr was regenerated by washing either with HCl or NaOH for 10 s. Four successive cycles of saturation and washing were made with the same HPN-Pr. The percentage of P removed in each cycle is depicted in Figure 7.7.

Cyclic saturation of the HPN-Pr without intermediary regeneration steps revealed that the material continues to present adsorption capacity. This fact might be due to the existence of a phosphate concentration gradient between the solution and the solid phase. This result is in agreement with the Freundlich adsorption model that best described phosphate adsorption on HPN-Pr. According to literature, the Freundlich model describes the adsorption process as a multilayer, where phosphate continues to adsorb after reaching the saturation in the presence of a concentration gradient [8,37].

The regeneration of the saturated HPN-Pr with HCl was effective, while with NaOH was not successful. In the first alkaline washing step, the adsorption capacity of the HPN-Pr decreased significantly and it was maintained constant in the next washing steps but considerably lower

than in of the initial material. Conversely, an increase in the phosphate adsorption capacity was observed in the first acidic washing step. Between the first and the second washing steps, a decrease in the amount of phosphate adsorbed was observed, and then was kept almost constant and similar to the adsorption capacity of the initial HPN-Pr. The increase in the phosphate adsorption capacity observed in the first acidic treatment might be due to the removal of chemical groups connected to the aluminium by weak bonds (e.g. OH), whose would raise the adsorption capacity of HPN-Pr. The alkaline washing step caused a decrease in the amount of aluminium nanoparticles present in the surface of HPN-Pr, as depicted in Table 7.2. This might have been caused by breakdown of weak chemical bonds between aluminium atoms in the surface of the HPN-Pr. Conversely, the acidic washing did not cause a variation in the percentage of aluminium detected in the surface of HPN-Pr (Table 7.2).

The phosphate species present in solution are dependent on pH [38]. Around pH 7.0, $H_2PO_4^-$ is the predominant species in solution (a weak acid with a pKa value of 7.2) and becomes a non-charged species in contact with an acidic solution [39]. This might explain the fact that phosphate was desorbed when HPN-Pr was washed with HCl, being the reaction as follows:

$$(AlPO_4)^- + 3H^+ \leftrightarrow -Al^{2+} + H_3PO_4 \qquad \text{Equation 7.5}$$

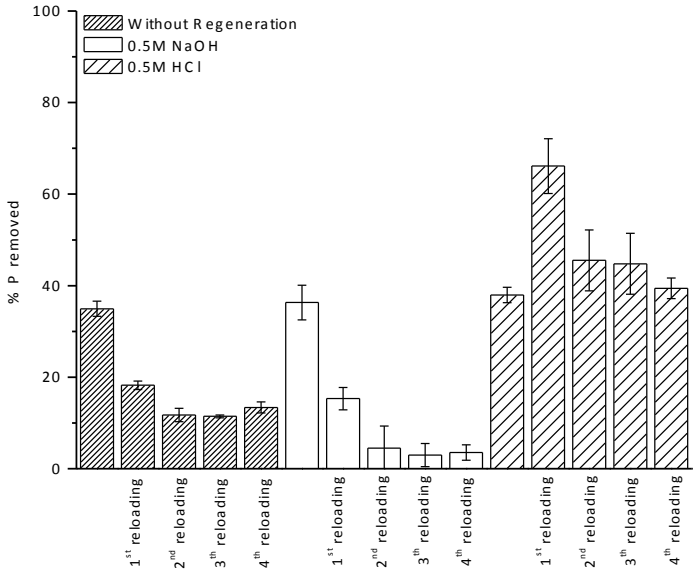


Figure 7.7 – Phosphate removal capacity of HPN-Pr with and without regeneration.

Table 7.2 – Aluminium and oxygen present on the surface of HPN-Pr before and after acidic and alkaline regeneration steps determined by EDS.

| HPN | Al (%) | O (%) |
|---|---|---|
| Virgin | 7.22 | 27.55 |
| HCl regeneration | 7.30 | 27.46 |
| NaOH regeneration | 3.65 | 23.37 |

### 7.3.4 TECHNOLOGY IMPLEMENTATION

The HPN-Pr presented in this work was mainly developed for the remediation of freshwater bodies (e.g. lakes, dams) and phosphate recovery. In this context, it is important to elucidate the possible ways to implement this technology. From an industrial point of view, the HPN-Pr can be produced in many shapes (pellets, rods, films and complex profiles). The topography at the bottom of the reservoirs, as well as their trophic state will determine the best way to apply the material. The HPN-Pr might be applied as a layer covering the sediments or as a 3D-structure like a coral reef that might be removed from the water reservoir when charged with phosphate. The first option would allow a more homogeneous distribution of the material in the surface of the sediment; however, its capacity to remove P would decrease along time due to the deposition of a new layer of sediment on top of it. The main advantage of the second option is that the material could be removed from the water body preventing phosphate solubilisation in the long term. Additionally, P could be recovered and reused as a fertiliser according to Donnert and Salecker (1999) [13].

## 7.4 CONCLUSIONS

The hybrid nanocomposites studied on the present work reveals as new and effective material to remove P from eutrophic natural waters. While HPN-Pr removes 0.80±0.01 mgP/g at the pH interval from 2.0 to 6.5, HPN-acac removes 1.27±0.02 mgP/g at the pH interval 6.0 to 8.5. However, determinations of aluminium concentration in batch tests indicated that HPN-acac transferred higher levels of this ion to solution, which makes this unviable for natural applications. HPN-Pr shows to be chemically stable, with adsorption mechanism described by Freundlich adsorption model. Moreover, HPN-Pr could be regenerated by washing it with HCl 0.5 M.

Regeneration, allows the recovery of phosphorus adsorbed by HPN-Pr, which can be again introduced on commercial cycle contributing this way to the sustainability of this mineral resource each time more scarce.

HPN-Pr is a material to treat natural eutrophic waters preferentially by proper application, compared with to other common phosphorus removal agents, it does not increase the water turbidity, sludge production or contaminate with toxic compounds.

## 7.5 BIBLIOGRAPHY

[1] Correll, D.L. 1999. Phosphorus: A Rate Limiting Nutrient in Surface Waters. *Poultry Sci*ence 78(5):674–682.

[2] Carmichael, W.W. 1991. Toxic freshwater blue-green algae (cyanobacteria): an overlooked health threat. *Health Environment Digest* 5:1–4.

[3] Selman, M. Greenhalg, S. 2009. Eutrophication: polices, action, and strategies to address nutrient pollution. *World Resources Institute* N° 3.

[4] Zheng, S. Chen, J. Jiang, X. Li, X. 2011. A comprehensive assessment on commercially-available standard anion resins for tertiary treatment of municipal wastewater. *Chemival Engineering Journal* 169(1-3):194–199.

[5] Hickey, C.W. Gibbs, M.M. 2009. Lake sediment phosphorus release management – Dicision support and risk assessment framework. *New Zealand Journal of Marine and Freshwater Research* 43(3):819–856.

[6] Nyenje, P.M. Foppen, J.W. Uhlenbrook, S. Kulabako, R. Muwanga, A. 2010. Eutrophication and nutrient release in urban areas of sub-Saharan Africa — A review. *Science Total Environment* 408(3):447–455.

[7] Lewandowski, J. Schauser, I. Hupfer, M. 2003. Long term effects of phosphorus precipitations with alum in hypereutrophic Lake Susser See (Germany). *Water Research* 37(13):3194–3204.

[8] Genz, A. Kornmüller, A. Jekel, M. 2004. Advanced phosphorus removal from membrane filtrates by adsorption on activated aluminium oxide and granulated ferric hydroxide. *Water Research* 38(16):3523–3530.

[9] Kõiva, M. Liirab, M. Mandera, U. Mõtlepb, R. Vohlaa, C. Kirsimäe, K. 2010. Phosphorous removal using Ca-rich hydrated oil shale ash as filter material. The effect of different phosphorus loadings and wastewater compositions. *Water Research* 44(18):5232–5239.

[10] Lan, Y.Z. Zhang, S. Wang, J.K. Smith, R.W. 2006. Phosphorous removal using steel slag. *Acta Metall. Sinica (English Letters)* 19(6):449–554.

[11] Yuan, G. Wu, L. 2007. Allophane nanoclay for the removal of phosphorus in water and wastewater. *Science Technology Advanced Materials* 8(1-2):60–62.

[12] Hano, T. Takanashi, H. Hirata, M. Urano, K. Eto, S. 1997. Removal of phosphorus from wastewater by activated alumina adsorbent. *Water Science Technol*ogy 35(7):39–46.

[13] Donnert, D. Salecker, M. 1999. Elimination of phosphorus from municipal and industrial waste water. *Water Science Technology* 40(4-5):195–202.

[14] Miller, N. 2005. Locally available adsorbing materials, sediment sealing and flocculants for chemical remediation of lake and stream. *Analytical & Environmental Consultants*:15–32.

[15] Zeng, L. Li, X. Liu, 2004. Adsorptive removal of phosphate from aqueous solutions using iron oxide tailings. *Journal Water Research* 38(5):1318–1326.

[16] Zhang, G. Liu, H. Liu, R. Qu, J. 2009. Removal of phosphate from water by a Fe-Mn binary oxide adsorbent. *Journal Colloid Interface Science* 335(2):168–174.

[17] Oliveira, M. Nogueira, R. Machado, A.V. 2012. Synthesis of aluminium nanoparticles in a pp matrix during melt processing: effect of the alkoxide organic chain. *Reactive & Functional Polymers DOI: 10.1016/j.reactfunctpolym.2012.06.022.*

[18] Kosmulski, M. 2002. The pH-Dependent Surface Charging and the Points of Zero Charge. Journal of Colloid Interface Science 253(1):77-87.

[19] Smičiklas, I.D. Milonjić S.K. Pfendt, P. Raičević, S. 2000. The point of zero charge and sorption of cadmium (II) and strontium (II) ions on synthetic hydroxyapatite. Separation and Purification Technology 18(3):185-194.

[20] Eaton, A.D. Clesceri, L.S. Greenberg, A.E. 1995. *Standard Methods for the Examination of Water and Wastewater,* 19th ed, American Public Health Association, Washington DC, 4-113–4-114.

[21] Galarneu, E. Gehr, R. 1997. Phosphorus removal from wastewaters: experimental and theoretical support for alternative mechanism. *Water Research* 31(2):328–338.

[22] Claret, F. Schäfer, T. Bauer, A. Buckau, G. 2003. Generation of humic and fulvic acid from Callovo-Oxfordian clay under high alkaline conditions. *Science Total Environment* 317(1-3):189–200.

[23] MacLeod, C. Whitfield, P.H. 1996. Seasonal and long-term variations in water quality of the Columbia river at Revelstoke. B.C. *Northwest Science* 70(1):55–65.

[24] Markich, S.J. Brown, P.L. 1998. Relative importance of natural and anthropogenic influences on the fresh surface water chemistry of the Hawkesbury-Nepean River, south-eastern Australia. *Science Total Environment* 217(3):201–230.

[25] Olías, M. Nieto, J.M. Sarmiento, A.M. Cerón, J.C. Cánovas, C.R. 2004. Seasonal water quality variations in a river affected by acid mine drainage: the Odiel River (south west Spain). *Science Total Environment* 333(1-3)267–281.

[26] Drizo, A. Frost, C.A. Grace, J. Smith, K.A. 1999. Physical-chemical screening of phosphate removing substrates for use in constructed wetland systems. *Water Research* 33(17):3595–3602.

[27] Sakadevan, K. Bavor, H.J. 1998. Phosphate adsorption characteristics of soils, slags and zeolite to be used as substrate in constructed wetland systems. *Water Research* 32(2):393–399.

[29] Chouyyok, W. Wiacek, R.J. Pattamakomsan, K. Sangvanich, T. Grudzien, R.M. Fryxell, G.E. 2010. Phosphate Removal by Anion Binding on Functionalized Nanoporous Sorbents. *Environment Science Technology* 44(8):3073–3078.

[30] Hongshan, L. Songqiang, L. 2003. Biochemical Mechanism of the eutrophication and its prevention - the deep treatment of waste water and its denitrification and dephosphorization. *Marine Science Bulletin* 5(1):32–39.

[31] Hupfer, M. Rübe, B. Schmieder, P. 2004. Origin and diagenesis of polyphosphate in lake sediments: A 31P-NMR study. *Limnology Oceanography* 49(1):1–10.

[32] Georgantas, D.A. Grigoropoulou, H.P. 2007. Orthophosphate and metaphosphate ion removal from aqueous solution using alum and aluminium hydroxide. *Journal Colloid Interface Science* 315(1):70–79.

[33] Razali, M. Zhao, Y.Q. Bruen, M. 2007. Effectiveness of a drinking-water treatment sludge in removing different phosphorus species from aqueous solution. *Separation Purification Technology* 55(3):300–306.

[34] Kuroda, D. 1987. Simultaneous adsorption of phosphate and ammonium ions from industrial wastewater onto the same adsorbent. *Kagaku To Kogyo* 61:378–383.

[35] Benyoucef, S. Amrani, M. 2011. Adsorption of phosphate ions onto low cost Aleppo pine adsorbent. *Desalination* 275(1-3):231–236.

[36] Mortula, M.M. Gagnon, G.A. 2009. Alum residuals as a low technology for phosphorus removal from aquaculture processing water. *Aquaculture Engineering* 36(3):233–238.

[37] Zhang, J. Shen, Z. Mei, Z. Li, S. Wang, W. 2011. Removal of phosphate by Fe-coordinated amino-functionalized 3D mesoporous silicates hybrid materials. *Journal Environment Science* 23(2):199–205

[38] Oliveira, M. Ribeiro, D. Nobrega, J.M. Machado, A.V. Brito, A.G. Nogueira, R. 2011. Removal of Phosphorus from Water Using Active Barriers: $Al_2O_3$ Immobilized on to Polyolefins. *Environment Technology* 32(9):989–995.

[39] Awual, M.R. Jyo, A. El-Safty, S. Tamada, M. Seko, N. 2011. A weak-base fibrous anion exchanger effective for rapid phosphate removal from water. *Journal Hazardous Materials* 188(1-3):264–171.

CHAPTER

# 8 A NOVEL HYBRID POLYMER NANOCOMPOSITE BIOFILM REACTOR FOR PHOSPHORUS REMOVAL: START UP AND OPERATION

The eutrophication phenomenon is one of the main challenges regarding the ecological quality of surface waters, being the phosphorus bioavailability its main driver. In this context, a novel hybrid polymer nanocomposite (HPN-Pr) biofilm reactor aiming at integrated chemical phosphorus adsorption and biological removal was conceived. The experimental assays pointed to a removal of 1.2 mgP/g of reactive phosphate (SRP) and 1.01 mgP/g of total phosphorus at steady-state. A mathematical adsorption-biological model was applied to predict the reactor performance. The model indicated that biological activity has a positive effect on reactor performance increasing the levels of SRP removed.

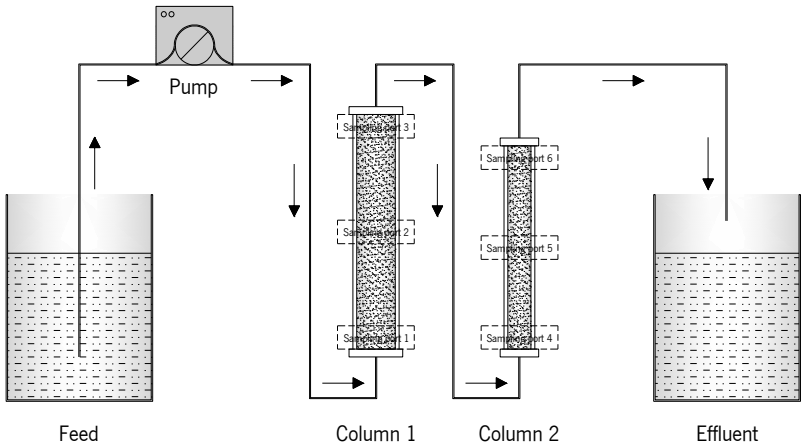


Oliveira, M. Rodrigues, A.L. Ribeiro, D. Machado, A.V. Brito, A.G. Nogueira, R. 2012. A novel hybrid polymer nanocomposite biofilm reactor for phosphorus removal: start up and operation. Submitted to *Science of Total Environment.*

## 8.1 INTRODUCTION

The leaching of surplus fertilizers from agriculture practices and the discharge of phosphorus (P) rich wastewaters are among the most significant anthropogenic pressures on river basins [1,2]. As a consequence, a severe loss of ecosystem biodiversity occurs and water abstraction is at risk when toxins are released after cyanobacteria blooms [3]. The eutrophication of waters bodies is noticed since the 1950s, yet the phenomenon is far from being solved today and affects 53 % of European lakes, among many others around the world [4]. The European Water Framework Directive (WFD-2000/60/EC) imposed the restoration of water bodies quality until 2015, but derogations have been claimed when eutrophication is the main pressure. Indeed, even when external P sources are eliminated, a slow rehabilitation process is observed because of the re-dissolution of P accumulated in sediments [5,6]. Furthermore, polyphosphates can also have a crucial role, since it can gradually hydrolyse into phosphates [2,7,8].

Biological nitrogen removal is well known in water and wastewater treatment processes [9]. On the contrary, biological P-removal is only applied in wastewater treatment plants [10]. Chemical P-removal is based on precipitation or adsorption processes using aluminium, iron and calcium salts or industrial by-products [11-15]. Nevertheless, these methods may cause water contamination, sludge disposal problems and do not allow P recycling [15-19].

In this context, the aim of this paper was to assess the efficiency of a new bioreactor using a hybrid polymer nanocomposite (HPN-Pr) media for integrated P adsorption and biological removal. The specific goals were i) to evaluate pH effects and the efficiency for polyphosphate removal and ii) to test the (HPN-Pr) bioreactor performance regarding soluble reactive phosphorus (SRP) and total P elimination.

## 8.2 MATERIALS AND METHODS

### 8.2.1 HPN-PR SYNTHESIS

HPN-Pr is a hybrid nanocomposite containing 1.4 % in aluminium that results from the reaction of polypropylene grafted with maleic anhydride (PP-g-MA) with aluminium isopropoxide ($Al(Pr\text{-}i\text{-}O)_3$) and was synthesised by reactive extrusion using a sol-gel reaction in the melt. The density of the nanocomposite was increased to 1.2 g/dm$^3$ with antimony trioxide ($Sb_2O_3$). The HPN-Pr was

milled in pellets with 3 mm length. A more detailed description of the synthesis process and properties of the HPN-Pr can be found on Oliveira et al. 2012 and Oliveira et al. 2012 [20,21].

### 8.2.2 ANALYTICAL METHODS

The concentrations of soluble reactive (SRP) and total P were measured as phosphate by ascorbic acid method (Method 4500P-E) according to the Standard Methods (1998) [22]. Polyphosphate was quantified as phosphate in samples that have been previously digested (Method 4500P-E) [22]. For the quantification of total solids (TS) and total P in the biofilm grown on the surface of the HPN-Pr particles, approximately 1 g of the material was taken in each sampling port of the columns after 50 days of operation (Figure 8.1) and was intensively shaken on a vortex during 1 min to release the biofilm from the material. The TS of the biofilm suspension was measured by the gravimetric method according to the Standard Methods (1998) [22]. Total phosphate was measured after digestion of the biofilm suspension as previously described. The phosphate adsorbed on the HPN-Pr was quantified after the biofilm removal step. For that, the material was washed with 10 mL 0.5 M HCl solution for 1 h as described in Oliveira et al. 2012 [23]. Afterwards, the solution was neutralised and phosphate was measured as previously described.

### 8.2.3 REACTOR OPERATION I: PRE-FEASIBILITY STUDIES WITHOUT BIOFILM

#### *8.2.3.1 pH effects on phosphate removal by HPN-Pr*

Experiments were done in a column of 260 mm length and 30 mm diameter filled with 50 g of HPN-Pr. The fixed bed porosity was 0.4 determined by gravimetric method. A synthetic water containing 200 µgP/L, with initial pH of 5, 6, 7 and 8, was passed in upflow mode at a rate of 0.5 mL/min. The empty bed hydraulic retention time was 2.5 h. The experiments were done in duplicate and stopped when the equilibrium concentration in the liquid phase was reached. Potassium dihydrogenophosphate ($KH_2PO_4$, Merck) was used as phosphate source.

#### *8.2.3.2 Polyphosphate removal by HPN-Pr at pH 6*

The experimental set-up used to determine the removal of polyphosphate by HPN-Pr was already described in section 8.2.3.1. A polyphosphate solution containing 100 µg/L of P with an initial pH of 6 was passed upflow through the column at rate of 0.5 mL/min. The experiments were done in duplicate and pentasodiumtripolyphosphate ($Na_5P_3O_{10}.6H_2O$, Sigma Aldrich) was used as polyphosphate source.

### 8.2.4 REACTOR OPERATION II: START-UP OPERATION WITH BIOFILM GROWTH

#### *8.2.4.1 Water characterisation*

Cávado river provided the feed water used in the experiments. The Cávado watershed is an agriculture intensive region in the northern Portugal where eutrophication pressures are reported. The average water pH was 6.6 and the total phosphate and phosphate concentrations were 267 µgP/L and 265 µgP/L, respectively. Carbon TC and TOC, TSS and SSV were determined according Standard Methods [22]. The water sample collected in September 2011 and was stored at 4 °C before use. Table 8.1 presents the water quality characterisation.

Table 8.1 – Characterization of Cávado river water quality.

| **SRP** (µg/L) | **Total P** (µg/L) | **pH** | **Carbon TC** (µg/L) | **Carbon TOC** (µg/L) | **TSS** (mg/L) | **SSV** (mg/L) |
|---|---|---|---|---|---|---|
| 265.5±1.01 | 267.1±11.2 | 6.56 | 232.9±11.8 | 214.3±16.6 | 0.60±0.03 | 0.50±0.04 |

#### *8.2.4.2 Column reactor set-up*

The experimental bioreactor set-up consisted in two connected columns as depicted in Figure 8.1. The first column was 300 mm length and 50 mm diameter and the second column 260 mm length and 30 mm diameter. Both columns were filled with 400 g of HPN-Pr. The river water was pumped upflow at a flow rate of 0.5 mL/min and the total hydraulic retention time in both columns was 10.4 h. Samples were taken daily during the first 30 days of operation and twice a week afterwards until the end of the experiments that lasted 50 days. The biofilm on the surface of the HPN-Pr was quantified as total solids.

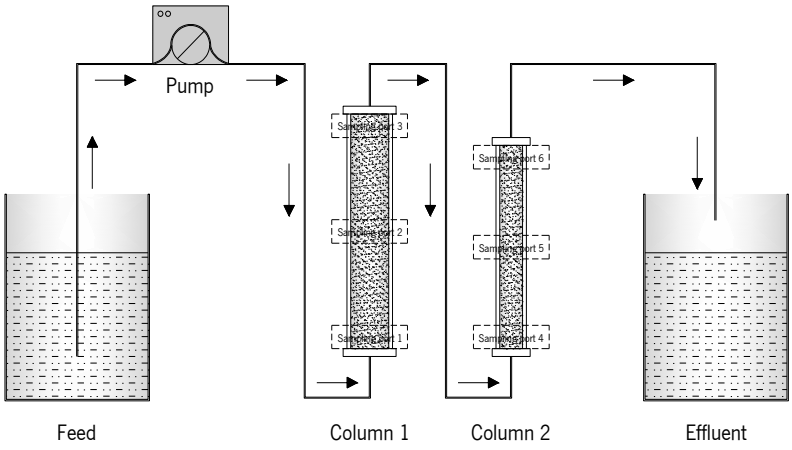


Figure 8.1 – Schematic of the experimental set-up.

### *8.2.4.3 Mathematical simulation*

The phosphate removal was hypothesized to occur sequentially, first by physic-chemical adsorption on the HPN-Pr support and then by a biological metabolism. In order to test this hypothesis, a mathematical model was used based on the saturated soil compartment of AQUASIM [24]. The adsorption process was described by a Freundlich isotherm (Equation 8.1) and the biological consumption by a Monod-type equation (Equation 8.2).

$$S=K_f \times C^{\alpha} \qquad \text{Equation 8.1}$$

$$R=\frac{\mu_{max} \times C}{Km+C} \qquad \text{Equation 8.2}$$

The parameters of the Freundlich isotherm were determined in a previous work [23], while the parameters of the Monod equation were estimated through the model adjustment to experimental data. The kinetic parameters are presented in Table 8.2.

Table 8.2 – Kinetic parameters used in the model

| Parameter | Value | Units |
|---|---|---|
| Adsorption constant, alpha | 0.56 | - |
| Adsorption constant, $K_F$ | 0.76 | $mg^{1-n}.g^{-1}.L^{n}$ |
| Maximum growth rate, $\mu_{max}$ | 0.12 | $h^{-1}$ |
| Half saturation coefficient, $K_m$ | 55 | µg/L |

The cross sectional area of columns 1 and 2 was 511 and 259 $cm^2$ and the length was 300 and 260 mm respectively.

## 8.3 RESULTS AND DISCUSSION

### 8.3.1 REACTOR OPERATION I: PRE-FEASIBILITY STUDIES WITHOUT BIOFILM

#### *8.3.1.1 pH effects on phosphate removal by HPN-Pr*

The influence of pH on the phosphate removal capacity of HPN-Pr is depicted in Figure 8.2. The phosphate removal capacity ($C/C_0$) was expressed as the ratio between the phosphate concentrations at outlet (C) and inlet ($C_0$). The experimental results indicated that the phosphate removal by HPN-Pr increased slightly when the pH decrease, attaining 12±1 μgP/g at pH 5.0, 11±2 μgP/g at pH 6.0, 9.1±0.2 μgP/g at pH 7.0 and 8.30±0.06 μgP/g at pH 8.0. The phosphate removal capacity of HPN-Pr is related to its superficial charge and the zero point charge is around pH 7.5 (Oliveira et al. 2012) [23]. Therefore, at a higher pH the HPN-Pr material presents a negative surface charge and repulses the phosphates anions ($H_2PO_4^-$, $HPO_4^{2-}$, $PO_4^{3-}$) [25]. Thus, pH values below the $pH_{ZPC}$ are more favourable to phosphate removal performance, since the surface of the HPN-Pr is positively charged and attracts phosphates anions.

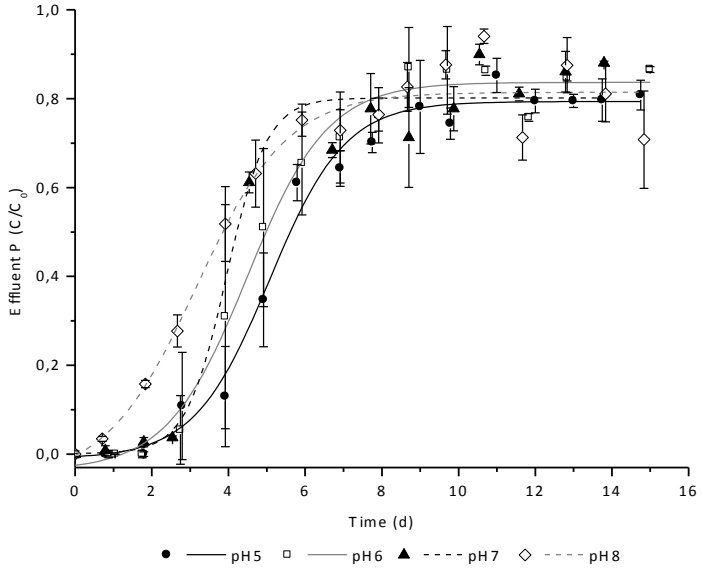


Figure 8.2 – Phosphate removal capacity of HPN-Pr at different pH values.

#### *8.3.1.2 Polyphosphate removal by HPN-Pr at pH 6*

The performance of HPN-Pr to eliminate polyphosphate was assessed at pH 6 and the results are depicted in Figure 8.3. The polyphosphate removal capacity was 12.7±0.6 µgP/g and is strongly related to $Al^{3+}$ content of HPN-Pr (1.4 %) and specific mass transfer area. Indeed, an adsorption capacity of 520±10 µgP/g was obtained in a previous study where $Al^{3+}$ concentration was 3.3 % and the particle size was much lower, 0.2 mm [23]. Moreover, Razali et al. (2007) reached a very high capacity of 23.5 mgP/g using a by-product with 46 % of $Al_2O_3$ and an $Al^{3+}$ concentration of 51 % [26].

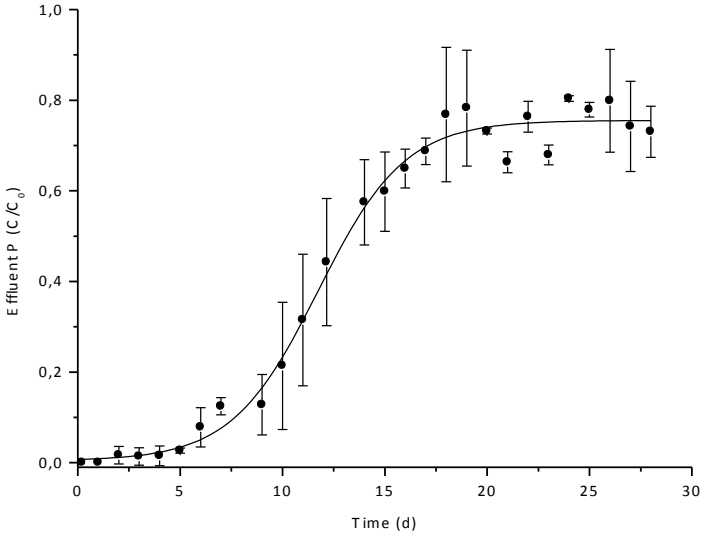


Figure 8.3 – Removal of polyphosphate by HPN-Pr at pH 6.

### 8.3.2 REACTOR OPERATION II: START-UP OPERATION WITH BIOFILM GROWTH

#### *8.3.2.1 Phosphorous removal test*

The Cávado river water was used to determine the bioreactor P-adsorption capacity in real conditions. The experimental results for total phosphate and SRP are depicted in Figure 8.4 and Figure 8.5.

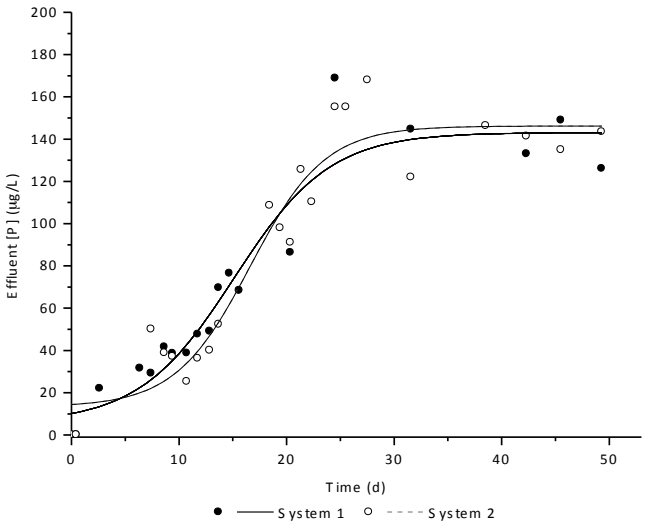


Figure 8.4 – Profile concentration of total phosphate at the outlet of both systems.

The total phosphate removal was 1.04 mgP/g and 0.98 mgP/g in system 1 and 2, respectively. Therefore, the results indicated that HPN-Pr is unable to remove all P species, since these can come out in organic particles and increase the total phosphate concentration after digestion process. However, regarding to SRP in Figure 8.5, HPN-Pr removal attained 100 % along the first 12 days of operation. The amount of SRP removed was 1.36 mgP/g and 1.04 mgP/g for systems 1 and 2, respectively. The concentration of phosphate at the outlet of both systems stabilized after 50 days of operation, but the reactor did not saturated and maintained a removal capacity of 55 % for system 1 and 62 % for system 2. This pattern might be explained by a multi-layer adsorption of phosphate on HPN-Pr as was suggested by the adsorption isotherm and bioconsumption kinetics [23,27].

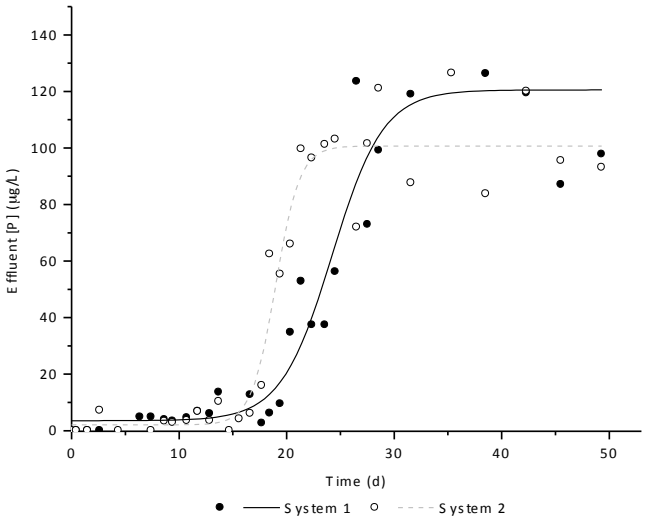


Figure 8.5 – Reactive phosphorus concentration of phosphate at the outlet of both systems.

Other studies indicate that phosphate removal depends on the type of adsorbent. Razali et al. (2007) removed 50.7 mgP/g of phosphate using aluminium sludge from a water treatment coagulation process [26]. Kabayama et al. (2003) removed 11.3 mgP/g from a 1 mM disodium hydrogen phosphate aqueous solution passing through the column containing aluminium oxide hydroxide [28]. Drizo et al. (1999) assess the phosphate removal by shale and bauxite clays and obtained 0.73 mgP/g and 0.35 mgP/g, respectively [29]. Aluminium wastes from a water treatment plant adsorbed 0.48 mgP/g and 0.14 mgP/g, when used in aquaculture wastewater treatment [30].

The pH value of the effluent was around 7.0, which was slightly higher than the influent one, 6.6. This increase might be due to an experimental variation or to the excretion of alkaline compounds by bacteria.

#### *8.3.2.2 Biofilm assessment*

The operation of the bioreactor led to the formation of a biofilm over the HPN-Pr particles, as can be seen in Figure 8.6. The presence of biofilm becomes visible at the end of the second week when a change in particles colour from white to yellowish did occur.

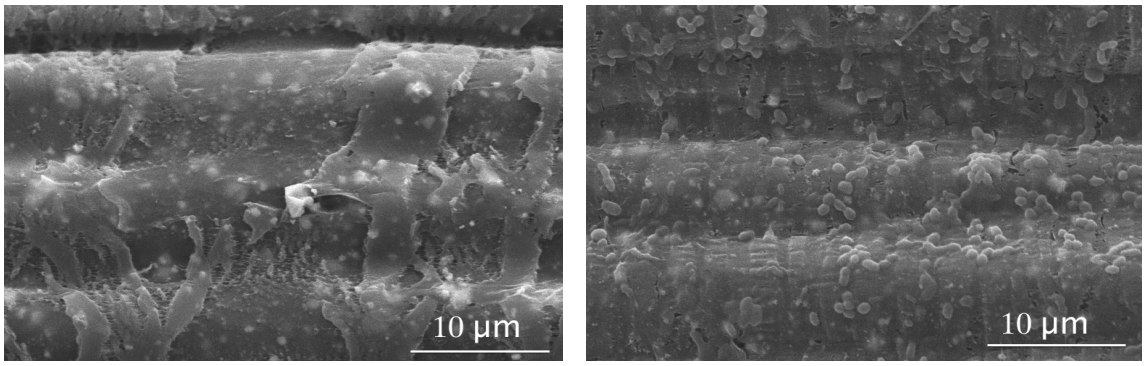


(a) (b)

Figure 8.6 – SEM pictures of the HPN-Pr surface: a) clean; b) with biofilm.

The bacterial diversity was assessed by DGGE patterns of partial 16S rRNA gene amplicons. The DGGE band-pattern of the biofilm formed on HPN-Pr indicated the presence of several ribotypes, which reveals a high microbial diversity. This result is in accordance with other ones that found out a similar microbial diversity in natural aquatic ecosystems [31,32]. SEM micrograph from the

HPN-Pr surface confirms the presence of a well-established microorganism community (Figure 8.6).

The biofilm formed after 50 days was quantified as total solids (TS) at 3 different columns heights, Figure 8.7a and b. The data indicate that biofilm concentration was proportional to bulk liquid carbon and macro-nutrients. However, the higher concentration of biofilm at the button column 2 was due to the biofilm formed inside the pipe that made the connection between columns.

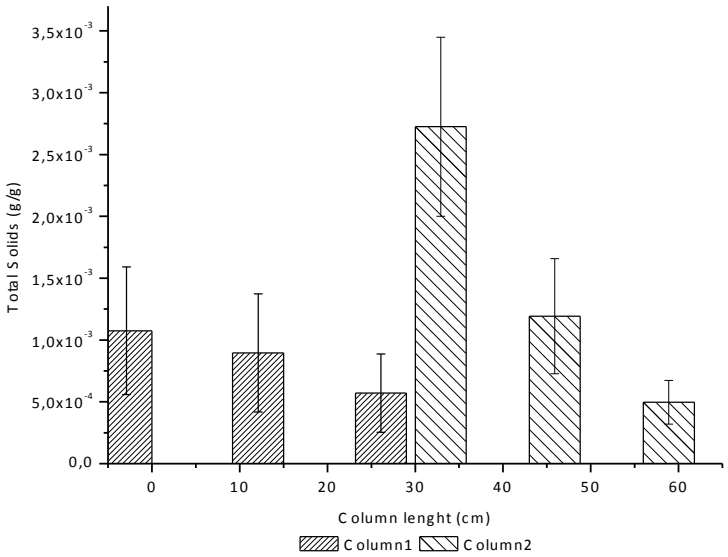


(a)

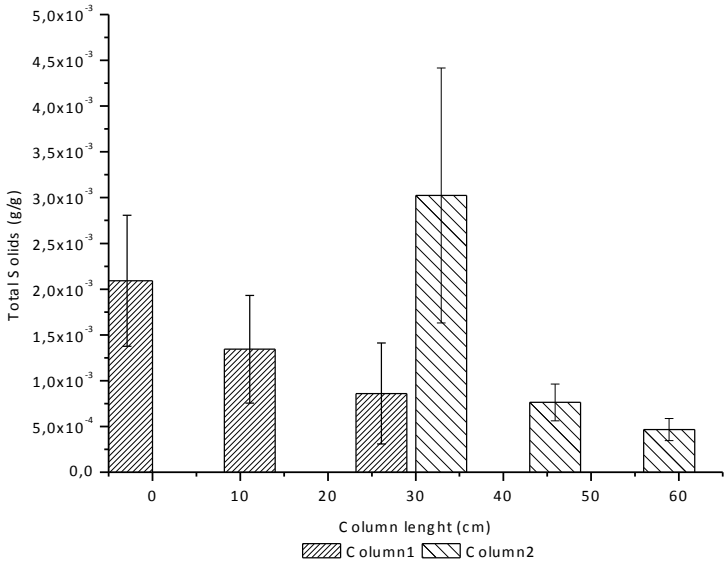


(b)

Figure 8.7 – Biofilm total solids distribution: a) System 1; b) System 2.

*8.3.2.3 Phosphate removal by adsorption on HPN-Pr particles and biofilm metabolism*

The amount of phosphate present in the biofilm and HPN-Pr particles was assessed as indicated in Methods section. To measure a concentration profile, the samples were taken at three distinct points of each system (Figure 8.1). The results showed that both biological and physic-chemical processes contribute to phosphate removal, since P was quantified on biofilm and on HPN-Pr surface. Therefore, the biofilm formation on HPN-Pr particles did enhance performance removal when compared to a pure physic-chemical process. As it can be observed in Figure 8.8, the highest amount of phosphate was consumed at the bottom of the columns and decreased along its height. These results are in accordance with biofilm concentration profile along the reactor.

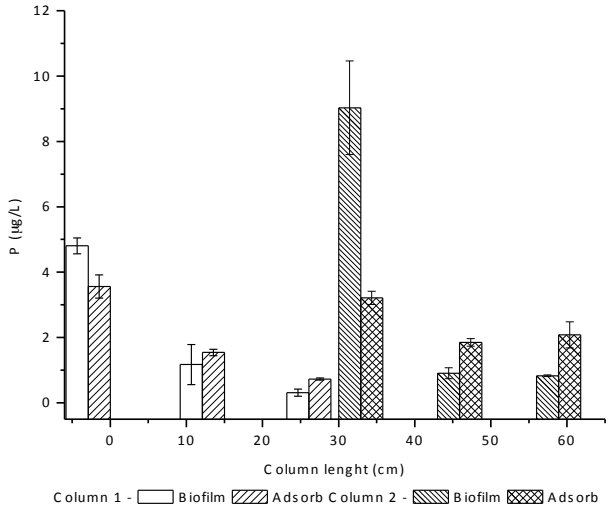


(a)

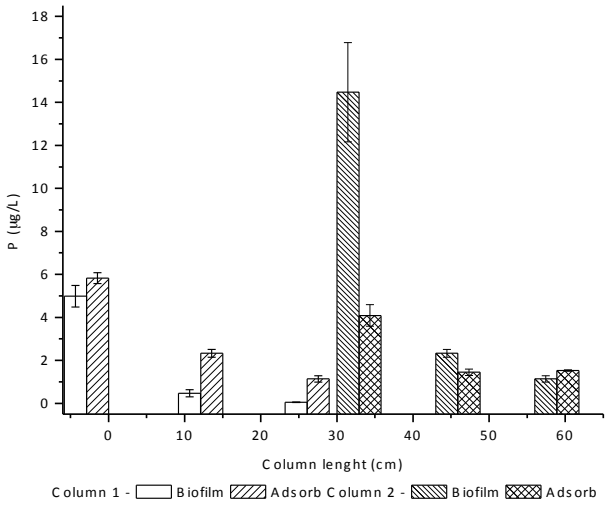


(b)

Figure 8.8 – Distribution of the amount of phosphate in the biofilm and adsorbed to the HPN-Pr particles: a) System 1; b) System 2.

### *8.3.2.4 Mathematical modelling of P removal*

The mathematical modelling was assessed using the following Freundlich and Monod equations:

$$S=0.76\times C^{0.56} \qquad \text{Equation 8.3}$$

$$R=\frac{0.12\times C}{55+C} \qquad \text{Equation 8.4}$$

The phosphate adsorption on HPN-Pr is a much faster reaction than the biofilm formation. The biofilm growth is limited by P availability until HPN-Pr reaches saturation (Figure 8.9: t=400 h). After this point, phosphate concentration in the bulk liquid trigger biofilm growth until it reaches the equilibrium (Figure 8.9: t=1200 h). To compare the effects of phosphate removal by adsorption process and biomass growth, this process was inactivated in the model, allowing phosphate removal to occur by adsorption processes only. The results are presented in Figure 8.9 (full line).

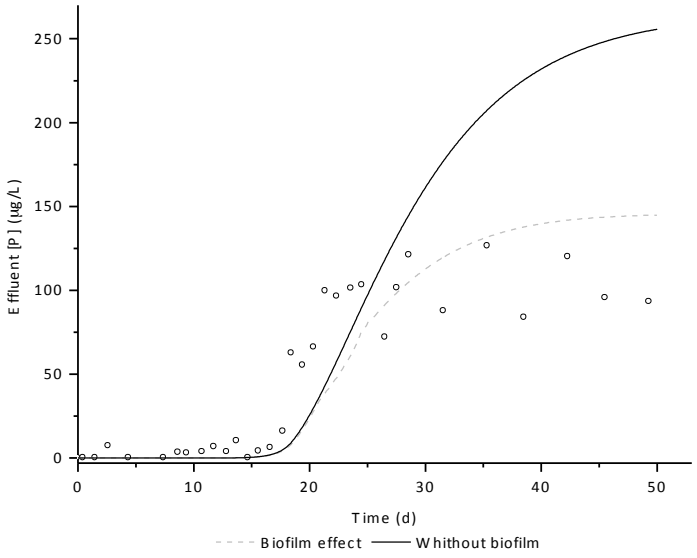


Figure 8.9 – Predicted average values for phosphate removal by HPN-Pr with and without the presence of biofilm.

We can conclude that if phosphate removal by biofilm doesn't occur, the reactive phosphate concentration will rise and will reach saturation earlier (comparing sketched and full line in Figure 8.9). When HPN-Pr is fully saturated, phosphate concentration at inlet (250 µg/L of P) will be the same at outlet (Figure 8.9: t=1200 h), revelling that no more phosphate can be removed by this process. Thus, adsorption process is more important in a short-time perspective (until saturation) while biofilm growth presents advantages to face reactive phosphate in a long-term perspective.

However, we may foresee that biofilm growth will reach a limit and biomass will tend to wash-out. In that case, reactive phosphate will continue to be removed but organic particulate phosphate concentration may rise at reactor outlet. Therefore, in order to prevent excessive biomass growth in the reactor, adsorption/regeneration cycles of HPN-Pr could be done for semi-continuous phosphate removal and to recover the P that was adsorbed. A future P removal application in wastewater treatment processes may be foreseen based in this hybrid technology also.

## 8.4 CONCLUSION

The hybrid polymer nanocomposite biofilm reactor is a novel and promising integrated technology combining adsorption and biological processes in order to eliminate phosphate from natural waters. Removal performance attained 1.20 mgP/g of SRP and 1.01 mgP/g of total P reaching saturation around 50 %.

## 8.5 BIBLIOGRAPHY

[1] Smith, V.H. Tilman, G.D. Nekola, J.C. 1999. Eutrophication: impacts of excess nutrient inputs on freshwater, marine and terrestrial ecosystems. *Environmental Pollution* 100(1-3):179–196.

[2] Correll, D.L. 1999. Phosphorus: A Rate Limiting Nutrient in Surface Waters. *Poultry Science* 78(5):674–682.

[3] Morse, G.K. Brett, S.W. Guy, J.A. Lester, J.N. 1998. Review: Phosphorus removal and recovery technologies. *The Science of the Total Environment* 212(1):69–81.

[4] Nyenje, P.M. Foppen, J.W. Uhlenbrook, S. Kulabako, R. Muwanga, A. 2010. Eutrophication and nutrient release in urban areas of sub-Saharan Africa - A review. *Science Total Environment* 408(3):447–455.

[5] Martins, G. Ribeiro, D. Pacheco, D. Cruz, J.V. Cunha, R. Gonçalves, V. Nogueira, R. Brito, A.G. 2008. Prospective scenarios for water quality and ecological status in Lake Sete Cidades (Portugal): the integration of mathematical modelling in decision processes. *Applied Geochemistry* 23(8):2171–2181.

[6] Ribeiro, D. Martins, G. Nogueira, R. Cruz, J.V. Brito, A.G. 2008. Phosphorus fractionation in lake volcanic sediments (Azores – Portugal). *Chemosphere* 70(7):1256–1263.

[7] Hongshan, L. Songqiang, L. 2003. Biochemical Mechanism of the eutrophication and its prevention - the deep treatment of wastewater and its denitrification and dephosphorization. *Maritime Science Bulletin* 5:32–39.

[8] Hupfer, M. Rübe, B. Schmieder, P. 2004. Origin and diagenesis of polyphosphate in lake sediments: A 31P-NMR study. *Limnology and Oceanography* 49(1):1–10.

[9] Lee, K. Rittmann, B.E. 2002. Applying a novel autohydrogenotrophic hollow-fiber membrane biofilm reactor for denitrification of drinking water. *Water Research* 36(8):2040–2052.

[10] Slater, F.R. Johnson, C.R. Blackall, L.L. Beiko, R.G. Bond, P.L. 2010. Monitoring associations between clade-level variation, overall community structure and ecosystem function in enhanced biological phosphorus removal (EBPR) systems using terminal-restriction fragment length polymorphism (T-RFLP). *Water Research* 44(17):4908–4923.

[11] Genz, A. Kornmüller, A. Jekel, M. 2004. Advanced phosphorus removal from membrane filtrates by adsorption on activated aluminium oxide and granulated ferric hydroxide. *Water Research* 38(16):3523–3530.

[12] Kõiva, M. Liirab, M. Mandera, U. Mõtlepb, R. Vohlaa, C. Kirsimäe, K. 2010. Phosphorous removal using Ca-rich hydrated oil shale ash as filter material. The effect of different phosphorus loadings and wastewater compositions. *Water Research* 44(18):5232–5239.

[13] Lewandowski, J. Schauser, I. Hupfer, M. 2003. Long term effects of phosphorus precipitations with alum in hypereutrophic Lake Susser See (Germany). *Water Research* 37(13):3194–3204.

[14] Yuan, G. Wu, L. 2007. Allophane nanoclay for the removal of phosphorus in water and wastewater. *Science Technology Advanced Materials* 8(1-2):60–62.

[15] Donnert, D. Salecker, M. 1999. Elimination of phosphorus from municipal and industrial waste water. *Water Science Technology* 40(4-5):195–202.

[16] Hano, T. Takanashi, H. Hirata, M. Urano, K. Eto, S. 1997. Removal of phosphorus from wastewater by activated alumina adsorbent. *Water Science Technology* 35(7):39–46.

[17] Miller, N. 2005. Locally available adsorbing materials, sediment sealing and flocculants for chemical remediation of lake and stream. *Analytical & Environmental Consultants*.

[18] Zeng, L. Li, X. Liu, J. 2004. Adsorptive removal of phosphate from aqueous solutions using iron oxide tailings. *Water Research* 38(5):1318–1326.

[19] Zhang, G. Liu, H. Liu, R. Qu, J. 2009. Removal of phosphate from water by a Fe-Mn binary oxide adsorbent. *Journal of Colloid Interface Science* 335(2):168–174.

[20] Oliveira, M. Nogueira, R. Machado, A.V. 2012. Synthesis of aluminium nanoparticles in a PP matrix during the melt: effect of the alkoxide organic chain. *Reactive and Functional Polymers DOI: 10.1016/j.reactfunctpolym.2012.06.022.*

[21] Oliveira, M. Nogueira, R. Machado, A.V. 2012. Hybrid nanocomposite preparation in a batch mixer and a twin-screw extruder. *Submitted to Advances in Polymer Technology.*

[22] Eaton, A.D. Clesceri, L.S. Greenberg, A.E. 1995. Standard Methods for the Examination of Water and Wastewater, 19th ed, American Public Health Association, Washington DC, 4-113–4-114.

[23] Oliveira, M. Machado, A.V. Nogueira, R. 2012. Phosphorus removal from eutrophic waters with an aluminium hybrid nanocomposite. *Water, Air & Soil Pollution DOI: 10.1007/s11270-012-1239-9*.

[24] Reichert, P. 1994. AQUASIM – a tool for simulation and data analysis of aquatic systems. *Water Science Technology* 30(2):21–30.

[25] Xiong, J. He, Z. Mahmood, Q. Liu, D. Yang, X. Islam, E. 2007. Phosphate removal from solution using steel slag through magnetic separation. *Journal of Hazardous Materials* 152(1):211–215.

[26] Razali, M. Zhao, Y.Q. Bruen, M. 2007. Effectiveness of a drinking-water treatment sludge in removing different phosphorus species from aqueous solution. *Separation Purification Technology* 55(3):300–306.

[27] Benyoucef, S. Amrani, M. 2011. Adsorption of phosphate ions onto low cost Aleppo pine adsorbent. *Desalination* 271(1-3):231–236.

[28] Kabayama, M. Sakiyama, T. Kawasaki, N. Nakamura, T. Araki, M. Tanada, S. 2003. Characteristics of phosphate ion adsorption-desorption onto aluminium oxide hydroxide for preventing eutrophication. *Journal of Chemical Engineering of Japan* 36(4):499–505.

[29] Drizo, A. Frost, C.A. Grace, J. Smith, K.A. 1999. Physical-chemical screening of phosphate removing substrates for use in constructed wetland systems. *Water Research* 33(17):3595–3602.

[30] Mortula, M.M. Gagnon, G.A. 2007. Alum residuals as a low technology for phosphorus removal from aquaculture processing water. *Aquacultural Engineering* 36(3):233–238.

[31] Newton, R.J. Jones, S.E. Eiler, A. McMahon, K.D. Bertilsson, S. 2011. A guide to the natural history of freshwater lake bacteria. *Microbiology and Molecular Biology Reviews* 75(1):14–49.

[32] Besemer, K. Singer, G. Limberger, R. Chlup, A.K. Hochedlinger, G. Hödl, I. 2007. Biophysical controls on community succession in stream biofilms. *Applied Environmental Microbiology* 73(15):4966–4974.

CHAPTER

# 9 CONCLUSIONS AND FUTURE WORK

## 9.1 CONCLUSIONS

The research present in this thesis aimed to develop a new polymeric material able to remove phosphorus (P) from natural eutrophic water. Therefore, this research began by a simple mixing of PE and PE-g-MA with aluminium oxide, forming thin plates in a hot press (Chapter 3). The effect of pH and the capacity of the prepared composites to remove P were assessed by batch contacting tests. The obtained results showed that even though the composites were able to remove P, the process revealed to be very slow and the polymer matrix functioned as a barrier and did not allow the P to reach the aluminium oxide particles. In chapter 4, hybrid nanocomposites of PP containing Al were prepared in an internal mixer using two Al precursors, $Al(Pr\text{-}i\text{-}O)_3$ and $Al(acac)_3$. The characterization done demostrated that $Al(Pr\text{-}i\text{-}O)_3$ allowed a faster and more extensive reaction. Morphological analysis showed that Al was homogeneously dispersed in the PP matrix with particles diameter around 200 nm. Moreover, improvements on thermal stability and crosslinking levels proved that Al was covalently bond to PP.

Chapter 5, describes the preparation of EVAs nanocomposites using $Al(Pr\text{-}i\text{-}O)_3$ as Al precursor. The EVA was investigated to obtained nanocomposites with higher density. The results, showed that EVA with higher VA content promotes higher levels of reaction and better Al particles distribution.

Focus on the polymer industrial production, Chapter 6 deal with the scale-up production of the developed nanocomposite in a twin screw extruder. The nanocomposite prepared exhibited a good dispersion of Al nanoparticles with a diameter around 85 nm.

Regarding to P removal capacity of prepared hybrid nanocomposites, Chapter 7 demonstrates the removal capability of the nanocomposites developed. However, water contamination was detected with the nanocomposite prepared with $Al(acac)_3$. Moreover, nanocomposite prepared with $Al(Pr\text{-}i\text{-}O)_3$ showed to be efficient on P as polyphosphate removal for pH values lower than 7. Removal process was fitted by Freundlich model, which indicate a multilayer removal mechanism. Furthermore, the material can be regenerated by acidic washing treatment.

The nanocomposite that exhibited better P removal capacity without water contamination was tested with real water using a column as reactor. The reactor showed to be efficient on P removal, where both physic-chemical and biological processes contributed to enhanced performance. The bioreactor worked during 50 days reaching a saturation level of 50 %.

Therefore, this study contributed for the development of a new solution to remove and recovery P from natural waters based on a new nanocomposite that can be produce at industrial scale. Moreover, the present thesis give an important contribution on sol-gel synthesis in the melt, showing that it is possible to produce polymer nanocomposites without presence of solvents.

## 9.2 SUGGESTIONS FOR THE FUTURE WORK

The research present in this dissertation showed that is possible to produce nanocomposites of polymer/Al by sol-gel reaction directly in the melt without additional treatments and that they are efficient on P removal. Although, a large number of studies have been publish on field of hybrid nanocomposites, many fundamental questions on the synthesis of nanocomposites as well as the interaction between nanocomposite and P are still not completely understand.

Taken in consideration the results and conclusions of the present research, some future work can be recommended:

- To investigate with more detail the nanocomposite synthesis in order to have a more controlled reaction extension.
- To investigate the chemical bonding between polymer and P in order to promote a more efficient recovery treatment.
- To identified the interaction between nanocomposite surface and biofilm to understand if material degradation can occurred with exposure time.
- To developed a reactor to be implemented in pilot scale test.